Nanocomposite Catalysts for Soot Combustion and Propane Steam Reforming

by

Hong He

M. S., Chemical Engineering Practice
Massachusetts Institute of Technology, 2003

M. S., Chemical Engineering
Tsinghua University, 2001

B. E., Chemical Engineering
Tsinghua University, 1998

Submitted to the Department of Chemical Engineering
in Partial Fulfillment of the Requirements for the Degree of

Doctor of Philosophy in Chemical Engineering

at the

MASSACHUSETTS INSTITUTE OF TECHNOLOGY

February 2007

Author: _____
Department of Chemical Engineering
December 13, 2006

Certified by: _____
Prof. Jackie Y. Ying
Adjunct Professor of Chemical Engineering
Thesis Supervisor

Accepted by: _____
Prof. William M. Deen
Professor of Chemical Engineering
Chairman, Departmental Committee on Graduate Studies

Nanocomposite Catalysts for Soot Combustion and Propane Steam Reforming

by

Hong He

M. S., Chemical Engineering Practice
Massachusetts Institute of Technology, 2003

M. S., Chemical Engineering
Tsinghua University, 2001

B. E., Chemical Engineering
Tsinghua University, 1998

Submitted to the Department of Chemical Engineering on December 13, 2006
in Partial Fulfillment of the Requirements for the Degree of
Doctor of Philosophy in Chemical Engineering

Abstract

A nanocomposite system, CuO-Ag/CeO_2, has been successfully developed to complete carbon black combustion by 400°C. This novel catalyst has excellent potential for application in the emission control of soot particulates generated by diesel engines. In this work, CuO was coated onto nanocrystalline supports, such as alumina, ceria, zirconia and titania. The best activity and catalyst reducibility were achieved by CuO supported on CeO_2, a material known for its redox property and oxygen storage capacity. A CuO loading of 20–40 wt% presented the optimal balance between CuO content and dispersion, providing for 50% carbon black combustion at 390°C. To further improve the catalytic activity, Ag was introduced as an additive to CuO/CeO_2. CuO-Ag/CeO_2 demonstrated superior reducibility. The optimal CuO-Ag loading was 40 wt%, with a Cu/Ag molar ratio of 1. 50% carbon black conversion was achieved at 304°C over the optimal catalyst, and complete combustion was attained well below 400°C.

A nanocomposite system of nickel aluminate ($NiAl_2O_4$), Re and V has been synthesized for propane steam reforming. Nickel aluminate nanocrystals with various Ni/Al molar ratios were prepared by chemical co-precipitation. They were pretreated in H_2 prior to propane steam reforming to obtain highly dispersed Ni species. The Al in nickel aluminate acted as a spacer to provide uniform Ni dispersion. The catalyst with a Ni/Al molar ratio of 1.10 showed the highest reducibility and the highest active surface area. It gave rise to the best propane conversion and H_2 yield. H_2 yield was improved with increasing reaction temperature up to 700°C, and more H_2 could be produced at higher H_2O/C molar ratios.

Various metal promoters were introduced by impregnation or vapor grafting to improve the catalytic activity and coke resistance of the optimal nickel aluminate catalyst.

Catalytic activity could be improved by introducing metal promoters in the order of Re > Rh > Pt > Ir > Pd > Ru > V. These selected additives provided increased reducibility and active surface area. In particular, 1 wt% Re-promoted nickel aluminate gave rise to the best catalytic activity and H_2 yield. Although Re was the most effective promoter at improving low-temperature activity, it only lowered the coking rate of nickel aluminate slightly. To inhibit coke formation over Re-promoted nickel aluminate, V was introduced as an additive. The optimal nickel aluminate system with 2 wt% Re and 2 wt% V demonstrated the highest catalytic activity and H_2 yield at low H_2O/C ratios. Coking rate was reduced dramatically with the V additive, which promoted carbon gasification. The excellent activity, coke resistance and thermal/hydrothermal stability of Re,V-promoted nickel aluminate nanocomposite would be attractive towards H_2 generation for fuel cell applications, especially in portable devices.

Thesis Supervisor: Jackie Y. Ying
Title: Adjunct Professor of Chemical Engineering

Acknowledgments

First and foremost, I am grateful to Prof. Jackie Ying for her invaluable advice and guidance on my thesis, and for her endless support and encouragements. I would like to thank Prof. Klavs F. Jensen and my thesis committee members, Prof. William H. Green, Prof. Kenneth A. Smith, and Prof. Bernhardt L. Trout for their helpful advice and suggestions.

I am indebted to members of the Nanostructured Materials Research Laboratory (NMRL) for being there for me in the laboratory, and for their insightful discussions and assistance. I thank my seniors, Dr. Neeraj Sangar, Dr. Steven Weiss, Dr. Su Seoung Lee, Dr. Pemakorn Pitukmanorom and Jianyi Cui for their guidance and expertise, especially in initiating my projects. I appreciate working with Dr. Justin McCue, Dr. Jason Sweeney, Dr. Suniti Moudgil, Dr. Tseh-Hwan Yong, Noreen Zaman, and Cindy Ren.

I would like to thank Dr. Hao Wang, Michael Frongillo and Dr. Yong Zhang for their assistance with transmission electron microscopy, Elizabeth Shaw for her help with X-ray photoelectron spectroscopy, Dr. Anthony Garratt-Reed for his assistance with scanning transmission electron microscopy, and Dr. Alexander Mitsos for his help with theoretical calculations. I would also like to acknowledge Linda Mousseau for her assistance. Financial support from the U.S. Army Research Office through the MURI program (DAAD19-01-1-0566) is gratefully acknowledged.

I wish to express my special thanks to my friends at MIT, Wei Chai, Wenchao Sheng, Jianyi Cui, Xiaojun Huang, Qun Shi, Minggang She and Huan Zhang, and my old friends from China, Lin Fang, Huading Zhang, Wenli Wang, Chong Gu and Yuanqing He. Their support, encouragement and friendship have made my life colorful and enjoyable.

Finally, I thank my family profoundly for their love, faith, support and encouragements. I am very fortunate that my parents, Jingqi Yu and Zunmin He, my husband, Yunpeng Yin, and my younger brother, Yi He, are always there for me. This thesis would not have been accomplished without their dedication.

Contents

List of Figures

List of Tables

Chapter 1. Background and Research Motivation

1.1 Soot Combustion

1.1.1 Soot Formation

Diesel engine is widely used in both stationary and mobile power generation. Heavy-duty vehicles such as trains, trucks, buses, tractors, ships and airplanes are diesel-powered. Diesel engine has become increasingly popular in passenger vehicles due to its high efficacy, durability and improved fuel economy. Compared to gasoline engine, the higher compression ratio of diesel engine leads to better efficiency in converting heat to work, and the higher operation temperatures result in more complete fuel combustion and reduce emissions of unburned hydrocarbons and carbon monoxide. However, diesel engine generates pollutants in the form of particulate matter (PM) or soot. Formed by incomplete combustion of fossil fuels in diesel engine, PM consists of elemental carbon (with an average formula of C_8H), inorganic oxides and hydrocarbons (often referred to as soluble organic fraction (SOF)), including some highly toxic polyaromatic hydrocarbons (PAHs). Many studies have shown that PM carries various mutagens and can penetrate deeply into the human lung due to its small particle size.

Since diesel soot particulate is harmful to both human health and the environment, stricter emission control has been established. Several approaches, including improving the engine design, developing fuel additives and tuning the combustion process, have been developed to reduce diesel engine emissions. Nevertheless, post-combustion treatment has become necessary to meet the stricter standard, and one promising strategy involves the use of particle traps and oxidation catalysts to convert soot particles into gaseous products. As shown in Figure 1.1, platinum catalyst (Johnson Matthey) was applied to oxidize NO to obtain NO_2, which facilitated the oxidation of soot particulate.

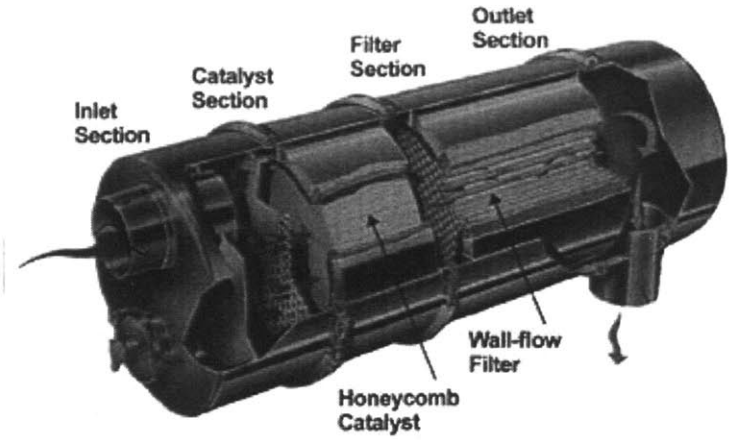

Figure 1.1 A particulate filter system in diesel engine (Johnson Matthey).

1.1.2 Catalysts for Soot Combustion

An ideal soot combustion catalyst should possess the following properties:

- Low temperature activity. Soot would be oxidized only at temperatures higher than 600°C in uncatalyzed combustion processes. Active catalysts are needed to eliminate the soot at temperatures typical of diesel exhausts (200–400°C).
- Thermal stability. Diesel stack temperatures can exceed 600°C at full load. Thus, it is important for the catalyst to be thermally stable.
- Chemical stability. The diesel soot consists of various hydrocarbons and inorganic materials besides elemental carbon. The catalysts employed for soot oxidation have to be chemically stable.
- High selectivity for CO_2. CO emission would require a specific post-converter. It would be much more convenient to be able to completely oxidize soot to CO_2.
- Low cost. If the catalyst is to be widely applied to diesel engine emissions control, it should be economically viable.

Over the past two decades, various materials, including noble metals, transition metal oxides, mixed oxides, pervoskites and spinels, have been studied for the combustion of soot and other carbonaceous materials (such as carbon black) as the substituent for soot. The catalysts examined could be divided into three categories: single-component catalysts, multicomponent catalysts and complex metal oxides.

A large number of single metal oxides that undergo redox cycles during the oxidation process, such as V_2O_5, Cr_2O_3, MoO_3, WO_3, MnO_2, Fe_2O_3, NiO, CuO and CeO_2, along with carbonates and hydroxides, have been examined for soot combustion [1-4]. These catalysts provide higher catalytic activity under tight contact versus loose contact.

To further improve the catalytic activity, multicomponent catalysts based on vanadium, copper and cobalt were studied extensively [4-19]. The catalysts containing copper have been shown to be most promising for soot oxidation, allowing for maximum combustion rate at 300–500°C [5-8]. A higher catalytic activity has been demonstrated by $CuO/\gamma\text{-}Al_2O_3$ compared to $Pt/\gamma\text{-}Al_2O_3$ and $Pd/\gamma\text{-}Al_2O_3$ for the combustion of motorcycle soot [20]. Neeft *et al.* [4] studied the effect of silver-based catalyst on model soot combustion. The results showed that the Ag/Mn-containing system provided much higher catalytic activity than Ag_2O and MnO_2 separately due to the synergistic effect associated with oxygen spillover.

Perovskites ($A_{1-x}A'_xB_{1-y}B'_yO_{3\pm\delta}$) with A, A'= La, K, Na and Rb; B, B'= Li, Mn, Cr and Fe have been studied. Of these, $La_{0.8}Cr_{0.9}Li_{0.1}O_3$ exhibited the highest catalytic activity with an optimal combustion temperature of 400°C [21]. Temperature-programmed reduction (TPR) study indicated that the high activity resulted from the high specific surface concentration of active oxygen species. Spinels (AB_2O_4) that have been examined for soot combustion included ACr_2O_4 (A = Cu, Mg, Co and Mn), AFe_2O_4 (A = Cu, Co and Ni) and $LiMn_2O_4$ [22-25]. Compared to the simple metal oxides and their physical mixtures, spinels showed a higher catalytic activity, with an optimal combustion temperature of ~ 400°C.

1.1.3 Research Motivation and Approach

The catalysts reported thus far were not active enough to eliminate soot at temperatures typical of diesel exhausts (200–400°C). The best catalysts in the literature could barely ignite soot or carbon black combustion below 400°C. Moreover, some of them were difficult to synthesize and handle.

In this thesis, a new catalytic system was developed to ignite the carbon black oxidation below 300°C, and achieve 100% conversion by 400°C. It involved a nanocomposite of supported CuO and Ag. CuO is known for its high activity for soot

combustion [2], chemical stability under moderate conditions, and availability. Ag is also an active material for soot combustion, and is much cheaper than noble metals [4]. It is applied as a promoter for CuO in our catalyst design. Alumina (Al_2O_3), zirconia (ZrO_2), yttria-stabilized zirconia (3 mol% Y_2O_3-ZrO_2) and titania (TiO_2) were examined as support materials for their high thermal resistance, and ceria (CeO_2) was tested as a support material for its excellent redox properties. The catalysts were synthesized by co-precipitation method. Their composition was optimized based on their catalytic activity in carbon black combustion. A combination of characterization techniques were employed to reveal the structure-property relationships for the catalysts. Kinetic analysis was also performed on selected catalysts.

1.2 Steam Reforming of Hydrocarbons

1.2.1 Introduction

Hydrogen is of increasing interest as a clean and efficient energy source. It may be applied towards powering vehicles, running turbines or fuel cells to produce electricity, and generating heat and electricity for buildings. Due to the relatively low volumetric energy density of hydrogen, its storage and transportation present a significant challenge. Hence, on-board hydrogen production is being examined extensively for the safe and practical application of hydrogen.

Currently, steam reforming is the most widely used process for producing H_2 from coal, natural gas, propane, methane, gasoline, light diesel, dry biomass, and biomass-derived liquid fuels (such as methanol and ethanol). In this process, H_2 is extracted not only from fuels, but also from water. Compared to partial oxidation and autothermal reforming processes, steam reforming can provide higher quality hydrogen feedstock with lower costs.

This thesis examines the production of high-quality H_2 for fuel cell application. Propane is an attractive fuel especially for portable devices because its liquid property under moderate pressure makes it easy to store and transport. The overall steam reforming of propane is represented as:

$$C_3H_8 + 3H_2O \rightarrow 3CO + 7\,H_2 \qquad (1.1)$$

with the water-gas shift reaction (WGS),

$$CO + H_2O \rightarrow CO_2 + H_2 \quad (1.2)$$

At the same time, methane can be produced via propane dehydrogenation, and CO and CO_2 methanation,

$$C_3H_8 \rightarrow CH_4 + 2C + 2H_2 \quad (1.3)$$

$$CO + 3H_2 \rightarrow CH_4 + H_2O \quad (1.4)$$

$$CO_2 + 4H_2 \rightarrow CH_4 + 2H_2O \quad (1.5)$$

Besides propane dehydrogenation, carbon can also be formed by CO disproportionation, and CH_4 and CO_2 decomposition.

$$2CO \rightarrow C + CO_2 \quad (1.6)$$

$$CH_4 \rightarrow C + 2H_2 \quad (1.7)$$

$$CO_2 \rightarrow C + O_2 \quad (1.8)$$

Controlled by reaction thermodynamics, hydrogen production is favored at high temperatures in the steam reforming process. However, coke formation would be promoted under these conditions as well. Therefore, the ideal catalysts for steam reforming should display the following characteristics:

- High catalytic activity. It is important for the catalyst to provide high fuel efficiency under the operating temperatures of the fuel cells.
- High selectivity for hydrogen production. Various by-products including hydrocarbons, CO and CO_2 may be produced in the steam reforming process. It is critical for the catalyst to possess high selectivity for hydrogen to provide high-quality feedstock to fuel cells.
- Excellent hydrothermal and mechanical stabilities. The introduction of water and the high temperatures involved in the steam reforming process would require the catalyst to be hydrothermally and mechanically stable in order to prolong catalyst lifetime.
- Superior coke resistance. Coke formation on catalysts can block the active site, and spall or pulverize catalyst particles to increase pressure drop of the catalyst bed. Therefore, excellent coke resistance is necessary for the catalyst to achieve stable catalytic activity and economical steam reforming processes.

1.2.2 Catalysts for Steam Reforming of Hydrocarbons

The first detailed study on the catalytic steam reforming of methane was published in 1924 [26]. Since then, numerous patents were issued, and a broad range of catalyst compositions have been examined. The elements that have been investigated in literature as promising catalysts or promoters for steam reforming of hydrocarbons are marked in Figure 1.2.

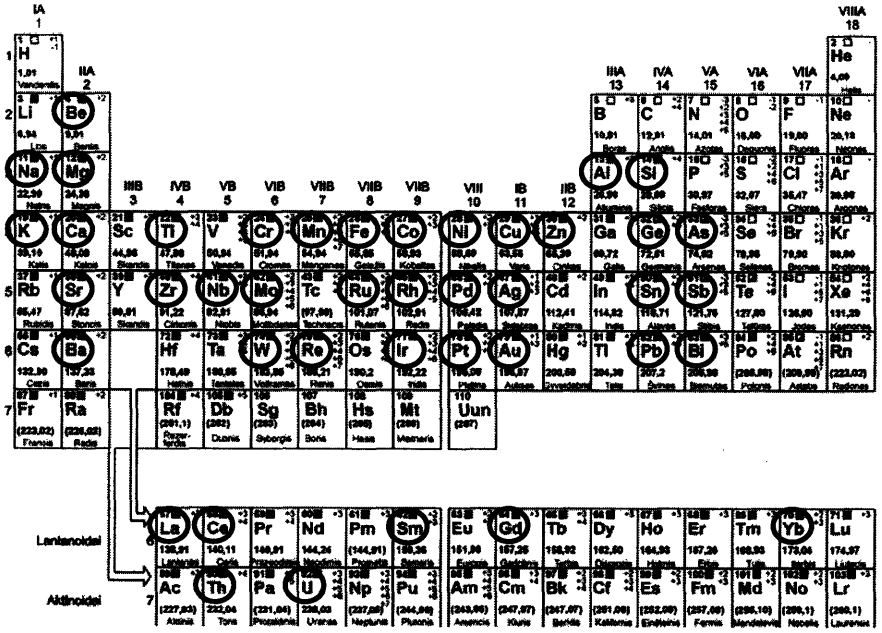

Figure 1.2 The elements that are circled have been studied in the steam reforming of hydrocarbons in the literature.

For the steam reforming reaction, the metals of group VIII in the periodic table were of special interest [26]. Most research has focused on Fe, Co, Ni, Ru, Rh, Pd, and Pt. Despite their high catalytic activity and excellent coke resistance [27-31], the noble metals are too expensive for wide industrial applications. Ni, Co and Fe are more promising for general commercial usage with their lower costs. However, Co and Fe are not stable in the metallic state at the H_2O/H_2 ratios typical of steam reforming conditions [26]. Therefore, Ni may be the most promising catalyst for industrial applications, although it presents a major coking problem.

To improve the coke resistance and catalytic activity of nickel-based catalysts, various metal promoters have been introduced. Alkali and alkaline-earth metals are known to improve coke resistance by promoting the reaction between steam and carbon [32-34]. Significant reduction in coke formation during steam reforming has been achieved by introducing group IVA and group VA elements, such as Ge, Sn, Pb, As, Sb and Bi [34, 35]. In addition, improved coke resistance has been obtained with Mo addition [36-39]. Precious metals, including Ru, Rh, Pd, Pt and Re, have been shown to increase the activity of nickel-based catalysts [32, 40]. Co-Ni/Al_2O_3 catalyst displayed excellent performance in steam reforming reaction under low H_2O/C molar ratios [40-43]. Natesakhawat *et al.* [44, 45] reported that the presence of Ce enhanced the catalytic activity and coke resistance of Ni/Al_2O_3. The improved catalytic activity was mainly due to the easier reduction of nickel species and the higher nickel surface area. The higher coke resistance was attributed to the enhanced water adsorption and effective carbon gasification.

Another way to improve catalytic activity and coke resistance of conventional Ni/Al_2O_3 is through the use of complex oxides, such as nickel aluminate and barium hexaaluminate (BHA) [46]. Compared to Ni/Al_2O_3, the reduced $NiAl_2O_4$ provided higher nickel dispersion [47]. $NiAl_2O_4$ has been demonstrated with excellent catalytic activity and coke resistance in steam reforming reactions [46-48]. Ni-substituted barium hexaaluminate ($BaNi_{1.65}Al_{10.35}O_{19}$) has also shown higher catalytic activity and coke resistance than Ni/Al_2O_3 [49].

1.2.3 Research Motivation and Approach

The objective of this research was to develop a new catalyst to generate hydrogen efficiently for fuel cell systems, especially for potable devices. High catalytic activity, high selectivity for hydrogen, and superior coke resistance are necessary for this application.

In the literature, both noble metal systems and Ni-based catalysts have been studied for the steam reforming of hydrocarbons. Various metals were introduced as modifiers to improve the catalytic activity and/or stability. However, relatively little work has been done on the catalytic activity and stability of nickel aluminates in steam reforming process.

Although this spinel has to be reduced at relatively high temperatures, the excellent nickel dispersion and catalytic activity make it a promising catalyst for steam reforming.

In this thesis, nanocrystalline nickel aluminates with various Ni/Al molar ratios were prepared by chemical co-precipitation. The composition of the catalyst was optimized based on the catalytic activity (in terms of propane conversion), and selectivity for hydrogen production. The effects of catalyst pretreatment, reaction temperature, and H_2O/C molar ratio were examined for the optimal nickel aluminate catalyst. To further improve catalyst reducibility and minimize coke formation, various metal promoters were introduced to the optimal nickel aluminate by impregnation or vapor-grafting. A combination of characterization techniques were employed to establish the structure-property relationships of the catalysts.

1.3 References

[1] Ahlström, A. F., Odenbrand, C. U. I., *Appl. Catal.* **60**, 143 (1990).
[2] Neeft, J. P. A., Makkee, M., Moulijn, J. A., *Chem. Eng. J.* **64**, 295 (1996).
[3] Neeft, J. P. A., Makkee, M., Moulijn, J. A., *Fuel Process. Technol.* **47**, 1 (1996).
[4] Neeft, J. P. A., Makkee, M., Moulijn, J. A., *Appl. Catal. B: Environ.* **8**, 57 (1996).
[5] Badini, C., Saracco, G., Serra, V., *Appl. Catal. B: Environ.* **11**, 307 (1997).
[6] Badini, C., Saracco, G., Serra, V., Specchia, V., *Appl. Catal. B: Environ.* **18**, 137 (1998).
[7] Serra, V., Saracco, G., Badini, C., Specchia, V., *Appl. Catal. B: Environ.* **11**, 329 (1997).
[8] Bellaloui, A., Varloud, J., Mériaudeau, P., Perrichon, V., Lox, E., Chevrier, M., Gauthier, C., Mathis, F., *Catal. Today* **29**, 421 (1996).
[9] Badini, C., Mazza, D., Ronchetti, S., Saracco, G., *Mater. Res. Bull.* **34**, 851 (1999).
[10] Saracco, G., Badini, C., Russo, N., Specchia, V., *Appl. Catal. B: Environ.* **21**, 233 (1999).
[11] Fino, D., Russo, N., Badini, C., Saracco, G., Specchia, V., *AIChE J.* **49**, 2173 (2003).
[12] Fino, D., Saracco, G., Specchia, V., *Chem. Eng. Sci.* **57**, 4955 (2002).
[13] Fino, D., Fino, P., Saracco, G., Specchia, V., *Chem. Eng. Sci.* **58**, 951 (2003).
[14] Querini, C. A., Ulla, M. A., Requejo, F., Soria, J., Sedrán, U. A., Miró, E. E., *Appl. Catal. B: Environ.* **15**, 5 (1998).
[15] Querini, C. A., Cornaglia, L. M., Ulla, M. A., Miró, E. E., *Appl. Catal. B: Environ.* **20**, 165 (1999).
[16] Miró, E. E., Ravelli, F., Ulla, M. A., Cornaglia, L. M., Querini, C. A., *Catal. Today* **53**, 631 (1999).
[17] Pisarello, M. L., Milt, V., Peralta, M. A., Querini, C. A., Miró, E. E., *Catal. Today* **75**, 465 (2002).
[18] Milt, V. G., Pissarello, M. L., Miró, E. E., Querini, C. A., *Appl. Catal. B: Environ.*

41, 397 (2003).
[19] Milt, V. G., Querini, C. A., Miró, E. E., *Thermochim. Acta* **404**, 177 (2003).
[20] Chien, C. C., Huang, T. J., *Ind. Eng. Chem. Res.* **34**, 1952 (1995).
[21] Russo, N., Fino, D., Saracco, G., Specchia, V., *J. Catal.* **229**, 459 (2005).
[22] Rougier, A., Soiron, S., Haihal, I., Aymard, L., Taouk, B., Tarascon, J.-M., *Powder Technol.* **128**, 139 (2002).
[23] Shangguan, W. F., Teraoka, Y., Kagawa, S., *Appl. Catal. B: Environ.* **8**, 217 (1996).
[24] Shangguan, W. F., Teraoka, Y., Kagawa, S., *Appl. Catal. B: Environ.* **12**, 237 (1997).
[25] Shangguan, W. F., Teraoka, Y., Kagawa, S., *Appl. Catal. B: Environ.* **16**, 149 (1998).
[26] Rostrup-Nielsen, J. R., "Catalytic Steam Reforming." Mercedes-Druck, Berlin, 1984.
[27] Hiromichi, A., Kitagawa, J., Nishioka, Y., US Patent 4,988,661 (1989).
[28] Murata, K., Wang, L. S., Saito, M., Inaba, M., Takahara, I., Mimura, N., *Energy Fuels* **18**, 122 (2004).
[29] Kolb, G., Zapf, R., Hessel, W., Löwe, H., *Appl. Catal. A: Gen.* **277**, 155 (2004).
[30] Wang, X., Gorte, R. J., *Appl. Catal. A: Gen.* **224**, 209 (2002).
[31] Kusakabe, K., Sotowa, K. I., Eda, T., Iwamoto, Y., *Fuel Process. Technol.* **86**, 319 (2004).
[32] Kikuchi, R., Eguchi, K., *J. Jpn. Petroleum Inst.* **47**, 225 (2004).
[33] Rostrup-Nielsen, J. R., *J. Catal.* **33**, 184 (1974).
[34] Trimm, D. L., *Catal. Today* **49**, 3 (1999).
[35] Ul-Haque, I., Trimm, D. L., US Patent 5,595,719 (1997).
[36] Borowiecki, T., Giecko, G., Panczyk, M., *Appl. Catal. A: Gen.* **230**, 85 (2002).
[37] Borowiecki, T., Gac, W., Denis, A., *Appl. Catal. A: Gen.* **270**, 27 (2004).
[38] Borowiecki, T., Denis, A., Gac, W., Dziembaj, R., Piwowarska, Z., Drozdek, M., *Appl. Catal. A: Gen.* **274**, 259 (2004).
[39] Golebiowski, A., Stolecki, K., Prokop, U., Kuśmierowska, A., Borowiecki, T., Denis, A., Sikorska, C., *React. Kinet. Catal. Lett.* **82**, 179 (2004).
[40] Wang, L. S., Murata, K., Inaba, M., *Appl. Catal. A: Gen.* **257**, 43 (2004).
[41] Hardiman, K. M., Ying, T. T., Adesina, A. A., Kennedy, E. M., Dlugogorski, B. Z., *Chem. Eng. J.* **102**, 119 (2004).
[42] Furusawa, T., Tsutsumi, A., *Appl. Catal. A: Gen.* **278**, 195 (2005).
[43] Furusawa, T., Tsutsumi, A., *Appl. Catal. A: Gen.* **278**, 207 (2005).
[44] Natesakhawat, S., Oktar, O., Ozkan, U. S., *J. Mol. Catal. A: Chem.* **241**, 133 (2005).
[45] Natesakhawat, S., Watson, R. B., Wang, X. Q., Ozkan, U. S., *J. Catal.* **234**, 496 (2005).
[46] Al-Ubaid, A., Wolf, E. E., *Appl. Catal.* **40**, 73 (1988).
[47] Murthy, I. A. P. S., Swamy, C. S., *J. Mater. Sci.* **28**, 1194 (1993).
[48] Myers, D. B., "Steam Reforming of Methane with Nickel Aluminate-based Catalysts," M.S. Thesis, Massachusetts Institute of Technology, 2000.
[49] Machida, M., Teshima, T., Eguchi, K., Arai, H., *Chem. Lett.*, 231 (1991).

Chapter 2. Copper Oxide-based Catalysts for Soot Combustion

2.1 Introduction

Compared to gasoline engine, diesel engine can operate with a higher efficiency and for a longer time. Furthermore, diesel engine produces lower emissions of CO and unburnt hydrocarbons due to its more complete fuel combustion. Therefore, it is extensively applied in heavy-duty vehicles such as trains, trucks, buses, tractors, ships and airplanes. Diesel engine has also become increasingly popular in passenger transport due to its high fuel economy. However, it generates soot particulates, which carry various mutagens and can penetrate deeply into the lungs. Thus, diesel engine emissions control is necessary to prevent damages to the human and environmental health. This may be achieved through post-combustion treatment via the use of particle traps and oxidation catalysts.

A suitable soot combustion catalyst should eliminate the soot particles at temperatures typical of diesel exhaust (200–400°C). It should also possess excellent thermal and chemical stability and high selectivity for CO_2. Various materials have been studied for the catalytic combustion of soot or other carbonaceous materials. Single metal oxides such as, Co_3O_4, V_2O_5, MnO_2, CuO, CeO_2, Nb_2O_5, SnO_2 and PbO, as well as Ag, Pt, Pd metals, were investigated for soot oxidation with limited success [1–4]. Besides metals and oxides, base and alkali salts (e.g. LiCl, LiF, KCl, KF, CsCl, CsOH, $CsCO_3$, NH_4VO_3, $Cu(NO_3)_2$, $CuCl_2$, $CrCl_3$, $(NH_4)_6Mo_7O_{24}$, $MnCl_2$ and $RuCl_3$) were also examined for soot combustion [2, 5]. Multicomponent catalysts based on platinum, silver, copper, potassium, vanadium and cobalt, as well as mixed metal oxides, have been studied extensively to achieve higher catalytic activity than single-component catalysts [2, 6–20]. In addition, catalytic activities of perovskites (ABO_3) and spinels (AB_2O_4) have been reported for soot combustion [18, 21–23]. However, none of the catalysts mentioned above can eliminate soot particles completely at temperatures below 400°C.

The main objective of this research was to develop a new catalytic system to enable effective soot removal at temperatures below 400°C. Copper oxide was selected as the active ingredient due to its high activity for soot combustion [1, 8], good chemical stability

under moderate conditions, and availability. Alumina (Al_2O_3), zirconia (ZrO_2), yttria-stabilized zirconia (3 mol% Y_2O_3-ZrO_2 or 3YSZ) and titania (TiO_2) were screened as promising support materials because of their high thermal resistance. Ceria (CeO_2) was of special interest due to its excellent oxygen storage capability. Copper oxide was coated on different supports, and the resulting catalysts were compared for soot combustion. CuO/CeO_2 was found to provide the highest activity. To further improve the catalytic activity of CuO/CeO_2, silver was introduced as a promoter. In an attempt to increase the oxygen accessibility of ceria, metal dopants including Pr, Gd and Sm were also examined. Kinetic analysis was performed for the optimized catalytic system.

2.2 Experimental

2.2.1 Selection of Carbon Source

Since the composition of soot particulates generated in diesel engines depends on many factors, such as diesel property, engine load, engine speed, operating temperatures and environmental conditions, it is difficult to collect soot particles from engines with consistent properties. Therefore, several carbonaceous materials, including carbon black, amorphous carbon and industrial-model soot, have been used in the soot combustion studies [16]. In this work, carbon black (acetylene, Alfa Aesar) was chosen as the substitute for diesel soot. The properties of carbon black and soot particulates are summarized in Table 2.1. The C/H atomic ratio of soot particulates is 3, indicating the presence of a large amount hydrocarbons and oxygenated compounds, as well as carbon particles. In contrast, carbon black, which consists of solid carbon and negligible hydrocarbons, has a much higher C/H atomic ratio of 83. Since hydrocarbons are more reactive than solid carbon, the results obtained from the combustion of carbon black would be conservative compared to those from soot combustion [4, 12].

Table 2.1 Properties of carbon black and soot particulates.

	Carbon Black (Alfa Aesar)	Soot Particulates [1]
C Content (wt%)	99.7	90.1
H Content (wt%)	0.1	2.4
Surface Area (m^2/g)	75	60–85
Particle Size (nm)	41	20 ± 3 (at 75% load)

2.2.2 *Catalyst Synthesis*

Nanocrystalline CuO-based catalysts were prepared by co-precipitation. $Al(NO_3)_3 \cdot 9H_2O$, $Ce(NO_3)_4 \cdot 6H_2O$, $Ti[OCH(CH_3)_2]_4$, $ZrOCl_2 \cdot 8H_2O$, $Y(NO_3)_3 \cdot 6H_2O$ (Alfa Aesar) were used as precursors for the synthesis of supports. Metal dopants were introduced to the supports using precursors such as $Pr(NO_3)_3 \cdot 6H_2O$, $Gd(NO_3)_3 \cdot 6H_2O$, $Y(NO_3)_3 \cdot 6H_2O$, $Sm(NO_3)_3 \cdot 6H_2O$ and $Sr(NO_3)_2$ (Alfa Aesar). $Cu(NO_3)_2 \cdot 3H_2O$ and $AgNO_3$ (Alfa Aesar) were used as the precursors for CuO and Ag.

In the synthesis of CuO-based catalysts, the precursors of the support material and its dopant were first dissolved at the desired molar ratio in deionized water at a total cation concentration of 0.2 M. The exception was titanium isopropoxide, which was dissolved in ethanol. The precursor solution was added dropwise to an organic base, tetraethylammonium hydroxide (TEAH, 40 wt% in water, Alfa Aesar), ethanol and deionized water. In the synthesis of supports with metal dopants, ammonium hydroxide (NH_4OH, 28.0–30.0% NH_3, Alfa Aesar) was used instead of TEAH. The amount of base used in the precipitation process was determined by multiplying an excess factor (1–15) with the theoretical value, which was the number of moles for hydroxide ions required to hydrolyze the metal cations to metal hydroxides. The final concentration of the base solution was 0.4 M, which was calculated by dividing the moles of the base by the total volume, including added solvent volume and base volume.

The precipitate of the support material was aged for 2 h at room temperature. Then the deionized water solution of copper nitrate and silver nitrate was introduced with a specific Cu/Ag molar ratio, while keeping the total concentration of cations constant. The resulting precipitate was aged for 18 h, recovered by centrifuge, washed by water to remove excess base and residual metal salts, and dried overnight in air at room temperature. Fine powders were then obtained by grounding the dried materials in a mortar-and-pestle. Catalysts were prepared by calcination at 400°C in air for 3 h.

2.2.3 *Catalyst Characterization*

Surface area of the catalysts was determined by nitrogen adsorption analysis (Micromeritics ASAP 2000) using the 5-point BET (Brunauer-Emmett-Teller) method. Powder X-ray diffraction (XRD) (Siemens D5000 θ-θ Diffractometer, 45 kV, 40 mA, Cu-

Kα) was used for phase identification and grain size analysis. Scherrer's analysis of <110> diffraction peak broadening was employed to obtain the volume-averaged crystallite size. X-ray photoelectron spectroscopy (XPS) (Kratos AXIS Ultra Imaging X-ray Photoelectron Spectrometer) was used to characterize the surface copper and silver species. The catalyst microstructure and composition were examined by scanning transmission electron microscopy (STEM) (Vacuum Generators HB603) and energy-dispersive X-ray (EDX) spectroscopy.

Catalyst reducibility was studied by temperature-programmed reduction (TPR) under a reducing atmosphere using a Perkin Elmer System 7HT Thermal Gravimetric Analyzer (TGA). Typically, 20 mg of calcined catalysts were first pretreated at 400°C for 60 min with a stream of air to ensure complete oxidation and to eliminate surface contaminants. The sample was then cooled to 50°C, and purged with helium for 10 min to remove weakly absorbed oxygen. Next, a stream of 5% H_2 in He was introduced, and the temperature was ramped to 400°C or 800°C at 5°C/min to record the weight loss.

2.2.4 Catalyst Activity

Catalytic soot combustion is a solid-solid-gas reaction between soot, catalyst and oxygen. Unlike a gas-solid reaction, the rate of solid-solid reaction depends on the intimate contact between two solid phases. Generally, a reaction carried out under loose contact, which is similar to the actual operating conditions of diesel engines, provides information on the apparent catalytic activity. A tight-contact reaction provides information on the intrinsic catalytic activity. Both types of contact conditions have been studied in literature [1, 2]. This study examined tight-contact samples achieved by grinding the catalyst and carbon black particles in a mortar-and-pestle.

Catalytic activity was studied with temperature-programmed oxidation (TPO) on a Perkin Elmer System 7HT TGA. A catalyst/carbon black weight ratio of 20 was used in all cases, unless otherwise specified. Typically, 20 mg of catalyst-carbon black mixture were loaded, and TPO was performed at 30–800°C at a ramp of 5°C/min in a stream of air (flow rate = 100 ml/min). Conversion of carbon black at a specific temperature could be determined by dividing the weight loss corresponding to that temperature by the total weight of carbon black in the sample.

2.2.5 Catalyst Selectivity

The selectivity of the catalysts was determined under steady-state conditions in a 1/4"-O.D. quartz tube reactor. 50 mg of catalyst-carbon black mixture were loaded in the reactor tube and placed between two quartz wool plugs. A type-K thermocouple located right below the catalyst bed was used in conjunction with an Omega temperature controller and a Lindberg tube furnace to maintain the catalyst bed at the desired temperature. A stream of air with a flow rate of 100 ml/min was introduced to oxidize carbon black. The temperature was increased from 30°C to 800°C at a ramp of 5°C/min. The product stream was analyzed by a Hewlett-Packard 6890 Gas Chromatograph (GC) equipped with molecular sieve 5A and Porapak Q columns, which allowed O_2, N_2, CO and CO_2 to be separated and quantified.

2.2.6 Kinetic Analysis

Kinetic parameters of solid-state reactions involving studies of TGA weight changes have been reported previously [24]. Compared to the conventional isothermal study, non-isothermal method makes it possible to obtain kinetic parameters such as reaction order and activation energy in one single experiment. However, the sample pan geometry, heating rate, temperature measurement and other factors could influence the final results. Fortunately, these effects could be mostly eliminated by the use of small samples.

The conversions of carbon black as a function of temperature in TPO study are the only data required to estimate the activation energy. Typically, 20 mg of catalyst-carbon black mixture were loaded in a custom-built quartz pan with a diameter of 7.7 mm. The temperature was measured precisely by a thermocouple positioned just beside the sample pan. The sample weight was determined by the balance, which was connected to the sample pan by a platinum wire. The activation energy of catalytic soot combustion was obtained by using the non-isothermal method, and the detailed calculation is presented later.

2.3 Results and Discussion

2.3.1 Screening of CuO-Coated Catalysts

2.3.1.1 Characterization

40 wt% of copper oxide was coated on Al_2O_3, ZrO_2, 3YSZ, TiO_2 and CeO_2, and calcined at 400°C. Figure 2.1 shows Cu $2p_{3/2}$ peaks corresponding to CuO/CeO_2, CuO/Al_2O_3, CuO/ZrO_2, CuO/3YSZ and CuO/TiO_2. The binding energies of 933.1–934.2 eV for Cu $2p_{3/2}$ and shake-up peaks (Table 2.2) were characteristic of CuO, confirming that copper oxide with a valence of +2 was present. Interestingly, while 40 wt% of CuO coated on CeO_2, Al_2O_3, ZrO_2 and 3YSZ exhibited similar XPS results, 40 wt% CuO/TiO_2 demonstrated two overlapped peaks at 933.1 and 934.2 eV. The latter indicated the lack of crystallinity of the copper oxide in CuO/TiO_2, which was confirmed by XRD results (Figure 2.2). Crystalline CuO peaks were found in CuO/CeO_2, CuO/Al_2O_3, CuO/ZrO_2 and CuO/3YSZ. However, only the ceria support has crystallized after calcination at 400°C. Table 2.2 shows that 40 wt% CuO/Al_2O_3 has the highest BET surface area and the largest CuO grain size. CuO/ZrO_2 and CuO/3YSZ showed relatively low surface areas and smaller CuO grain sizes. STEM/EDX showed that CuO was more uniformly dispersed on Al_2O_3 and TiO_2 (Figure 2.3).

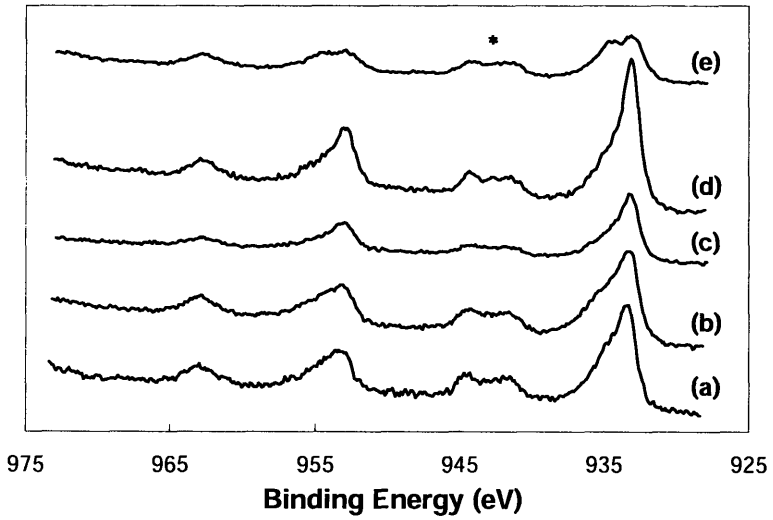

Figure 2.1 XPS spectra of Cu $2p_{3/2}$ in (a) 40 wt% CuO/CeO_2, (b) 40 wt% CuO/Al_2O_3, (c) 40 wt% CuO/ZrO_2, (d) 40 wt% CuO/3YSZ and (e) 40 wt% CuO/TiO_2, after calcination at 400°C in air. Shake-up peaks are denoted by *.

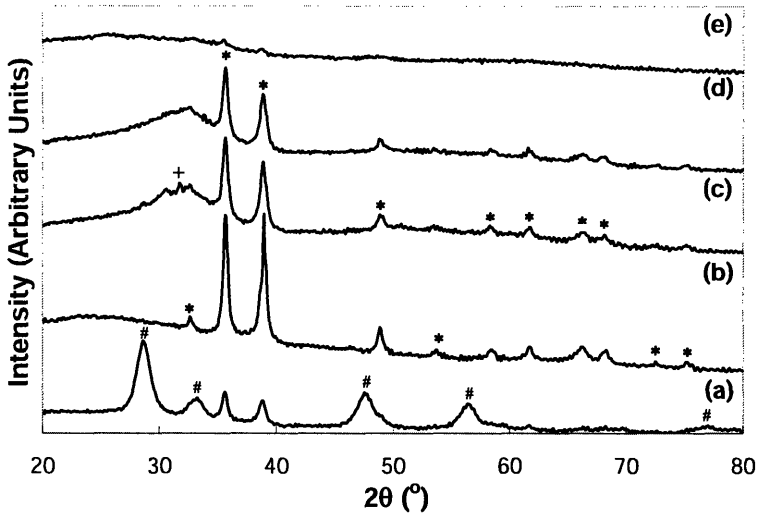

Figure 2.2 XRD patterns of (a) 40 wt% CuO/CeO_2, (b) 40 wt% CuO/Al_2O_3, (c) 40 wt% CuO/ZrO_2, (d) 40 wt% CuO/3YSZ and (e) 40 wt% CuO/TiO_2, after calcination at 400°C in air. XRD peaks of CuO, CeO_2 and ZrO_2 are denoted by *, # and +, respectively.

Table 2.2 Cu $2p_{3/2}$ binding energy, BET surface area and CuO grain size of 40 wt% CuO coated on different support materials, after calcination at 400°C in air.

Catalyst	Cu $2p_{3/2}$ Binding Energy (eV)	BET Surface Area (m^2/g)	CuO Grain Size (nm)
40 wt% CuO/CeO_2	933.3	116	18.5
40 wt% CuO/Al_2O_3	933.4	195	20.2
40 wt% CuO/ZrO_2	933.3	93	15.3
40 wt% CuO/3YSZ	933.1	104	15.4
40 wt% CuO/TiO_2	933.1, 934.2	139	—

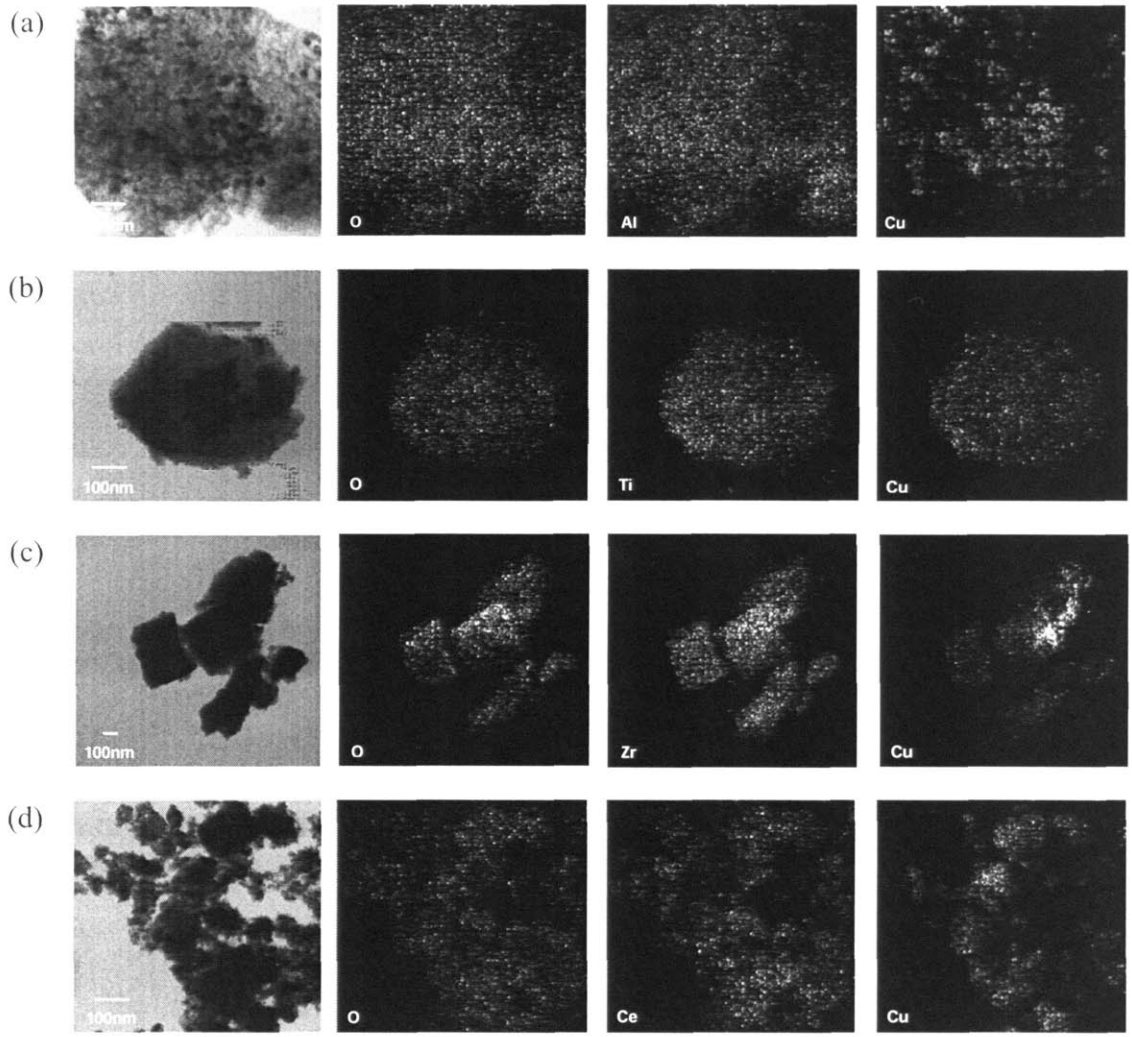

Figure 2.3 STEM/EDX image and elemental maps of (a) 40 wt% CuO/Al_2O_3, (b) 40 wt% CuO/TiO_2, (c) 40 wt% CuO/ZrO_2 and (d) 40 wt% CuO/CeO_2, after calcination at 400°C in air.

2.3.1.2 Catalyst Reducibility

Redox mechanism has been proposed to explain the catalytic oxidation over CuO-based catalysts [4, 25]. Hence, the reducibility and re-oxidizability of CuO would be critical for its catalytic activity. In the catalytic oxidation of carbon black, CuO transfers its oxygen to carbon black, and subsequently becomes reoxidized by air. The support may promote or inhibit this cycle.

TPR indicated that the reduction of CuO supported on various materials took place between 200°C and 400°C (Figure 2.4). The reduction of CuO accounted for the weight

loss observed. Although CeO_2 itself could only initiate reduction above 600°C, it promoted CuO's reducibility as a support material. In contrast, Al_2O_3 negatively impacted the reducibility of CuO. CuO supported on ZrO_2, 3YSZ and TiO_2 needed to be reduced at higher temperatures than unsupported CuO.

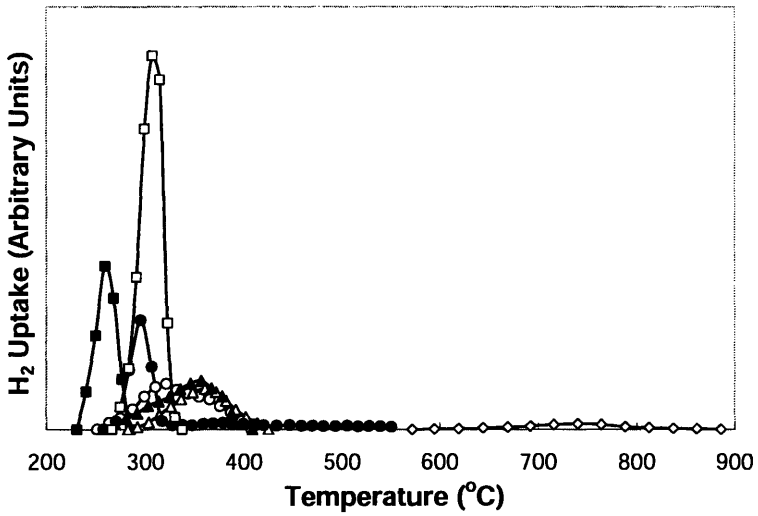

Figure 2.4 TPR profiles of (■) 40 wt% CuO/CeO_2, (●) 40 wt% CuO/Al_2O_3, (○) 40 wt% CuO/ZrO_2, (▲) 40 wt% CuO/3YSZ, (Δ) 40 wt% CuO/TiO_2, (□) CuO and (◊) CeO_2, after calcination at 400°C in air.

2.3.1.3 Catalytic Activity

The combustion of carbon black as a function of temperature over different catalysts is shown in Figure 2.5, and the temperatures corresponding to 10%, 50% and 90% conversion are reported in Table 2.3. Compared with non-catalytic combustion (initiated at 525°C and completed at 765°C), all catalysts studied promoted the oxidation of carbon black. CuO/CeO_2 showed the highest activity, and was superior to both CuO and CeO_2 catalysts. CuO/ZrO_2 and CuO/3YSZ achieved similar catalytic activities. CuO/Al_2O_3 and CuO/TiO_2 provided the lowest activity, although they possessed the highest BET surface areas. This study showed that the support's surface area was not critical. Rather, the promotional or inhibitive effect of the support material on CuO's reducibility were important. CeO_2, which was the only support that enabled CuO reducibility at a lower temperature, was the only support that led to better catalytic performance than pure CuO. Synergism between ceria and copper has been reported to improve the catalytic activity in

other oxidation reactions [26–28]. Similar effects between the oxygen ion conducting support and the base metal oxide could be responsible for the excellent performance of CuO/CeO_2 in the catalytic combustion of carbon black.

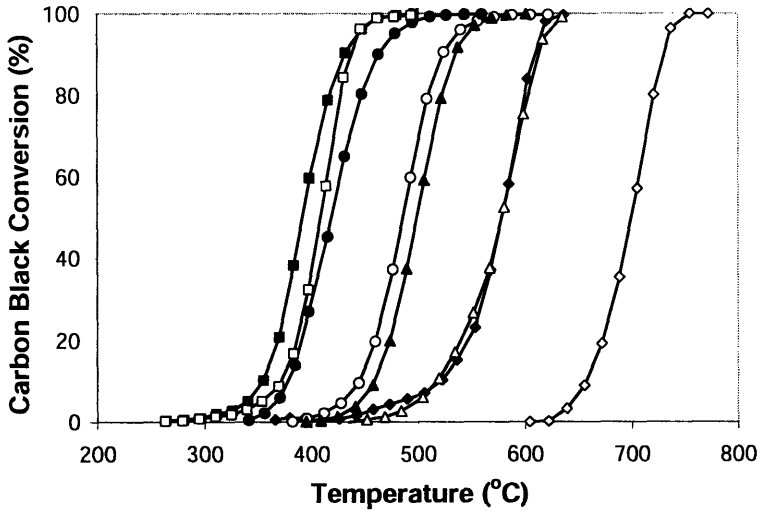

Figure 2.5 Carbon black conversion as a function of temperature over (■) 40 wt% CuO/CeO_2, (○) 40 wt% CuO/ZrO_2, (▲) 40 wt% CuO/3YSZ, (Δ) 40 wt% CuO/TiO_2, (♦) 40 wt% CuO/Al_2O_3, (□) CuO and (●) CeO_2, after calcination at 400°C in air. No catalyst is employed in ◊.

Table 2.3 Temperatures corresponding to 10%, 50% and 90% carbon black conversions over various catalysts, after calcination at 400°C in air.

Catalyst	Temperature (°C)		
	10% Conversion	50% Conversion	90% Conversion
40 wt% CuO/CeO_2	355	391	428
40 wt% CuO/ZrO_2	445	486	523
40 wt% CuO/3YSZ	459	498	534
40 wt% CuO/TiO_2	517	580	613
40 wt% CuO/Al_2O_3	524	581	609
CuO	371	411	438
CeO_2	381	422	467
—	657	700	728

2.3.2 Optimization of CuO/CeO_2 System

Different loading of copper oxide was coated onto ceria, and calcined at 400°C. XPS spectra of Cu $2p_{3/2}$ revealed that copper was present in a valence of +2 (i.e. CuO with

a binding energy of 933.3–933.9 eV), and illustrated the characteristic shake-up peaks (Figure 2.6). The peak intensities increased with increasing CuO loading.

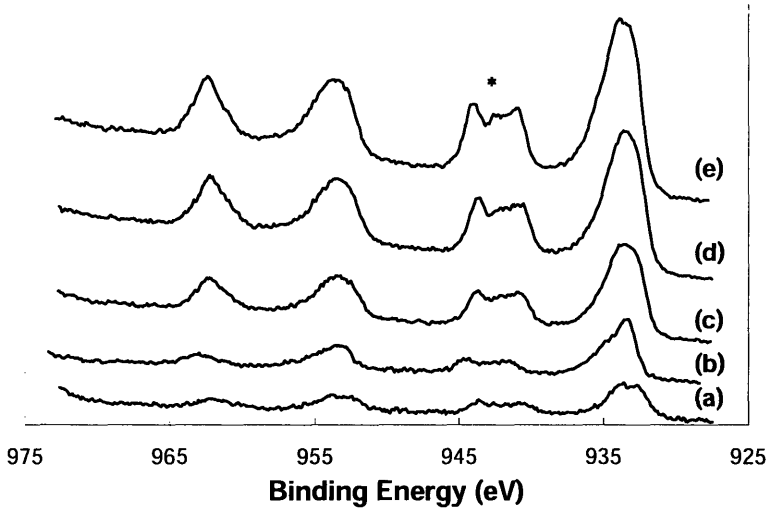

Figure 2.6 XPS spectra of Cu $2p_{3/2}$ for (a) 20 wt% CuO/CeO_2, (b) 40 wt% CuO/CeO_2, (c) 60 wt% CuO/CeO_2, (d) 80 wt% CuO/CeO_2 and (e) CuO, after calcination at 400°C in air. Shake-up peaks are denoted by *.

XRD patterns indicated the presence of crystalline CuO and CeO_2 phases in CuO/CeO_2 systems with 20–80 wt% CuO (Figure 2.7). Increasing CuO loading led to more intense and sharper CuO peaks, corresponding to an increased grain size from 18 nm to 23 nm (Figure 2.8). With increased CuO loading, the CeO_2 peaks diminished in intensity and became broader, corresponding to a reduced grain size from 7 nm to 5 nm. This study illustrated that CeO_2 helped increased the dispersion of CuO and the BET surface area of the system. The increased CuO reducibility (Figure 2.9) could be partially attributed to these physical effects.

Figure 2.10 showed that crystalline CuO peaks were no longer detected after CuO/CeO_2 catalysts and CuO were subjected to TPR study between 30°C and 400°C in 5% H_2 in He. For CeO_2 coated with 40–80 wt% CuO, crystalline Cu peaks were detected after the TPR study, as in the case of pure CuO.

CuO/CeO_2 catalysts with various CuO loadings were tested in the combustion of carbon black. The temperatures corresponding to 50% carbon black conversion and maximum CuO reduction rate are presented in Figure 2.11. All CuO/CeO_2 catalysts demonstrated higher catalytic activity than pure CuO and CeO_2. The optimal CuO loading

was 20–40 wt%, which provided for 50% carbon black conversion at 391°C (Table 2.4). 20 wt% CuO gave rise to a higher dispersion and a lower temperature for maximum CuO reduction rate, whereas a higher CuO loading provided for a greater concentration of active sites.

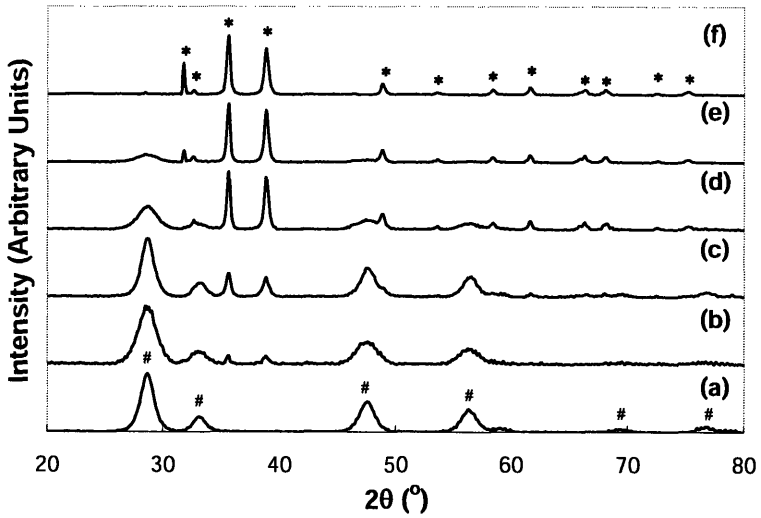

Figure 2.7 XRD patterns of 400°C-calcined (a) CeO_2, (b) 20 wt% CuO/CeO_2, (c) 40 wt% CuO/CeO_2, (d) 60 wt% CuO/CeO_2, (e) 80 wt% CuO/CeO_2 and (f) CuO. XRD peaks of CuO and CeO_2 are denoted by * and #, respectively.

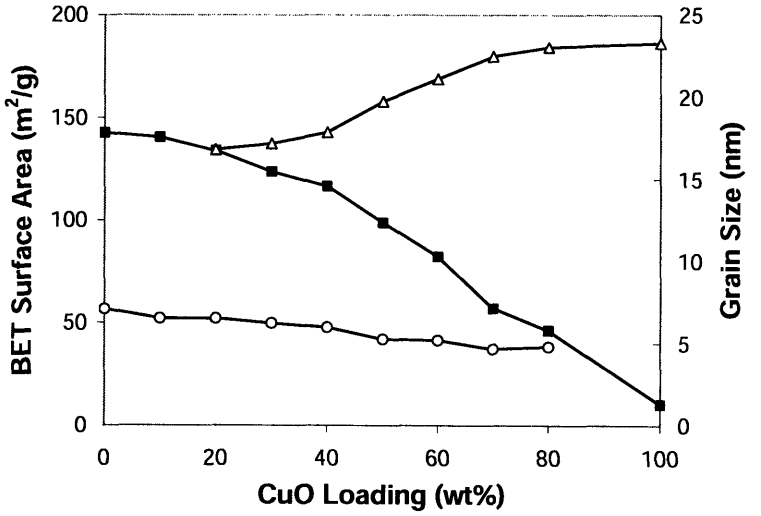

Figure 2.8 (■) BET surface area, and (Δ) CuO and (○) CeO_2 grain sizes of 400°C-calcined CuO/CeO_2 with the CuO loading specified.

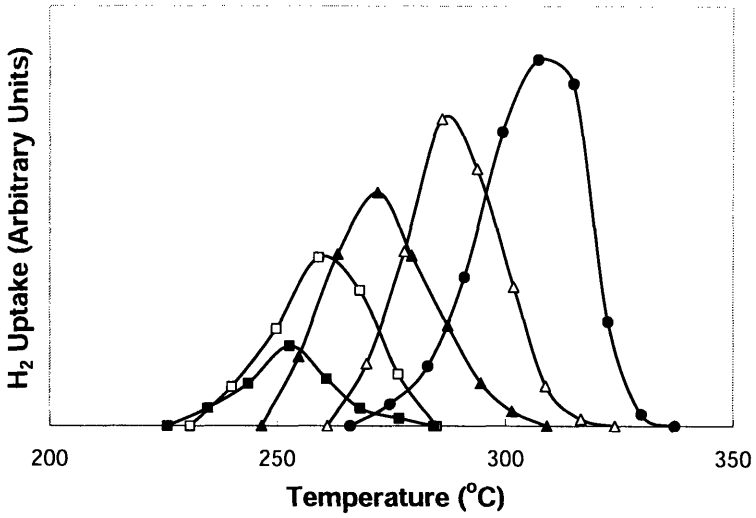

Figure 2.9 TPR profiles of (■) 20 wt% CuO/CeO_2, (□) 40 wt% CuO/CeO_2, (▲) 60 wt% CuO/CeO_2, (Δ) 80 wt% CuO/CeO_2 and (●) CuO, after calcination at 400°C in air.

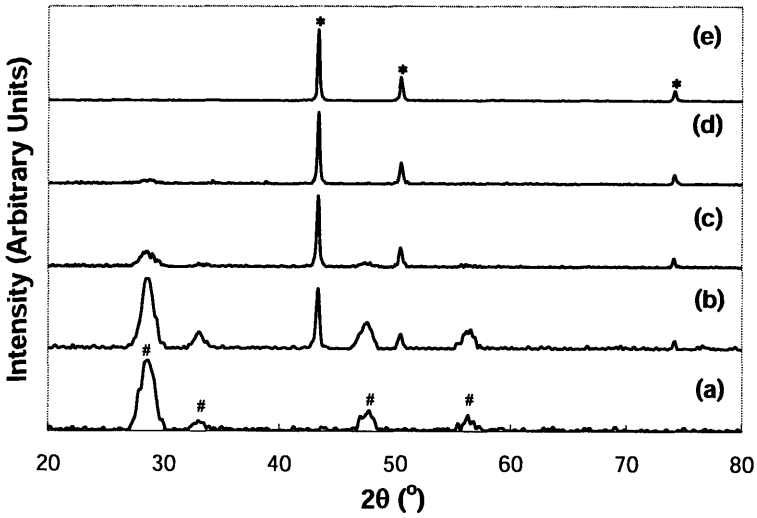

Figure 2.10 XRD patterns of 400°C-calcined (a) 20 wt% CuO/CeO_2, (b) 40 wt% CuO/CeO_2, (c) 60 wt% CuO/CeO_2, (d) 80 wt% CuO/CeO_2 and (e) CuO, after reduction at 400°C in 5% H_2 in He. XRD peaks of Cu and CeO_2 are denoted by * and #, respectively.

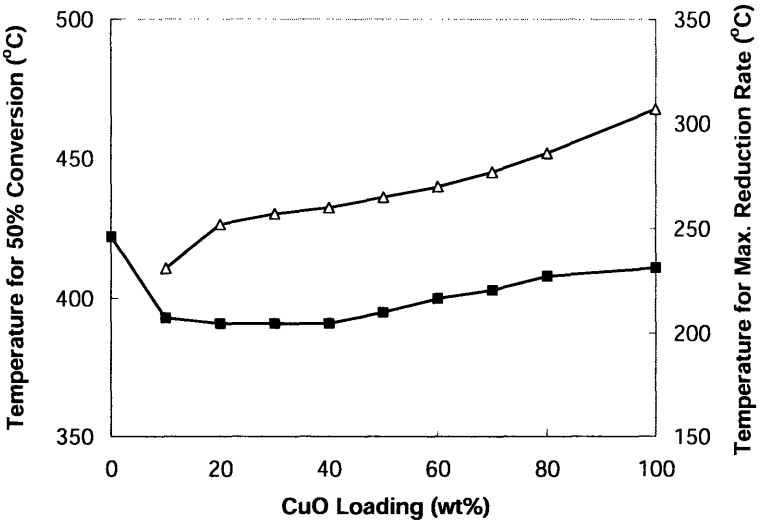

Figure 2.11 Temperatures corresponding to (■) 50% carbon black conversion and (Δ) maximum CuO reduction rate for 400°C-calcined CuO/CeO_2 with the CuO loading specified.

Table 2.4 Catalytic activity of CuO/CeO_2 and CuO, after calcination at 400°C in air.

Catalyst	Temperature (°C)		
	10% Conversion	50% Conversion	90% Conversion
20 wt% CuO/CeO_2	359	391	428
40 wt% CuO/CeO_2	355	391	428
60 wt% CuO/CeO_2	364	400	430
80 wt% CuO/CeO_2	375	408	435
CuO	371	411	438

2.3.3 Optimization of Modified CuO/CeO_2 Catalysts

2.3.3.1 Ag Promoter

Although CuO/CeO_2 provided excellent activity for the combustion of carbon black, it still did not meet all the necessary requirements for the application in diesel engines. To further improve the catalytic activity of CuO/CeO_2, silver was introduced as a promoter as it has been demonstrated to be active in carbon combustion [13]. CuO-Ag (molar ratio = 1:1) was coated onto ceria at a loading of 0–100 wt%, and calcined at 400°C. The normalized XPS spectra of Cu 2p and Ag 3d are shown in Figure 2.12. The characteristic binding energy of 933.2–933.9 eV and shake-up peaks indicated the presence of CuO (Figure 2.12(i)). The binding energy of 368.2–368.4 eV corresponded to metallic Ag

(Figure 2.12(ii)). The intensity of CuO and Ag peaks increased with increasing CuO-Ag loading.

The XRD patterns of CuO-Ag/CeO_2 are shown in Figure 2.13. Separate CuO and Ag phases were detected only when the CuO-Ag loading was above 20 wt%. Figure 2.14 shows that the XRD grain size of Ag increased from 28 nm to 40 nm as the CuO-Ag loading increased from 30 wt% to 100 wt%. The XRD grain sizes of CuO and CeO_2 did not change significantly with increasing CuO-Ag loading; they remained at ~ 33 and 7 nm, respectively. As the CeO_2 content was lowered, the BET surface area of CuO-Ag/CeO_2 decreased rapidly. The 20 wt% CuO-Ag/CeO_2 catalysts showed a lower surface area than the 20 wt% and 40 wt% CuO/CeO_2 catalysts. Figure 2.15 illustrates the reduced dispersion of CuO and Ag in CuO-Ag/CeO_2 as the CuO-Ag loading was increased from 40 wt% to 60 wt%.

Figure 2.16 shows the excellent reducibility of CuO-Ag/CeO_2, especially at low CuO-Ag loadings. Compared to the results shown in Figure 2.9, it was obvious that the CuO reducibility was enhanced by the Ag addition. Figure 2.17 showed that crystalline CuO peaks were no longer detected after CuO-Ag/CeO_2 catalysts and CuO-Ag were subjected to TPR study between 30°C and 400°C in 5% H_2 in He. For CeO_2 coated with 40–80 wt% CuO-Ag, crystalline Cu peaks were detected after the TPR study, as in the case of CuO-Ag.

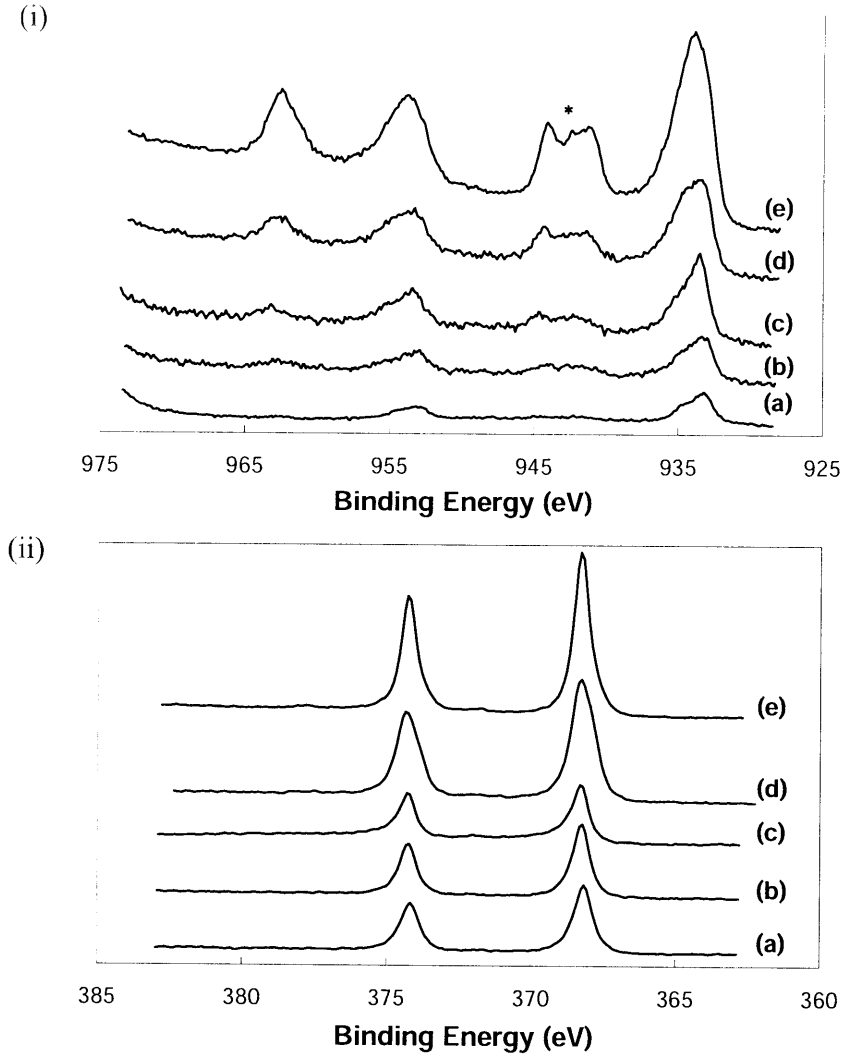

Figure 2.12 XPS spectra of (i) Cu 2p and (ii) Ag 3d for (a) 20 wt% CuO-Ag/CeO_2, (b) 40 wt% CuO-Ag/CeO_2, (c) 60 wt% CuO-Ag/CeO_2, (d) 80 wt% CuO-Ag/CeO_2 and (e) CuO-Ag, after calcination at 400°C in air. Shake-up peaks are denoted by *.

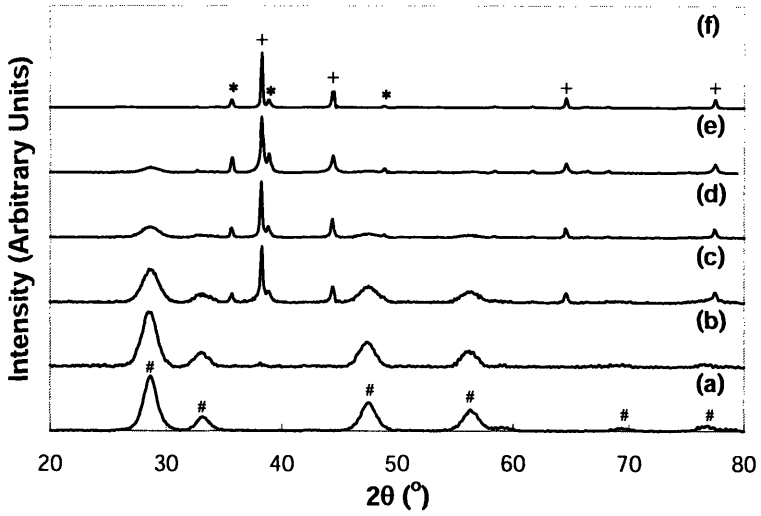

Figure 2.13 XRD patterns of 400°C-clacined (a) CeO_2, (b) 20 wt% CuO-Ag/CeO_2, (c) 40 wt% CuO-Ag/CeO_2, (d) 60 wt% CuO-Ag/CeO_2, (e) 80 wt% CuO-Ag/CeO_2 and (f) CuO-Ag. XRD peaks of CuO, Ag and CeO_2 are denoted by *, + and #, respectively.

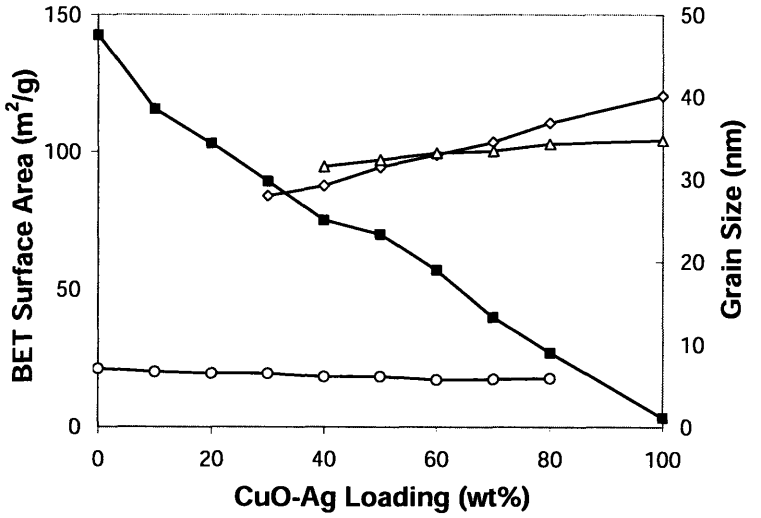

Figure 2.14 (■) BET surface area, and (Δ) CuO, (◊) Ag and (○) CeO_2 grain sizes of 400°C-calcined CuO-Ag/CeO_2 with the CuO-Ag loading specified.

(a)

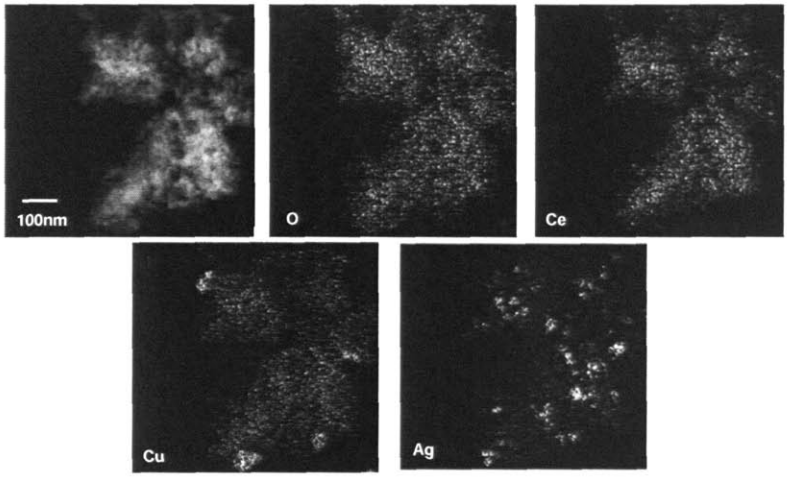

(b)

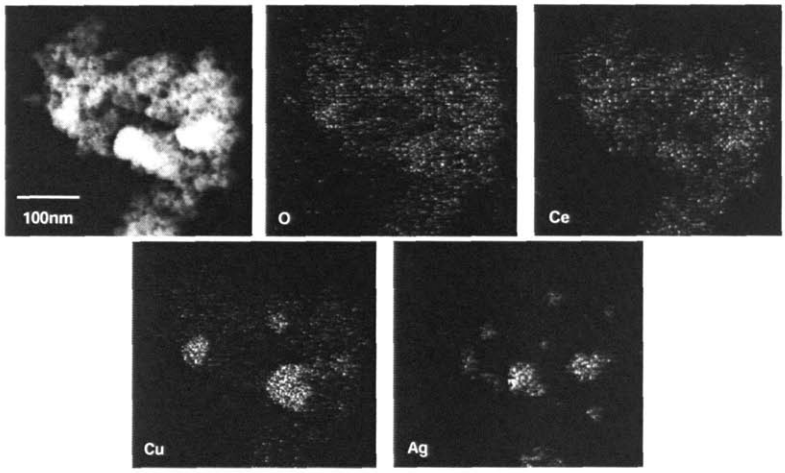

Figure 2.15 STEM/EDX image and elemental maps of (a) 40 wt% CuO-Ag/CeO_2 and (b) 60 wt% CuO-Ag/CeO_2, after calcination at 400°C in air.

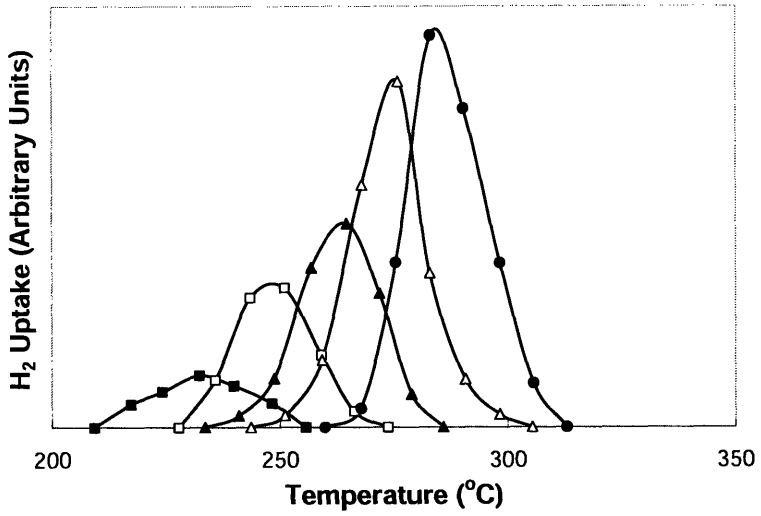

Figure 2.16 TPR profiles of (■) 20 wt% CuO-Ag/CeO_2, (□) 40 wt% CuO-Ag/CeO_2, (▲) 60 wt% CuO-Ag/CeO_2, (Δ) 80 wt% CuO-Ag/CeO_2 and (●) CuO-Ag, after calcination at 400°C in air.

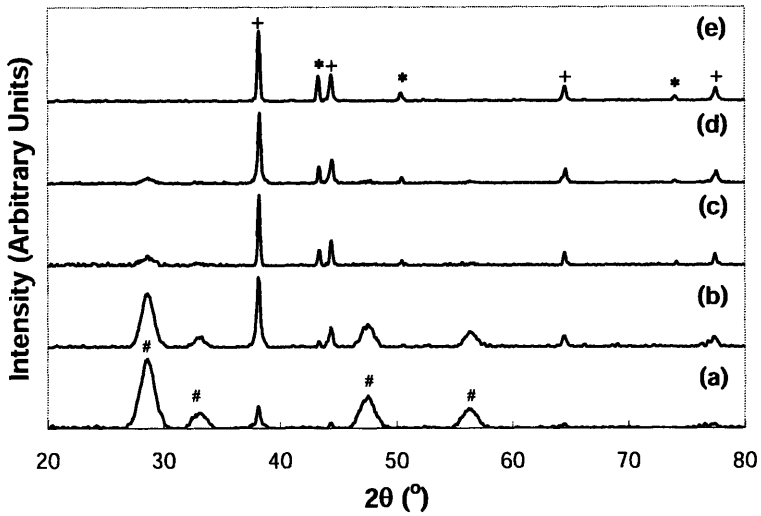

Figure 2.17 XRD patterns of 400°C-calcined (a) 20 wt% CuO-Ag/CeO_2, (b) 40 wt% CuO-Ag/CeO_2, (c) 60 wt% CuO-Ag/CeO_2, (d) 80 wt% CuO-Ag/CeO_2 and (e) CuO-Ag, after reduction at 400°C in 5% H_2 in He. XRD peaks of Cu, Ag and CeO_2 are denoted by *, + and #, respectively.

CuO-Ag/CeO_2 catalysts with various CuO-Ag loadings were tested in the combustion of carbon black. The temperatures corresponding to 50% carbon black conversion and maximum CuO reduction rate are presented in Figure 2.18. Compared to the results in Figure 2.11, it was obvious that the catalytic activity for carbon black

combustion was increased significantly with the introduction of Ag. The optimal CuO/CeO_2 catalysts (20–40 wt% CuO) provided for 50% carbon black conversion at 391°C (Table 2.4). In contrast, the optimal $CuO\text{-}Ag/CeO_2$ catalyst (40 wt% CuO-Ag) achieved 50% conversion at a remarkably low temperature of 304°C.

As proposed earlier, the CuO reducibility was critical to the catalytic combustion activity. Figure 2.18 shows that the temperature for maximum reduction rate of $CuO\text{-}Ag/CeO_2$ was as low as 226°C, which was less than that achieved by CuO/CeO_2 (Figure 2.11). The synergism between CuO and Ag increased the CuO reducibility, possibly through more effective oxygen transfer. The enhanced combustion over $CuO\text{-}Ag/CeO_2$ could be explained by spill-over effects [25], whereby oxygen was adsorbed and activated on the donor (Ag) and transferred to the acceptor (CuO) for reaction.

Compared to 20 wt% $CuO\text{-}Ag/CeO_2$, 40 wt% $CuO\text{-}Ag/CeO_2$ has a higher concentration of active sites, and contained nanocrystalline instead of amorphous CuO and Ag. Compared to 60 wt% $CuO\text{-}Ag/CeO_2$, 40 wt% $CuO\text{-}Ag/CeO_2$ showed better CuO and Ag dispersions, and greater reducibility (Figures 2.14–2.16). This combination of characteristics might have led to the superior performance of 40 wt% $CuO\text{-}Ag/CeO_2$ in carbon black combustion (Table 2.5).

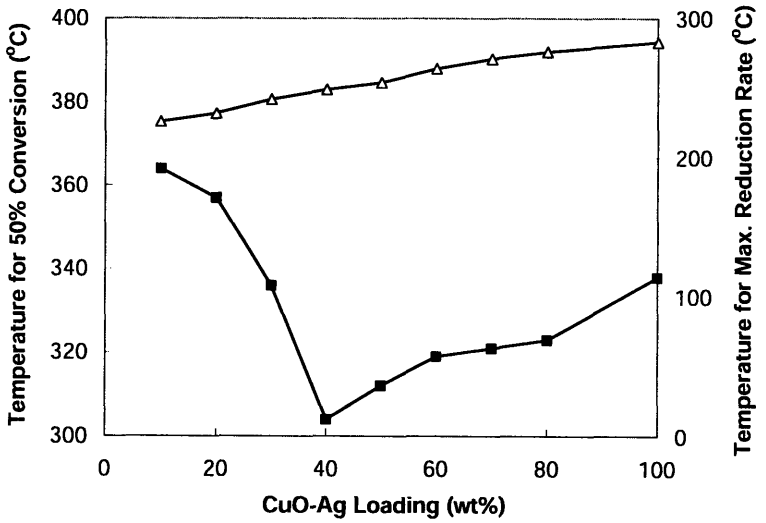

Figure 2.18 Temperatures corresponding to (■) 50% carbon black conversion and (Δ) maximum CuO reduction rate for 400°C-calcined $CuO\text{-}Ag/CeO_2$ with the CuO-Ag loading specified.

Table 2.5 Catalytic activity of CuO-Ag/CeO_2 and CuO-Ag, after calcination at 400°C.

Catalyst	Temperature (°C)		
	10% Conversion	50% Conversion	90% Conversion
20 wt% CuO-Ag/CeO_2	327	357	388
40 wt% CuO-Ag/CeO_2	264	304	340
60 wt% CuO-Ag/CeO_2	279	319	360
80 wt% CuO-Ag/CeO_2	284	323	360
CuO-Ag	286	338	376

2.3.3.2 Ceria Dopants

Recent studies have demonstrated that the addition of some transition metals such as Pr, Gd and Sm could improve the reducibility of ceria significantly [29]. To investigate the effect of metal dopants, Pr, Gd, Sm, Y and Sr were introduced into ceria to prepare 40 wt% CuO-Ag/$Ce_{1-y}M_yO_x$ where M = metal dopant. Table 2.6 indicates that no significant improvement on the catalytic activity was achieved by doping ceria. This could be due to the negligible or negative effect that the doped ceria have on the CuO reducibility in the TRP studies (not shown). This work suggested that CeO_2 support already provided effective synergism in CuO reduction, especially in the presence of Ag. Thus, doping of ceria did not further promote the CuO reduction or carbon black combustion.

Table 2.6 Catalytic activity of 40 wt% CuO-Ag/$Ce_{1-y}M_yO_x$, after calcination at 400°C in air.

Catalyst	Temperature for 50% Conversion (°C)
40 wt% CuO-Ag/CeO_2	304
40 wt% CuO-Ag/$Ce_{0.6}Pr_{0.4}O_x$	312
40 wt% CuO-Ag/$Ce_{0.8}Pr_{0.2}O_x$	316
40 wt% CuO-Ag/$Ce_{0.85}Sm_{0.15}O_x$	328
40 wt% CuO-Ag/$Ce_{0.8}Y_{0.2}O_x$	337
40 wt% CuO-Ag/$Ce_{0.8}Gd_{0.2}O_x$	340
40 wt% CuO-Ag/$Ce_{0.8}Sr_{0.2}O_x$	377

2.3.4 Optimization of $(CuO)_x$-Ag_y/CeO_2 System

To study the effect of CuO and Ag molar ratio on catalytic activity, 40 wt% $(CuO)_x$-Ag_y/CeO_2 catalysts were synthesized and calcined at 400°C. Figure 2.19 shows that increasing CuO/Ag molar ratio led to the emergence of crystalline CuO phase at x/y = 1:1.5, and the disappearance of crystalline Ag phase at x/y above 10:1. The XRD grain

size of Ag increased from 14 nm to 30 nm with increasing CuO/Ag molar ratio, while the grain size of CuO decreased from 46 nm to 18 nm (Figure 2.20). The grain size of CeO_2 remained at ~ 6.1–7.5 nm for the range of CuO/Ag molar ratios examined. The BET surface area of the catalyst decreased with decreasing CuO/Ag molar ratio, which could be attributed to the greater tendency of Ag to agglomerate (Figure 2.21). The increased reducibility with decreasing CuO/Ag molar ratio is demonstrated in Figure 2.22, confirming the benefit of Ag addition in CuO reducibility.

The temperatures corresponding to 50% carbon black conversion for various 40 wt% $(CuO)_x$-Ag_y/CeO_2 catalysts are shown in Figure 2.23. The best catalytic performance was achieved by the catalyst with a CuO/Ag molar ratio of 1:1. Lower CuO/Ag molar ratio would result in lower CuO dispersion, while presenting less CuO active sites. Higher CuO/Ag molar ratio would not have the full benefit of Ag promotion in CuO reducibility (Figure 2.22).

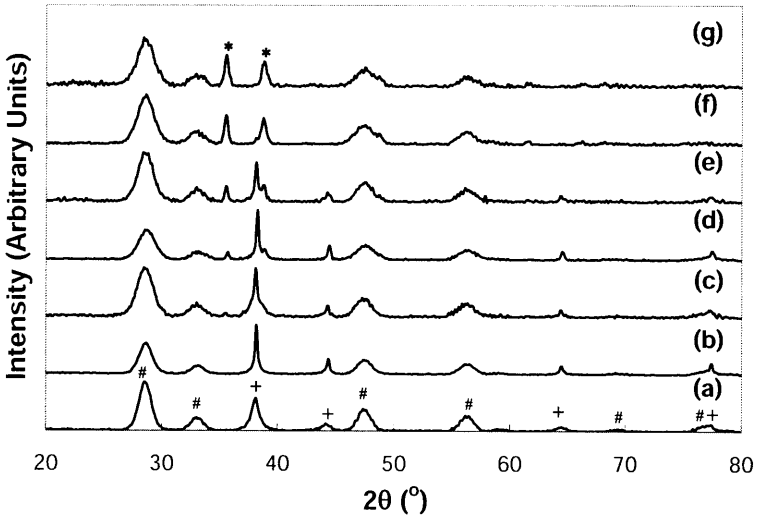

Figure 2.19 XRD patterns of 400°C-calcined 40 wt% $(CuO)_x$-Ag_y/CeO_2 where CuO/Ag molar ratio = (a) 1:100, (b) 1:10, (c) 1:1.5, (d) 1:1, (e) 1.5:1, (f) 10:1 and (g) 100:1. XRD peaks of CuO, Ag and CeO_2 are denoted by *, + and #, respectively.

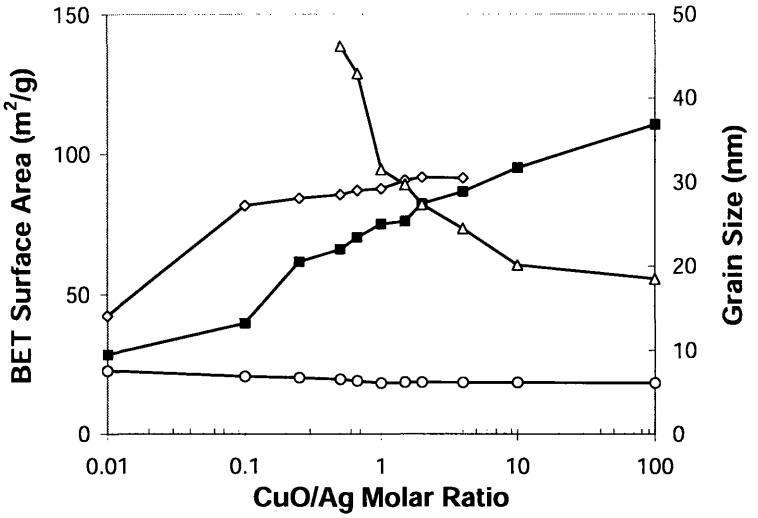

Figure 2.20 (■) BET surface area, and (Δ) CuO, (◊) Ag and (○) CeO_2 grain sizes of 40 wt% $(CuO)_x$-Ag_y/CeO_2 with the CuO/Ag molar ratio specified, after calcination at 400°C.

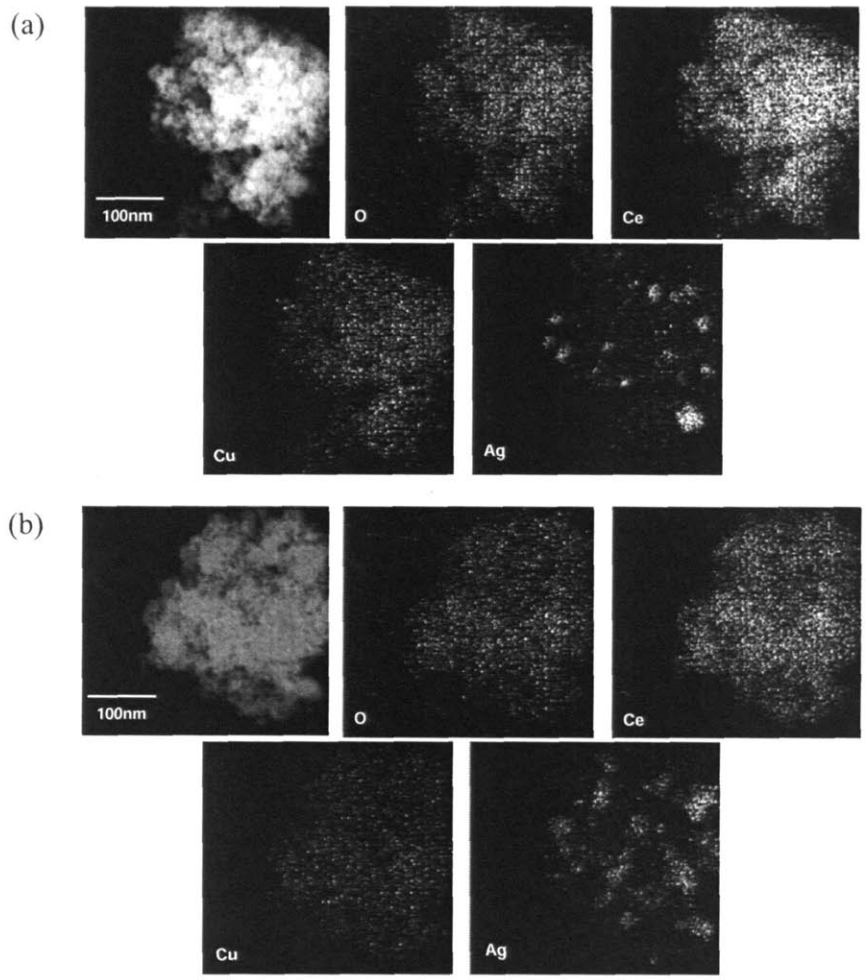

Figure 2.21 STEM/EDX image and elemental maps for 40 wt% $(CuO)_x$-Ag_y/CeO_2 where x/y ratio = (a) 4:1 and (b) 1:4, after calcination at 400°C in air.

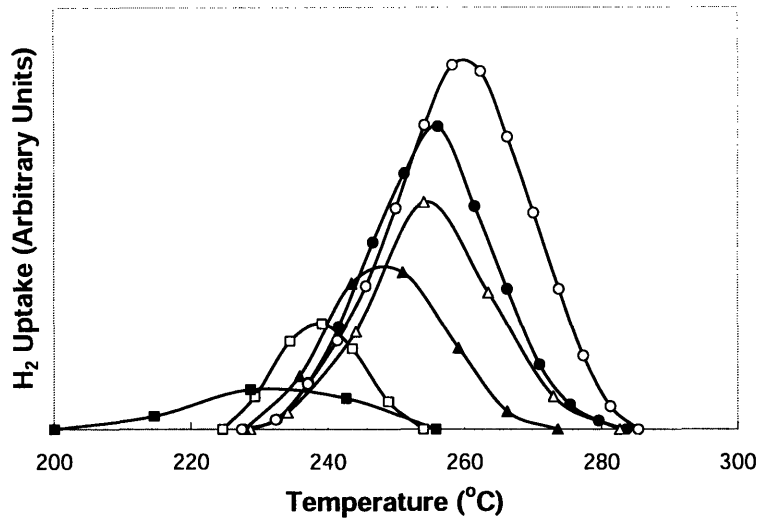

Figure 2.22 TPR profiles of 40 wt% $(CuO)_x$-Ag_y/CeO_2 where CuO/Ag molar ratio = (■) 1:4, (□) 1:2, (▲) 1:1, (Δ) 2:1, (●) 4:1 and (○) 100:1, after calcination at 400°C in air.

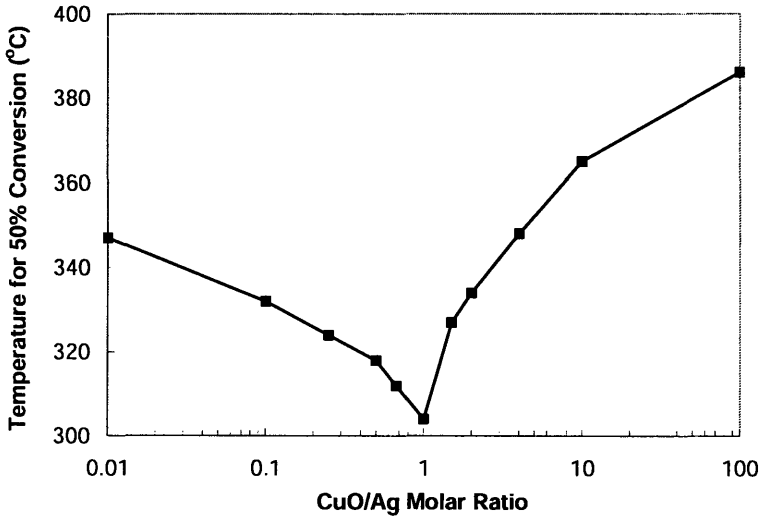

Figure 2.23 Temperature corresponding to 50% carbon black conversion for 40 wt% $(CuO)_x$-Ag_y/CeO_2 with the CuO/Ag molar ratio specified, after calcination at 400°C in air.

2.3.5 Effect of Catalyst/Carbon Black Weight Ratio

40 wt% CuO/CeO_2 and 40 wt% $CuO\text{-}Ag/CeO_2$ were each mixed with carbon black at various weight ratios by grinding with a mortar-and-pestle. The temperatures corresponding to 50% carbon black conversion are shown in Figure 2.24. With increasing catalyst/carbon black weight ratio, the temperature corresponding to 50% conversion decreased, due to the increase in contact area between catalyst and carbon black particles.

For 40 wt% CuO/CeO_2, the catalytic activity was not further enhanced beyond a catalyst/carbon black weight ratio of 8. In contrast, the catalytic activity of 40 wt% CuO-Ag/CeO_2 was increased with catalyst loading up to a catalyst/carbon black weight ratio of 15.

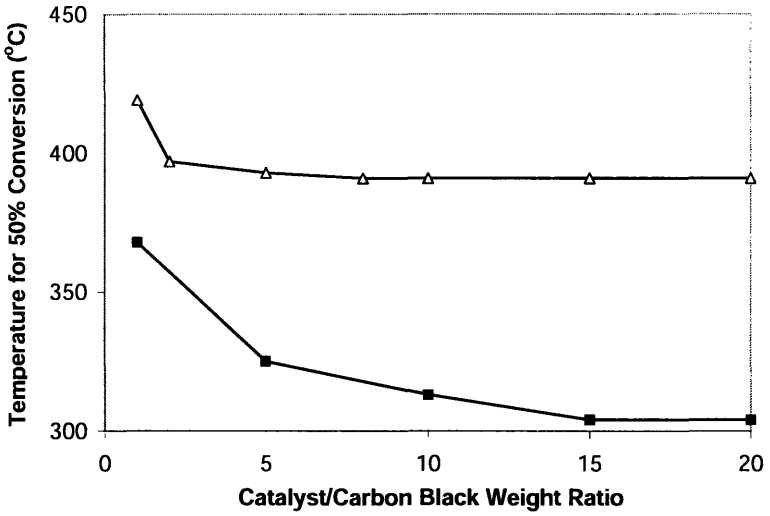

Figure 2.24 Temperature corresponding to 50% carbon black conversion over 400°C-calcined (Δ) 40 wt% CuO/CeO_2 and (■) 40 wt% CuO-Ag/CeO_2, at the catalyst/carbon black weight ratio specified.

2.3.6 Kinetic Analysis of Catalytic Soot Combustion

Kinetic analysis has been performed with TGA data in the literature [24]. It has been established that the surface area of soot was the key factor for the reaction rate with respect to carbon [30]. Our reaction selectivity studies showed that all the carbonaceous material was converted to carbon dioxide during combustion. Thus, carbon black combustion could be expressed as,

$$C + O_2 \rightarrow CO_2$$

The reaction was performed in excess O_2, therefore, the rate of carbon black consumption could be expressed as:

$$\frac{d\alpha}{dt} = k(1-\alpha)^n \qquad (2.1)$$

where α = fraction of carbon black decomposed at time t, n= order of reaction, and k= rate constant, which could be expressed as,

$$k = Ae^{-\frac{E_a}{RT}}; \tag{2.2}$$

where A = Arrhenius pre-exponential factor, and E_a = activation energy.

Combining the expression of linear heating rate (δ = 5°C/min),

$$\delta = \frac{dT}{dt} \tag{2.3}$$

with equations (2.1) and (2.2), the carbon black consumption rate was obtained as,

$$\frac{d\alpha}{dT} = \frac{A}{\delta} e^{-\frac{E_a}{RT}} (1-\alpha)^n \tag{2.4}$$

Upon rearrangement and integration, equation (2.4) became,

$$\int_0^{\alpha} \frac{d\alpha}{(1-\alpha)^n} = \frac{A}{\delta} \int_0^{T} e^{-\frac{E_a}{RT}} dT \tag{2.5}$$

Substituting $u = \frac{E_a}{RT}$, the right integration of equation (2.5) became,

$$\int_u^{\infty} e^{-u} u^{-b} du \cong u^{1-b} e^{-u} \sum_{m=0}^{\infty} \frac{(-b)^m}{u^{m+1}} \tag{2.6}$$

with $b = 2$. When the addition was expanded to two terms ($m = 0$ and $m = 1$), equation (2.5) was expressed by,

$$\frac{1-(1-\alpha)^{1-n}}{1-n} = \frac{ART^2}{E_a \delta}\left(1 - \frac{2RT}{E_a}\right) e^{-\frac{E_a}{RT}}. \tag{2.7}$$

Taking logarithms on both sides gave,

$$\log_{10}\left[\frac{1-(1-\alpha)^{1-n}}{T^2(1-n)}\right] = \log_{10}\frac{AR}{E_a \delta}\left(1 - \frac{2RT}{E_a}\right) - \frac{E_a}{2.3RT}. \tag{2.8}$$

Since $\frac{2RT}{E_a}$ was negligible compared to 1, the equation was simplified as

$$\log_{10}\left[\frac{1-(1-\alpha)^{1-n}}{T^2(1-n)}\right] = \log_{10}\frac{AR}{E_a \delta} - \frac{E_a}{2.3RT}. \tag{2.9}$$

Thus, a plot of $\log_{10}\left[\frac{1-(1-\alpha)^{1-n}}{T^2(1-n)}\right]$ against $\frac{1}{T}$ should yield a straight line, with a slope of $-\frac{E_a}{2.3R}$. In this work, the values of α and $\frac{d\alpha}{dT}$ were calculated based on the relationship

between carbon black conversion and temperature obtained from the TPO study. The activation energy was determined by fitting the value of $\frac{d\alpha}{dT}$, α and T in Equation (2.4), or from the slope of the straight line in Equation (2.9). Figure 2.25 illustrates the procedure of this analysis.

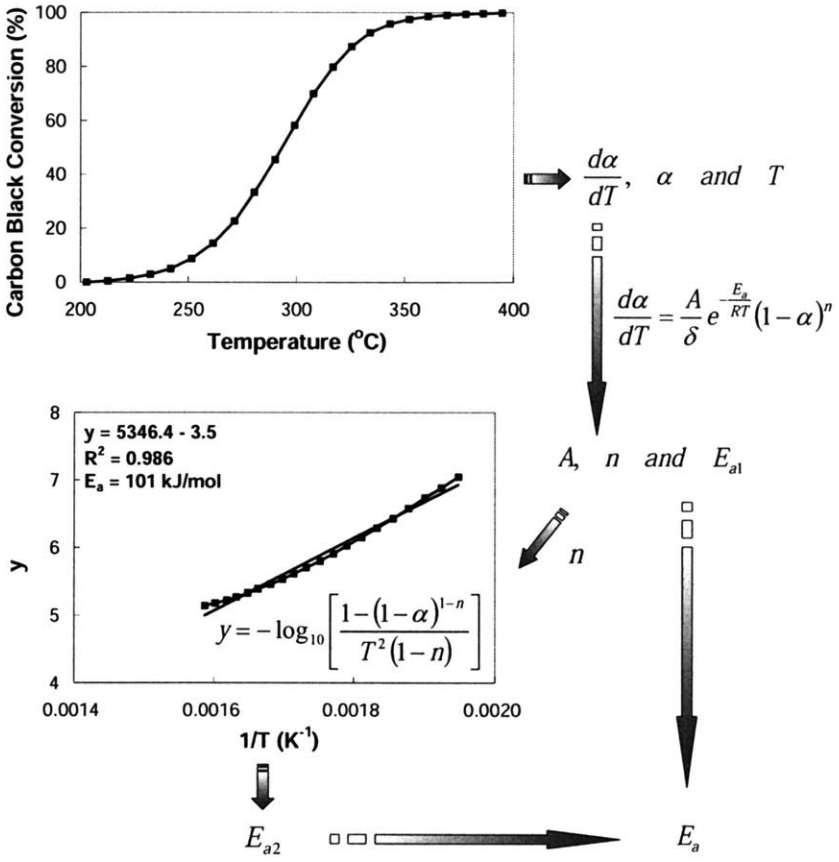

Figure 2.25 Procedure for kinetic analysis. (■) Experimental data and (solid line) regression data.

The activation energies for carbon black combustion over various catalysts are shown in Table 2.7. The best catalyst, 40 wt% CuO-Ag/CeO_2, which provided 50% carbon black conversion at the lowest temperature of 304°C, gave rise to the lowest activation energy of 100.9 kJ/mol. In contrast, uncatalyzed carbon black combustion would require a much higher activation energy of 172.9 kJ/mol. The activation energy obtained was not sensitive to the reaction order of carbon black (n). As reported in the literature, the value

of n should be between $\frac{2}{3}$ and 1 [33, 34]. In this range of n values, similar values have been obtained for the activation energy. Figure 2.26 shows the carbon black conversion as a function of time over 40 wt% CuO-Ag/CeO_2. The temperature was first increased from 30°C to 270°C or 305°C at a heating rate of 5°C/min, and then held for 10 h to complete the oxidation of carbon black isothermally. The time needed for the complete conversion of carbon black under 270°C or 305°C was dependent on the reaction rate under each condition.

Table 2.7 Activation energy of selected catalysts.

Catalyst	Activation Energy (kJ/mol)	Temperature for 50% Carbon Black Conversion (°C)
—	172.9	700
40 wt% CuO/Al_2O_3	150.4	581
40 wt% CuO/ZrO_2	137.1	486
40 wt% CuO/3YSZ	137.1	498
40 wt% CuO/TiO_2	149.9	580
CeO_2	121.6	422
20 wt% CuO/CeO_2	117.5	391
40 wt% CuO/CeO_2	117.3	391
60 wt% CuO/CeO_2	119.6	400
80 wt% CuO/CeO_2	120.9	408
CuO	121.0	411
20 wt% CuO-Ag/CeO_2	113.4	357
40 wt% CuO-Ag/CeO_2	100.9	304
60 wt% CuO-Ag/CeO_2	102.8	319
80 wt% CuO-Ag/CeO_2	104.8	323
CuO-Ag	105.5	338

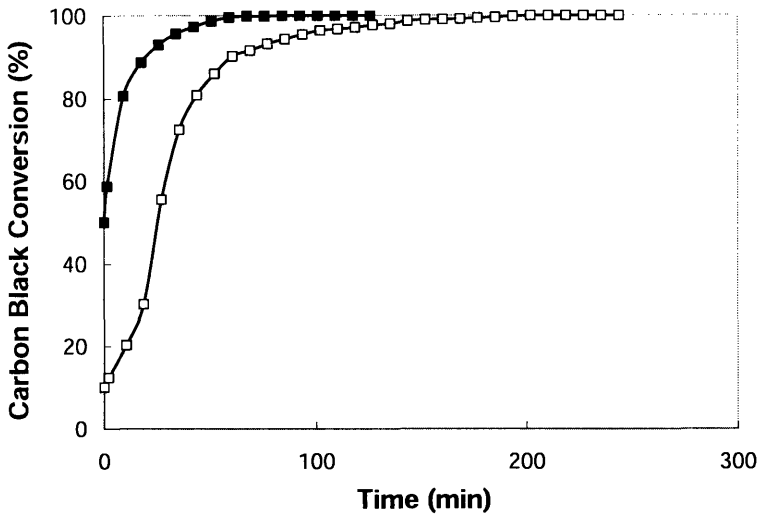

Figure 2.26 Carbon black conversion as a function of time over 40 wt% CuO-Ag/CeO_2 at (□) 270°C and (■) 305°C.

In literature, various methods have been applied to estimate the activation energy of catalytic soot combustion [10, 21, 30-32]. Ozawa method [31] and Redhead method [30] are referenced here for comparison with the results obtained above. The Ozawa method links the heating rate (δ) to the temperature with a specific soot conversion (T_α), as shown in the following equation:

$$\log(\delta) = B - 0.4567(E_a / RT_\alpha), \tag{2.10}$$

where B is a constant value depending on the reaction. Therefore, the activation energy can be obtained from the slope of the linear plot, $\log(\delta)$ vs. $1/T_\alpha$. In order to use this method, three different heating rates, 2°C/min, 5°C/min and 8°C/min, were applied to carbon black combustion over 40 wt% CuO-Ag/CeO_2. Figure 2.27 shows the carbon black conversion as a function of temperature under each heating rate. The temperature corresponding to 50% carbon black conversion (T_{50}) under a given heating rate was applied to calculate the activation energy. A linear plot was obtained for $\log(\delta)$ vs. $1/T_{50}$, which verified that Ozawa method was suitable for this application.

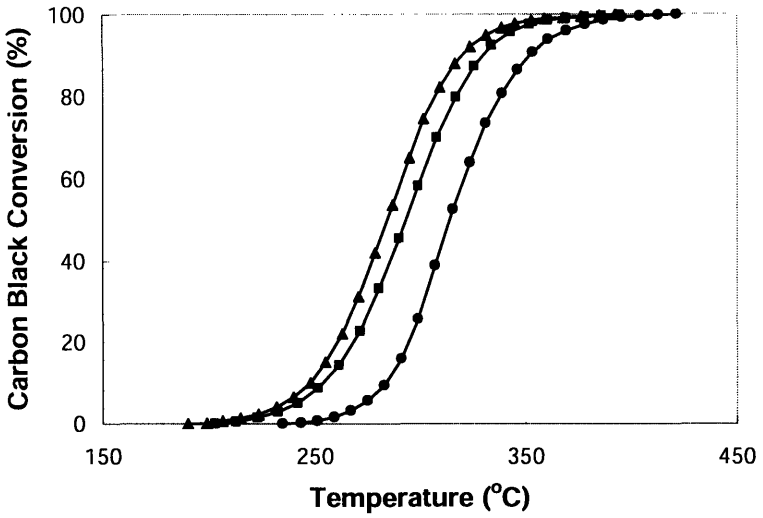

Figure 2.27 Carbon black conversion as a function of temperature over 40 wt% CuO-Ag/CeO_2 at a heating rate of (▲) 2°C/min, (■) 5°C/min or (●) 8°C/min.

The Redhead method is a simple method that provides a rough estimation of the activation energy for soot combustion using the following equation,

$$Ae^{-E_a/RT_P} = \frac{\delta E_a}{RT_P}. \tag{2.11}$$

Here, only the Arrhenius pre-exponential factor A, the temperature for maximum conversion rate T_P and heating rate δ are needed to obtain E_a. The results derived from the three different methods are compared in Table 2.8. They indicated that the heating rate has negligible effect on the activation energy calculated from the TGA data. The E_a value obtained by the Ozawa method was relatively high compared to those obtained by the TGA and Redhead methods.

Table 2.8 Activation energy calculated for 40 wt% CuO-Ag/CeO_2 subjected to different heating rates.

Method	E_a (kJ/mol)		
	2°C/min	5°C/min	8°C/min
TGA Method	103	101	101
Ozawa Method		124	
Redhead Method*	—	97	—

*$A = 10^9$.

2.4 Summary

CuO was shown to be highly effective towards the catalytic oxidation of carbonaceous materials. Ceria was shown to be a superior support for CuO than alumina, zirconia, yttria-stabilized zirconia and titania by significantly increasing the reducibility of CuO. The optimal CuO loading in CuO/CeO_2 was 20–40 wt%, which provided 50% carbon black conversion at a low temperature of 391°C. Ag was found to be an excellent promoter for CuO/CeO_2 as it further enhanced CuO's reducibility. The optimal CuO-Ag loading of 40 wt% led to 50% carbon black conversion at a remarkably low temperature of 304°C. The optimal CuO/Ag molar ratio was found to be 1:1. Doping of ceria did not lead to further improvement in the catalytic performance of 40 wt% $CuO\text{-}Ag/CeO_2$.

The activation energy of carbon black combustion over the optimized catalyst was calculated using TGA, Ozawa and Redhead methods. TGA data analysis showed that 40 wt% $CuO\text{-}Ag/CeO_2$ has an activation energy of ~ 101 kJ/mol, which was similar to that obtained by the Redhead method; Ozawa method led to a higher activation energy value.

2.5 References

[1] Neeft, J. P. A., Makkee, M., Moulijn, J. A., *Chem. Eng. J.* **64**, 295 (1996).
[2] Neeft, J. P. A., Makkee, M., Moulijn, J. A., *Appl. Catal. B: Environ.* **8**, 57 (1996).
[3] Fredrik Ahlström, A., Ingemar Odenbrand, C. U., *Appl. Catal.* **60**, 143 (1990).
[4] Chien, C. C., Huang, T. J., *Ind. Eng. Chem. Res.* **34**, 1952 (1995).
[5] Neeft, J. P. A., Makkee, M., Moulijn, J. A., *Fuel Process. Technol.* **47**, 1 (1996).
[6] Querini, C. A., Ulla, M. A., Requejo, F., Soria, J., Sedrán, U. A., Miró, E. E., *Appl. Catal. B: Environ.* **15**, 5 (1998).
[7] Querini, C. A., Cornaglia, L. M., Ulla, M. A., Miró, E. E., *Appl. Catal. B: Environ.* **20**, 165 (1999).
[8] Bellaloui, A., Varloud, J., Mériaudeau, P., Perrichon, V., Lox, E., Chevrier, M., Gauthier, C., Mathis, F., *Catal. Today* **29**, 421 (1996).
[9] Ciambelli, P., Corbo, P., Parrella, P., Scialò, M., Vaccaro, S., *Thermochim. Acta* **162**, 83 (1990).
[10] Badini, C., Saracco, G., Serra, V., *Appl. Catal. B: Environ.* **11**, 307 (1997).
[11] Serra, V., Saracco, G., Badini, C., Specchia, V., *Appl. Catal. B: Environ.* **11**, 329 (1997).
[12] Badini, C., Saracco, G., Serra, V., Specchia, V., *Appl. Catal. B: Environ.* **18**, 137 (1998).
[13] Badini, C., Mazza, D., Ronchetti, S., Saracco, G., *Mater. Res. Bull.* **34**, 851 (1999).
[14] Saracco, G., Badini, C., Russo, N., Specchia, V., *Appl. Catal. B: Environ.* **21**, 233 (1999).
[15] Ciambelli, P., Palma, V., Russo, P., Vaccaro, S., *J. Mol. Catal. A: Chem.* **204–205**, 673 (2003).

[16] Fino, D., Russo, N., Badini, C., Saracco, G., Specchia, V., *AIChE J.* **49**, 2173 (2003).
[17] Fino, D., Saracco, G., Specchia, V., *Chem. Eng. Sci.* **57**, 4955 (2002).
[18] Fino, D., Fino, P., Saracco, G., Specchia, V., *Chem. Eng. Sci.* **58**, 951 (2003).
[19] Jelles, S. J., van Setten, B. A. A. L., Makkee, M., Moulijn, J. A., *Appl. Catal. B: Environ.* **21**, 35 (1999).
[20] van Setten, B. A. A. L., van Dijk, R., Jelles, S. J., Makkee, M., Moulijn, J. A., *Appl. Catal. B: Environ.* **21**, 51 (1999).
[21] Fino, D., Russo, N., Saracco, G., Specchia, V., *J. Catal.* **217**, 367 (2003).
[22] Russo, N., Fino, D., Saracco, G., Specchia, V., *J. Catal.* **229**, 459 (2005).
[23] Rougier, A., Soiron, S., Haihal, I., Aymard, L., Taouk, B., Tarascon, J.-M., *Powder Technol.* **128**, 139 (2002).
[24] Coats, A. W., Redfern, J. P., *Nature* **201**, 68 (1964).
[25] Mul, G., Kapteijn, F., Doornkamp, C., Moulijn, J. A., *J. Catal.* **179**, 258 (1998).
[26] Ying, J. Y., Tschöpe, A., *Chem. Eng. J.* **64**, 225 (1996).
[27] Kundakovic, Lj., Flytzani-Stephanopoulos, M., *Appl. Catal. A: Gen.* **171**, 13 (1998).
[28] Liu, W., Flytzani-Stephanopoulos, M., *Chem. Eng. J.* **64**, 283 (1996).
[29] Sweeney, J. T., "Novel Metal Oxide Nanocomposites for Oxygen Storage, Sulfur Dioxide Adsorption and Hydrogen Sulfide Absorption," Ph.D. Thesis, Massachusetts Institute of Technology, 2002.
[30] Dernaika, B., Uner, D., *Appl. Catal. B: Environ.* **40**, 219 (2003).
[31] Badini, C., Saracco, G., Russo, N., Specchia, V., *Catal. Lett.* **69**, 207 (2000).
[32] Órfão, J. J. M., Martins, F. G., *Thermochim. Acta* **390**, 195 (2002).
[33] Yezerets, A., Currier, N. W., Kim, D. H., Eadler, H. A., Epling, W. S., Peden, C. H. F., *Appl. Catal. B: Environ.* **61**, 120 (2005).
[34] Bokova, M. N., Decarne, C., Abi-Aad, E., Pryakhin, A. N., Lunin, V. V., Aboukaïs, A., *Thermochim. Acta* **428**, 165 (2005).

Chapter 3. Steam Reforming of Propane over Nickel Aluminates

3.1 Introduction

Hydrogen has increasing appeal as a clean fuel as we face mounting challenges from fossil fuel shortage and environmental pollution. It is particularly attractive as a feedstock for fuel cell systems. Due to the difficulty of hydrogen storage, various on-board hydrogen production processes have been investigated. Steam reforming is of particular interest for hydrogen production in industrial processes since it can provide higher hydrogen concentration compared to partial oxidation and autothermal reforming, and is relatively cost effective.

NiO/Al_2O_3 is the most widely used industrial catalyst for steam reforming as it is active and economical. However, its poor resistance against coking presents a major problem. Coke deposition on catalysts surface significantly increases the pressure drop of the catalyst bed and deactivates the catalyst system. To improve coke resistance, $NiAl_2O_4$ has been used in place of NiO/Al_2O_3 since this spinel phase shows exceptional thermal stability [1]. Compared to NiO/Al_2O_3, $NiAl_2O_4$ results in a higher H_2 uptake during reduction, and a higher Ni dispersion in the reduced catalyst [2]. $NiAl_2O_4$ provides excellent catalytic activity and coking resistance when applied to the steam reforming of methane [1, 3]. However, it showed poor reducibility compared to NiO/Al_2O_3 [4, 5]. Thus, $NiAl_2O_4$ was not favored for steam reforming application. To make the nickel aluminate system more suitable for steam reforming catalysis, it would be critical to improve its reducibility.

Our objective was to develop a novel steam reforming catalyst suitable for fuel cell systems, especially for portable energy generation devices. Hence, high catalytic activity, excellent hydrothermal stability, good selectivity for hydrogen, and high resistance to coking are necessary characteristics. Nickel aluminates are active and coke-resistant, but have not been studied in detail by previous researchers for such application. In this work, nanocrystalline nickel aluminates were synthesized for propane steam reforming. Propane is of great interest for portable hydrogen production due to its liquid properties under moderate pressures. Nickel aluminates were optimized for propane steam reforming based on catalytic activity (defined as propane conversion as a function of temperature) and H_2

yield. In addition, the effects of pretreatments, reaction temperatures and feed compositions were examined. The effects of metal promoters on the reducibility, activity and coking resistance of the catalyst are discussed in Chapter 4.

3.2 Experimental

3.2.1 Catalyst Synthesis

Nanocrystalline nickel aluminates with various Ni/Al molar ratios were synthesized by wet-chemical precipitation. Nickel (II) nitrate ($Ni(NO_3)_2 \cdot 6H_2O$, 99.9985%, Alfa Aesar) and aluminum nitrate ($Al(NO_3)_3 \cdot 9H_2O$, 98–102%, Alfa Aesar) were dissolved in deionized water at a desired molar ratio. Ammonium hydroxide (NH_4OH, 28–30% NH_3, Alfa Aesar) and deionized water (at a volume ratio of 1:4) were used as the base solution. The base solution was added dropwise to the nitrate precursor solution to reach a pH of 8. The resulting suspension was heated to 45°C and aged for 24 h under stirring. Myers' work [3] has shown that the precipitation temperature was critical towards obtaining the desired phase of $NiAl_2O_4$, while longer aging time resulted in relatively low surface area. The precipitate was recovered by filtration, and washed with deionized water and ethanol. After drying at 110°C for 18 h, the powder was ground with a mortar-and-pestle, and sieved to 230 mesh. It was calcined at temperatures ranging from 500°C to 900°C for 4 h. In this work, stoichiometric (Ni/Al = 0.5), Ni-poor (Ni/Al < 0.5) and Ni-rich (Ni/Al > 0.5) systems were prepared. The Ni and Al contents were analyzed by inductively coupled plasma-atomic emission spectrometry (ICP-AES) (Desert Analytics, Tucson, AZ).

3.2.2 Catalyst Characterization

BET surface area of the catalysts was measured by nitrogen adsorption analysis (Micromeritics ASAP 2000). Hydrogen chemisorption was performed on a Micromeritics ASAP 2010 chemisoprtion system. Typically, 200 mg of calcined samples were first reduced in H_2 at a temperature that was 50°C lower than the calcination temperature for 2 h. The sample was then cooled to 35°C and evacuated to 10^{-5} mmHg. The chemisorption measurement was performed at equilibrium pressures between 100 and 500 mmHg. Assuming that chemisorption stoichiometry of H:Ni was 1:1, and the surface area occupied by one hydrogen atom was 0.065 nm^2, the Ni dispersion and metallic surface area could be

estimated [6, 7]. From the measured active surface area, the particle size of nickel could be calculated with the following equation:

$$d_H = \frac{5\times10^3 X_{N_i}\alpha_{N_i}}{\gamma_{N_i} A_{N_i}}. \tag{3.1}$$

where d_H = nickel particle size (nm), X_{N_i} = nickel content in the sample (wt%), α_{N_i} = degree of reduction (%), γ_{N_i} = specific density of nickel (8.908 g/cm^3), and A_{N_i} = active surface area of nickel (m^2/g catalyst).

The powder X-ray diffraction (XRD) patterns of catalysts after calcination, reduction, reaction and re-oxidation were obtained with a Siemens D5000 θ-θ X-ray diffractometer (45 kV, 40 mA, Cu-K_α). The volume-averaged crystallite size was calculated based on Scherrer's analysis of the XRD peak broadening. The morphologies of the catalyst before and after reaction were investigated with high-resolution transmission electron microscopy (HR-TEM) (JEOL 2010) at 200 kV. In addition, energy-dispersive X-ray (EDX) spectroscopy was performed to obtain the elemental mapping of a given area. The catalyst powder was dispersed on a copper grid coated with carbon film. The composition and elemental dispersion of the catalyst was investigated by a Vacuum Generators HB603 Scanning Transmission Electron Microscope (STEM) with energy dispersion X-ray (EDX) spectroscopy.

Temperature-programmed reduction (TPR) was conducted under a reducing atmosphere using a Perkin Elmer System 7HT Thermal Gravimetric Analyzer (TGA). 20 mg of calcined catalysts were first pretreated under air flow at a temperature that was 50°C lower than the calcination temperature for 1 h to remove the adsorbed contaminants. After cooling to 50°C and purging in He for 10 min, a stream of 5% H_2 in He was introduced at a flow rate of 100 ml/min. The temperature was ramped from 30°C to 900°C at a rate of 5°C/min to record the weight loss.

3.2.3 Catalyst Activity and Selectivity

The activity and selectivity of the catalysts were evaluated under steady state in a packed bed reactor (see Figure 3.1). 50 mg of catalysts were loaded into a 1/4"-O.D. quartz reactor tube, and placed between two quartz wool plugs. To control the reaction

temperature accurately, a type-K thermocouple located right below the catalyst bed was used in conjunction with an Omega temperature controller and a Lindberg tube furnace. The gas flow was metered using mass flow controllers (MFC), and water was injected by a syringe pump and vaporized in a pipe wrapped with heating tape. The catalyst was first pretreated at a temperature that was 50°C lower than the calcination temperature in a stream of 5% H_2 in He at a flow rate of 50 ml/min. The reduction time was varied from 2 to 16 h. Following the reduction process, 10% C_3H_8 in N_2 was introduced with H_2O at a H_2O/C molar ratio of 1–6, and the reaction was initiated at a temperature that was 100°C lower than the calcination temperature. A space velocity of 70,000 h^{-1} was used for the reactant gases in all runs. A water trap was placed right after the reactor to condense the unreacted water.

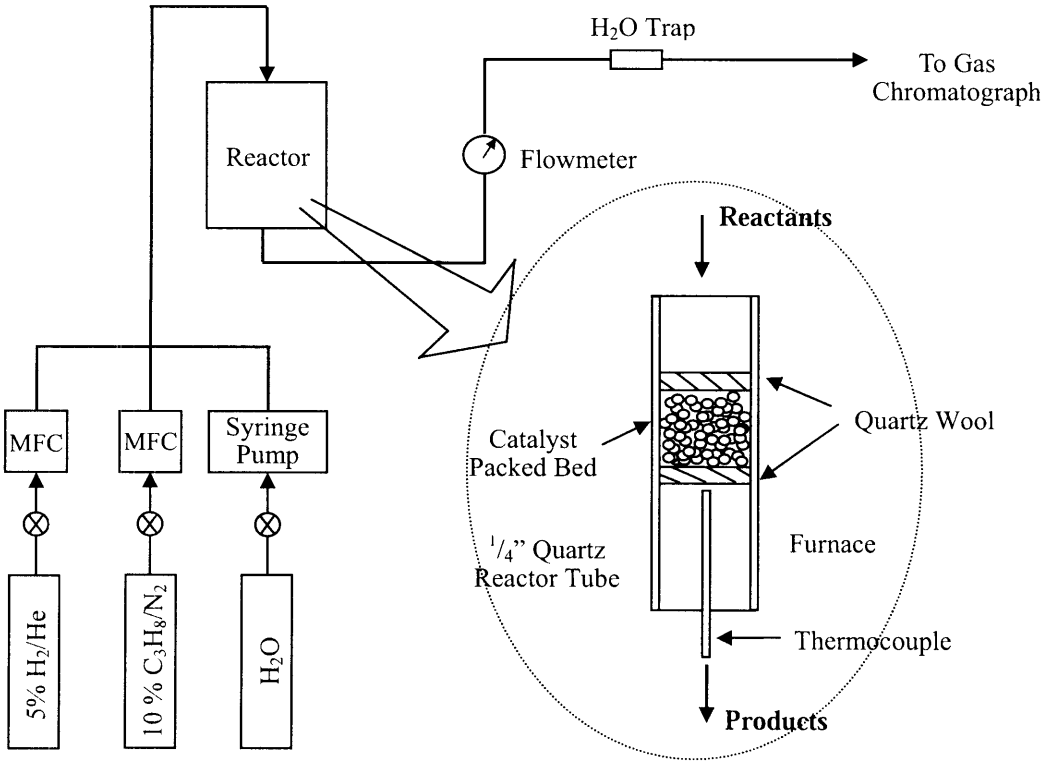

Figure 3.1 Schematic of the packed bed reactor set-up.

The product stream was analyzed by a Hewlett-Packard 6890 Gas Chromatograph (GC) equipped with molecular sieve 5A and Porapak Q chromatographic columns, which allowed CO, CO_2, CH_4, C_2H_4, C_2H_6, C_3H_6, C_3H_8, H_2 and N_2 to be separated and quantified.

N_2 was used as an internal standard to obtain precise quantification of the products. The conversion of propane was calculated by,

$$X_{C_3H_8} = \frac{n^{in}_{C_3H_8} - n^{out}_{C_3H_8}}{n^{in}_{C_3H_8}} \times 100. \tag{3.2}$$

The selectivity for the product with a number of carbon atoms in one molecule ($C_aH_bO_z$) was obtained from,

$$S_{C_aH_bO_z} = \frac{a \times n^{out}_{C_aH_bO_z}}{3 \times (n^{in}_{C_3H_8} - n^{out}_{C_3H_8})} \times 100. \tag{3.3}$$

To obtain a hydrogen yield of less than unity, the calculation was based on the reaction,

$$C_3H_8 + 6H_2O \rightarrow 3CO_2 + 10H_2, \tag{3.4}$$

whereby 1 mole of C_3H_8 could produce 10 moles of H_2. Since the H_2 signal from GC analysis was not sufficiently reliable, the yield of hydrogen was obtained from the balance of oxygen and hydrogen, as shown in the following equation:

$$Y_{H_2} = \frac{4 \times (n^{in}_{C_3H_8} - n^{out}_{C_3H_8}) + \sum z \times n^{out}_{C_aH_bO_z} - \sum \frac{b}{2} \times n^{out}_{C_aH_bO_z}}{10 \times (n^{in}_{C_3H_8} - n^{out}_{C_3H_8})} \times 100. \tag{3.5}$$

Carbon balances of ± 2% were achieved in all runs.

3.2.4 Coking Studies

The amount of coke deposited on the catalyst surface during a steam reforming reaction was investigated by temperature-programmed oxidation (TPO) using a Perkin Elmer System 7HT Thermal Gravimetric Analyzer (TGA). Typically, 20 mg of reacted catalysts were first pretreated in He at 500°C for 1 h to remove the adsorbed water and residual gases on the sample surface. After cooling down to 30°C rapidly, TPO was performed by ramping to 800°C at a rate of 5°C/min in a stream of air (flow rate = 100 ml/min). The weight loss associated with coke combustion was recorded.

3.3 Results and Discussion

3.3.1 Effect of Ni/Al Molar Ratio

3.3.1.1 Materials Characterization

Nickel aluminates of various Ni/Al molar ratios were synthesized and calcined at 700°C in air. XRD patterns showed that only $NiAl_2O_4$ phase was detected in the Ni-poor and stoichiometric materials (Figure 3.2). Both $NiAl_2O_4$ and NiO phases were found in materials with Ni/Al molar ratios of 0.75. NiO phase was dominant in materials with Ni/Al molar ratios of $\geq$ 1.00. Table 3.1 shows that the BET surface area of nickel aluminate decreased with increasing Ni loading due to increasing grain size. In contrast to pure NiO (24.5 nm and 10.1 m^2/g), nickel aluminates possessed a much finer grain size (< 9 nm) and a surface area that was an order of magnitude higher. This study illustrates the superior thermal stability of nickel aluminates against grain growth and surface area reduction.

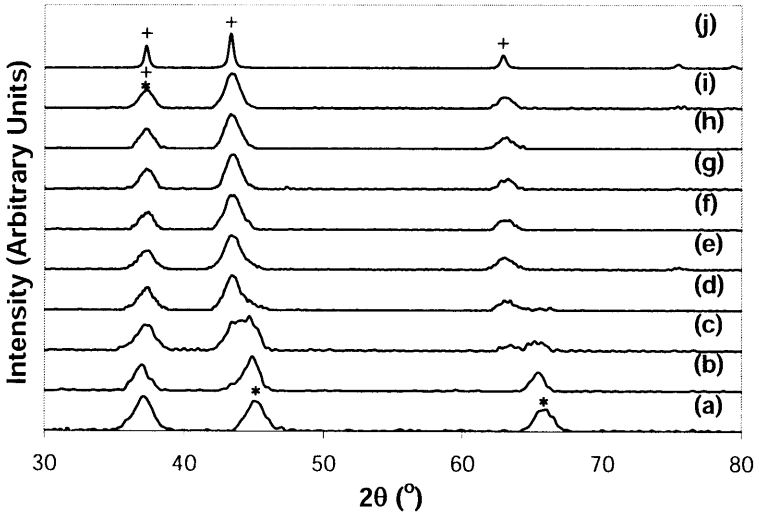

Figure 3.2 XRD patterns of nickel aluminates with Ni/Al ratios of (a) 0.25, (b) 0.50, (c) 0.75, (d) 1.00, (e) 1.10, (f) 1.25, (g) 1.50, (h) 1.75 and (i) 2.00, and (j) NiO, after calcination at 700°C in air. XRD peaks of $NiAl_2O_4$ and NiO are denoted by * and +, respectively.

Table 3.1 BET surface area and XRD grain size of nickel aluminates (with the Ni/Al ratios specified) and pure NiO, after calcination at 700°C in air.

Catalyst	BET Surface Area (m^2/g)	$NiAl_2O_4$ Grain Size (nm)	NiO Grain Size (nm)
Ni/Al = 0.25	202.5	6.4	—
Ni/Al = 0.50	194.2	7.0	—
Ni/Al = 0.75	185.4	8.7	8.1
Ni/Al = 1.00	168.8	—	8.2
Ni/Al = 1.10	162.5	—	8.5
Ni/Al = 1.25	159.9	—	8.6
Ni/Al = 1.50	153.5	—	8.8
Ni/Al = 1.75	147.3	—	8.8
Ni/Al = 2.00	145.6	—	8.9
NiO	10.1	—	24.5

Nickel metal is the active ingredient in steam reforming. Thus, the oxide catalyst has to be reduced prior to the reaction. The catalyst's reducibility and the resulting metal dispersion would affect the application temperature and catalytic activity. TPR profiles show that the Ni-poor and stoichiometric nickel aluminates have poor reducibility, with only one peak at 790°C and 740°C, respectively (Figure 3.3). In contrast, two peaks were detected at ~ 550°C and ~ 710°C in Ni-rich systems, and the reduction was initiated below 500°C. The low-temperature reduction could be attributed to the reduction of NiO phase present in the Ni-rich systems. In contrast, pure NiO showed only one TPR peak at 420°C, and the reduction was initiated at ~ 360°C. The high reducibility of pure NiO was due to the absence of polarizing effect of aluminum ions on Ni-O bonds [8]. Of the nickel aluminates, the sample with Ni/Al = 1.10 allowed for reduction at the lowest initiation temperature. This could be attributed to its Ni surface area being the highest (7.1 m^2/g), as determined by chemisorption (Figure 3.4). We note that pure NiO has a Ni surface area that was almost an order of magnitude smaller (0.8 m^2/g). The Ni particle sizes, d_H, in nickel aluminate systems were calculated from the active surface area (Equation. 3.1) to be 9–14 nm, which were quite consistent with the grain sizes obtained by XRD.

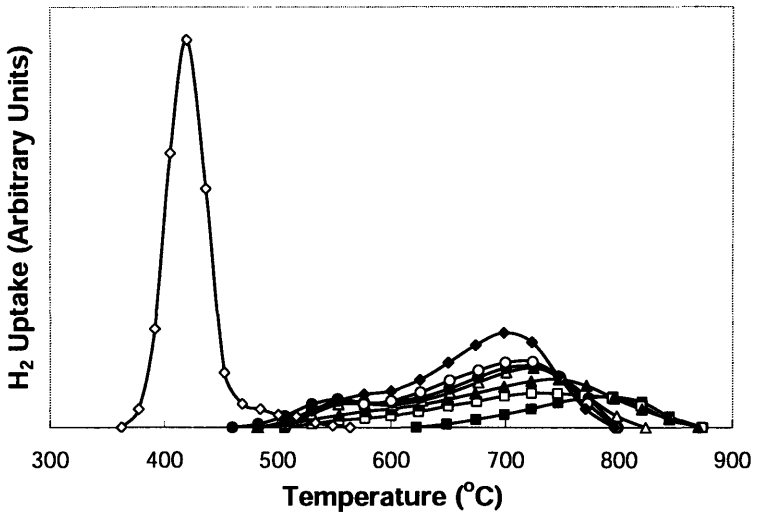

Figure 3.3 TPR profiles of nickel aluminates with Ni/Al ratios of (■) 0.25, (□) 0.50, (▲) 0.75, (Δ) 1.00, (●) 1.10, (○) 1.50 and (♦) 2.00, and (◊) NiO, after calcination at 700°C in air.

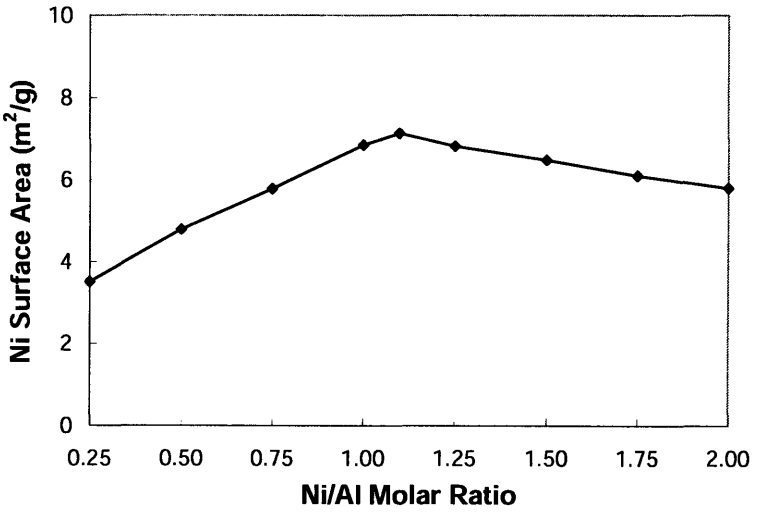

Figure 3.4 Active Ni surface area of nickel aluminates with various Ni/Al ratios after calcination at 700°C in air.

The composition and elemental dispersion of the reduced nickel aluminate (Ni/Al = 1.10) were studied by STEM. Figure 3.5 shows that nickel was uniformly dispersed on the aluminate support.

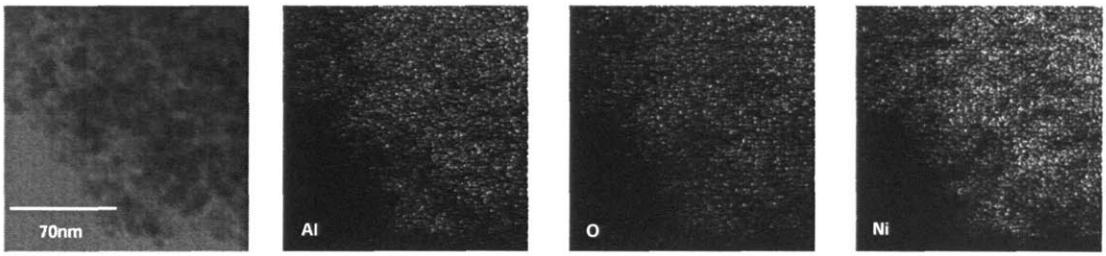

Figure 3.5 STEM/EDX image and elemental maps of 700°C-calcined nickel aluminate with Ni/Al = 1.10, after reduction at 650°C.

3.3.1.2 Catalytic Activity and Selectivity

Nickel aluminates were calcined at 700°C in air, and reduced in 5% H_2 in He for 12 h for complete reduction. They were then tested for propane steam reforming at a H_2O/C molar ratio of 2. Figure 3.6 shows that nickel aluminate with Ni/Al = 1.10 provided the best catalytic activity, demonstrating the lowest light-off temperature and achieving full propane conversion at 430°C. The existence of an optimal Ni loading in NiO/Al_2O_3 has been reported in the literature [7, 9, 10], although the value was different for different reactants in steam reforming reactions. For this reaction, the optimal catalytic activity of the nickel aluminate with Ni/Al = 1.10 could be attributed to the superior reducibility and active Ni surface area of the catalyst.

Pure NiO was also examined for the steam reforming of propane. However, due to severe coking, which blocked the gas pathway and increased the pressure drop of the catalyst bed, the reaction could not last more than 5 h. Hence, NiO was mixed with Al_2O_3 at a molar ratio of 1.1:0.5. Figure 3.6 shows that this mixture provided very low activity. Although pure NiO possessed superior reducibility compared to nickel aluminates, its low Ni surface area and poor coke resistance led to low catalytic activity.

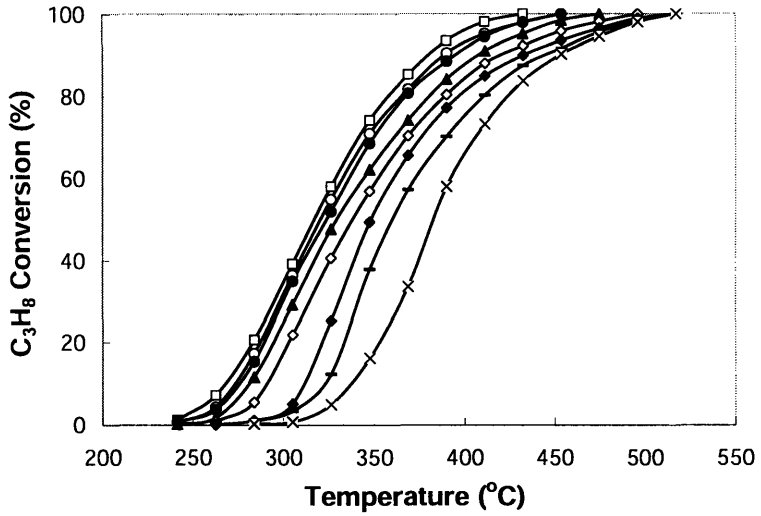

Figure 3.6 Propane conversion over nickel aluminates with Ni/Al ratios of (×) 0.25, (♦) 0.50, (◊) 0.75, (○) 1.00, (□) 1.10, (●) 1.50 and (▲) 2.00, and (—) NiO/Al_2O_3 mixture (molar ratio = 1.1:0.5), after calcination at 700°C in air. Catalytic testing was performed with a feed of 10% C_3H_8 in N_2 and H_2O at 70,000 h^{-1} and $H_2O/C = 2$.

The specific and intrinsic rates of nickel aluminates at 280°C are shown in Figure 3.7. They were normalized to catalyst weight and Ni surface area, respectively, and showed similar trends with respect to Ni/Al molar ratio. The highest specific rate was achieved with the nickel aluminate with Ni/Al = 1.10, which showed the highest propane conversion rate in Figure 3.6. The highest intrinsic reaction rate (16.5×10^{-7} mol/s·m^2) was also attained by the same catalyst. In contrast, the intrinsic rate of NiO/Al_2O_3 mixture at 280°C was only 6.3×10^{-7} mol/s·m^2. This could be due to its greater tendency to deactivate by coking.

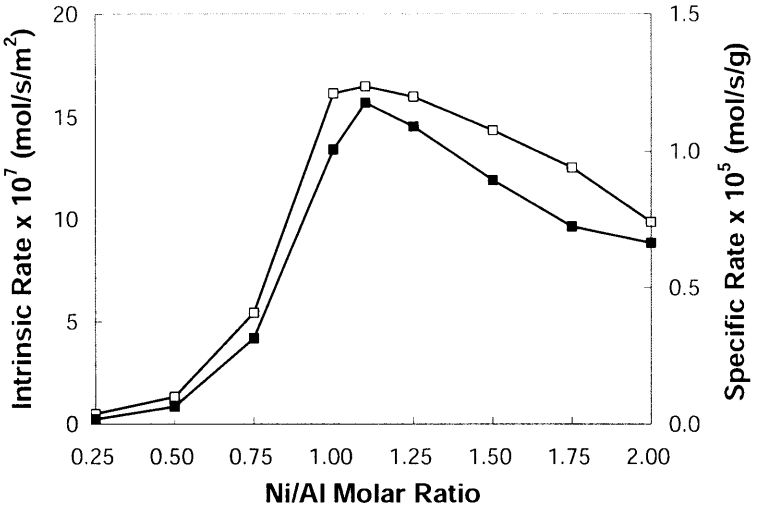

Figure 3.7 (■) Specific and (□) intrinsic reaction rates of nickel aluminates with various Ni/Al ratios in propane steam reforming. Reaction rates were obtained under differential conversions at 280°C with a feed of 10% C_3H_8 in N_2 and H_2O at 70,000 h^{-1} and H_2O/C = 2.

Figure 3.8 presents the average H_2 yield, selectivities for CH_4, CO and CO_2, and C_3H_8 conversion of nickel aluminates at 600°C for 12 h. C_3H_8 was completely converted over all nickel aluminates examined. The products only consisted of H_2, CH_4, CO and CO_2. The H_2 yield increased with increasing Ni/Al molar ratio up to 1.10, and decreased slightly with further increases in Ni/Al molar ratio. The opposite trend was observed in the selectivity for CH_4.

Figure 3.9 shows the structural evolution of nickel aluminate with Ni/Al = 1.10 after calcination, reduction, reaction, and re-oxidation. Both $NiAl_2O_4$ and NiO phases were detected in the fresh catalyst. After reduction at 650°C for 12 h, only metallic Ni was found in the catalyst, which corresponded to the active phase in propane steam reforming. The Ni phase underwent some grain growth from 7.5 nm to 13.6 nm after 12 h of steam reforming reaction (Table 3.2). Upon re-oxidation in air, both $NiAl_2O_4$ and NiO phases were detected again in the sample, with some grain growth. ICP-AES confirmed that the Ni/Al ratio remained unchanged after these treatments.

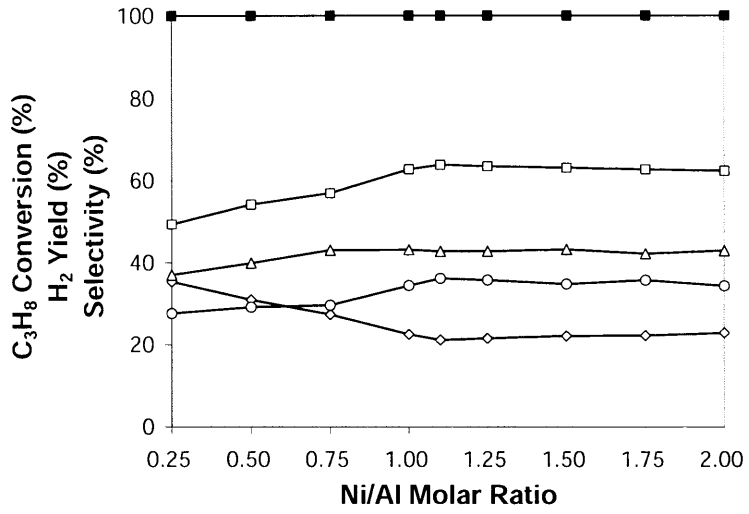

Figure 3.8 (□) H_2 yield, selectivities for (◊) CH_4, (○) CO and (Δ) CO_2, and (■) C_3H_8 conversion over nickel aluminates with various Ni/Al ratios in propane steam reforming at 600°C. Catalytic testing was performed with a feed of 10% C_3H_8 in N_2 and H_2O at 70,000 h^{-1} and $H_2O/C = 2$.

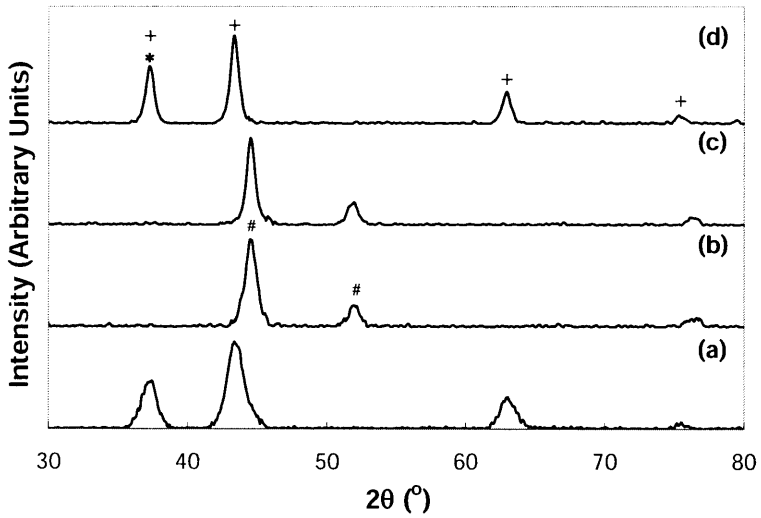

Figure 3.9 XRD patterns of nickel aluminate with Ni/Al = 1.10 after (a) calcination at 700°C, (b) reduction at 650°C, (c) reaction at 600°C, and (d) re-oxidation at 800°C. XRD peaks of $NiAl_2O_4$, NiO and Ni are denoted by *, + and #, respectively.

Table 3.2 NiO and Ni grain sizes of nickel aluminate with Ni/Al = 1.10 after calcination, reduction, reaction and re-oxidation.

Catalyst	NiO Grain Size (nm)	Ni Grain Size (nm)
Calcined at 700°C	8.5	—
Reduced at 650°C	—	7.5
Reacted at 600°C	—	13.6
Re-oxidized at 800°C	14.6	—

3.3.2 Effect of Calcination Temperature

The optimal nickel aluminate catalyst (Ni/Al = 1.10), the stoichiometric nickel aluminate (Ni/Al = 0.50) and the Ni-poor catalyst (Ni/Al = 0.25) were calcined at various temperatures between 500°C and 900°C. The Ni-poor system showed no crystalline peaks at temperatures below 700°C. Figure 3.10 shows that $NiAl_2O_4$ was the only phase detected in this material at 700–900°C. For the stoichiometric nickel aluminate, $NiAl_2O_4$ phase was detected at 600–900°C (Figure 3.11). The material was amorphous after calcined at 500°C. The nickel aluminate catalyst with Ni/Al = 1.10 possessed both NiO and $NiAl_2O_4$ phases upon calcination to 500–900°C, but the two phases overlapped in peak positions substantially when calcined at temperatures below 800°C (Figure 3.12).

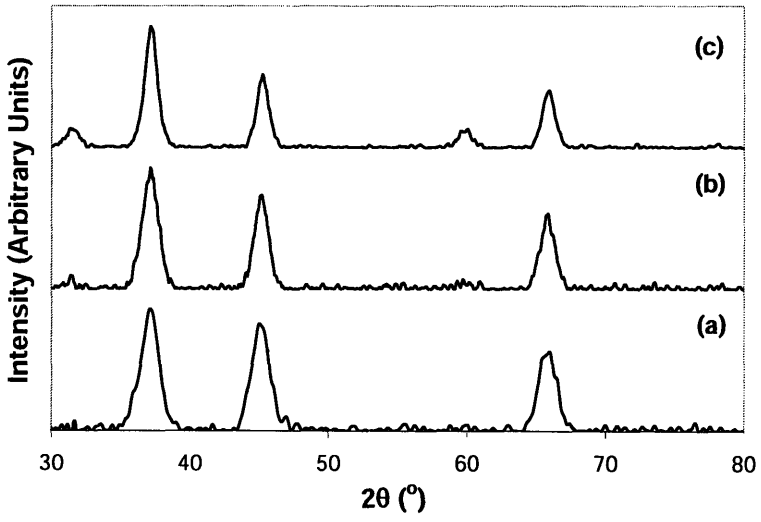

Figure 3.10 XRD patterns of nickel aluminate with Ni/Al = 0.25 after calcination at (a) 700°C, (b) 800°C and (c) 900°C. All XRD peaks are associated with $NiAl_2O_4$.

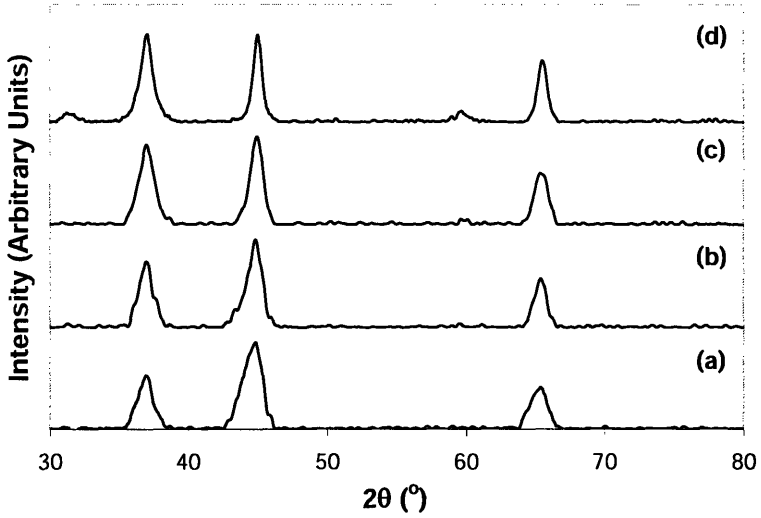

Figure 3.11 XRD patterns of nickel aluminate with Ni/Al = 0.50 after calcination at (a) 600°C, (b) 700°C, (c) 800°C and (d) 900°C. All XRD peaks are associated with $NiAl_2O_4$.

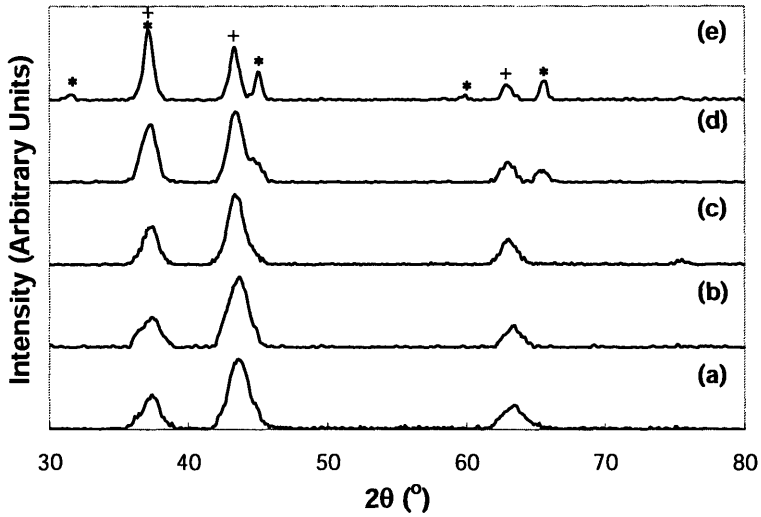

Figure 3.12 XRD patterns of nickel aluminate with Ni/Al = 1.10 after calcination at (a) 500°C, (b) 600°C, (c) 700°C, (d) 800°C and (e) 900°C. XRD peaks of $NiAl_2O_4$ and NiO are denoted by * and +, respectively.

This study illustrated that a higher Al content postponed nickel aluminate's crystallization till a higher calcination temperature, and provided finer grain sizes (Table 3.3). It also prevented the formation of a separate NiO phase, and offered a higher BET surface area (Figure 3.13). BET surface areas of nickel aluminates were shown to decrease steadily with increasing calcination temperature due to increased crystallinity and/or grain

growth. The nickel aluminates possessed remarkably high BET surface areas of > 60 m^2/g even after calcination at 900°C, showing their superior thermal stability to NiO, which only retained a BET surface area of 10 m^2/g after calcination at 700°C.

Table 3.3 $NiAl_2O_4$ and NiO grain sizes of nickel aluminates after calcination at the temperatures specified.

Catalyst	Phase	Calcined at 600°C	Calcined at 700°C	Calcined at 800°C	Calcined at 900°C
Ni/Al = 0.25	$NiAl_2O_4$	—	6.4	7.2	9.3
Ni/Al = 0.50	$NiAl_2O_4$	4.7	7.0	8.0	11.1
Ni/Al = 1.10	$NiAl_2O_4$	—	—	15.8	18.4
	NiO	7.7	8.5	10.0	12.8

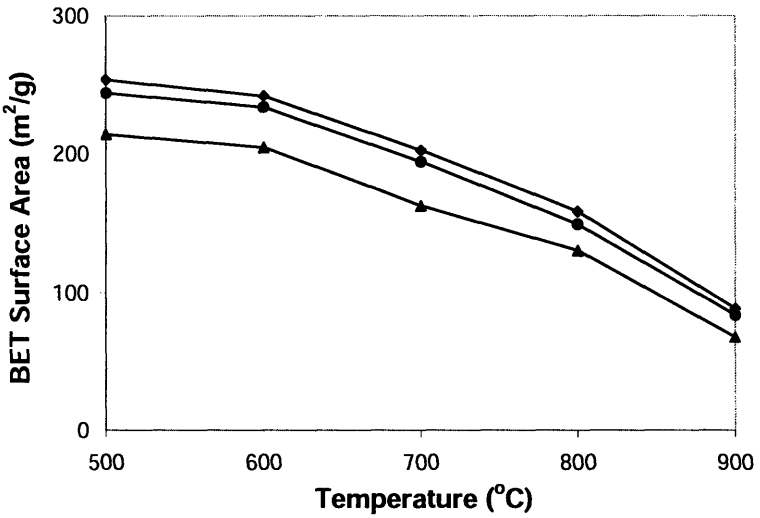

Figure 3.13 BET surface area of nickel aluminates with Ni/Al ratios of (♦) 0.25, (●) 0.50 and (▲) 1.10 as a function of calcination temperature.

The optimal nickel aluminate catalyst (Ni/Al = 1.10) was calcined at 500–900°C, and studied in H_2 atmosphere. For the sample calcined at 500°C, the reduction was initiated at ~ 390°C (Figure 3.14). The TPR profile was characterized by one broad peak from 390°C to 750°C. In contrast, the samples calcined at 600°C, 700°C, 800°C and 900°C showed two peaks in the TPR profile, and the two peaks became more discrete with increasing calcination temperature. This could be associated with the increasingly distinct formation of separate NiO and $NiAl_2O_4$ phases at higher calcination temperatures. The sample calcined at 900°C has a particularly intense low-temperature peak at ~ 600°C and a

small high-temperature peak at ~ 850°C. The former could be attributed to the reduction of NiO, which has emerged as a distinct and dominant crystalline phase with a grain size of 12.8 nm. Calcination at higher temperatures led to increased crystallinity and grain growth, thus, the samples would require a higher temperature for reduction to initiate.

Nickel aluminate with Ni/Al = 1.10 was calcined at 500–900°C, and was reduced for 2 h at a temperature that was 50°C lower than the calcination temperature. Figure 3.15 shows that the 700°C-calcined sample possessed the highest Ni surface area. Samples calcined and reduced at lower temperatures showed lower Ni surface area possibly due to incomplete reduction. On the other hand, calcination and reduction at higher temperatures might have led to lower Ni surface area due to grain growth and sintering.

Propane conversion of nickel aluminate with Ni/Al = 1.10 calcined at 500–900°C is illustrated in Figure 3.16. The 700°C-calcined sample showed the highest catalytic activity, while the 500°C-calcined sample displayed the lowest catalytic activity. The catalytic performance illustrated the same trend as the Ni surface area with regard to calcination temperature (Figure 3.15). This confirmed the direct correlation of propane conversion with Ni dispersion in the nickel aluminate system (Ni/Al = 1.10).

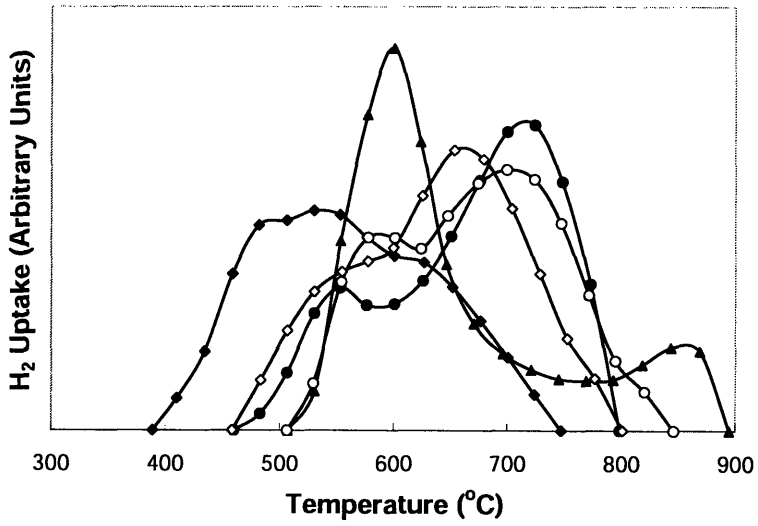

Figure 3.14 TPR profiles of nickel aluminate with Ni/Al = 1.10 after calcination at (♦) 500°C, (◊) 600°C, (●) 700°C, (○) 800°C and (▲) 900°C.

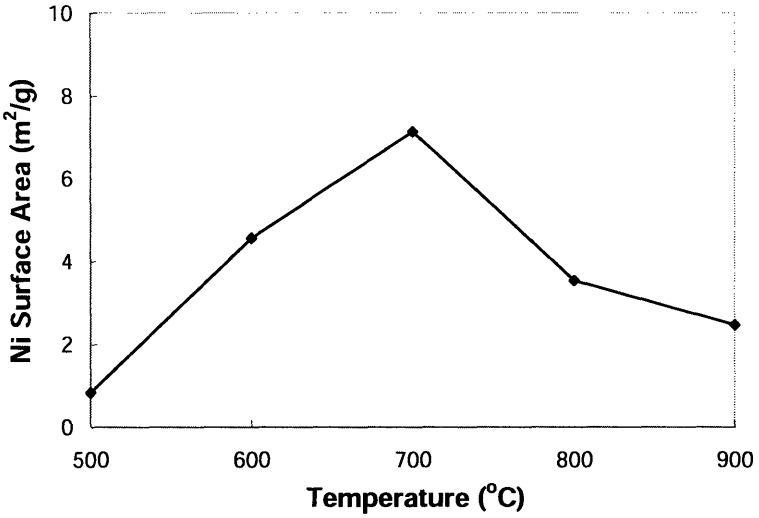

Figure 3.15 Ni surface area of nickel aluminate with Ni/Al = 1.10 as a function of calcination temperature.

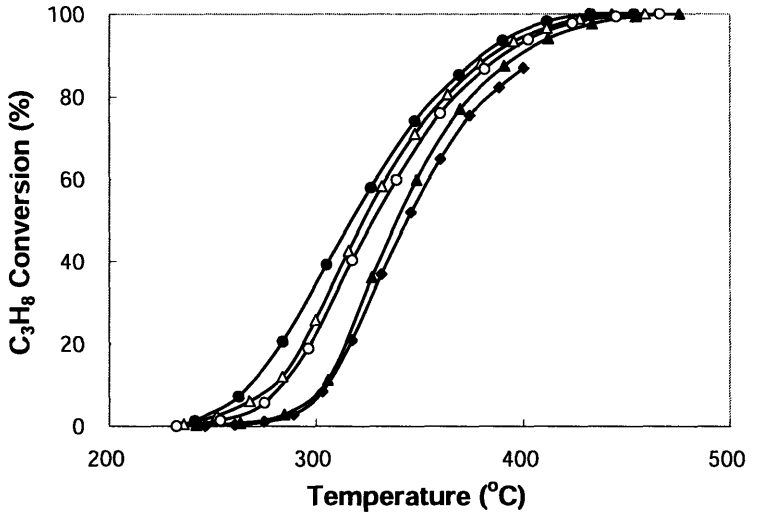

Figure 3.16 Propane conversion over nickel aluminate with Ni/Al = 1.10 after calcination at (♦) 500°C, (Δ) 600°C, (●) 700°C, (○) 800°C and (▲) 900°C. Catalytic testing was performed with a feed of 10% C_3H_8 in N_2 and H_2O at 70,000 h^{-1} and $H_2O/C = 2$.

Figure 3.17 shows the specific and intrinsic reaction rates at 280°C for nickel aluminate with Ni/Al = 1.10 calcined to different temperatures. Since the specific rate was normalized to catalyst weight, the trend should match the catalytic activity results in Figure 3.16. The 700°C-calcined sample displayed the highest specific and intrinsic reaction rates. As expected, the intrinsic reaction rate was not substantially affected by the calcination

temperature as it was normalized to the Ni surface area. The exception was the 900°C-calcined sample with a much lower intrinsic reaction rate (6.5×10^{-7} mol/s·m^2), which was similar to that of NiO/Al_2O_3 mixture (molar ratio = 1.1:0.5) (6.3×10^{-7} mol/s·m^2). This suggested that the lower intrinsic reaction rate could be attributed to the weaker interaction between Ni and Al in the 900°C-calcined sample, which led to significant deactivation due to coking.

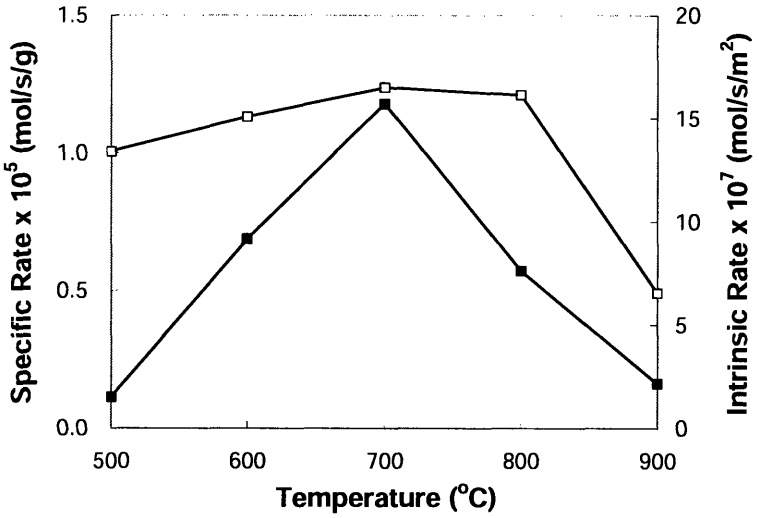

Figure 3.17 (■) Specific and (□) intrinsic reaction rates of nickel aluminate with Ni/Al = 1.10 as a function of calcination temperature. Reaction rates were obtained under differential conversions at 280°C with a feed of 10% C_3H_8 in N_2 and H_2O at 70,000 h^{-1} and $H_2O/C = 2$.

The average values of H_2 yield, selectivities for CH_4, CO and CO_2, and C_3H_8 conversion were obtained at a reaction temperature that was 100°C below the calcination temperature. Figure 3.18 shows that 88% conversion of propane was achieved at 400°C, while 100% conversion of propane was attained at ≥ 500°C. The selectivity for CH_4 decreased with increasing reaction temperature due to the enhanced H dissociation at high temperatures. Low reaction temperatures favored CO_2 production and inhibited CO production due to the exothermic water-gas shift reaction. High reaction temperatures enhanced H dissociation and C oxidation to generate more H_2 and CO_2, but these processes were in competition with the water-gas shift reaction. Consequently, the highest H_2 yield was achieved at 700°C, and the highest selectivity for CO_2 was obtained at 600°C.

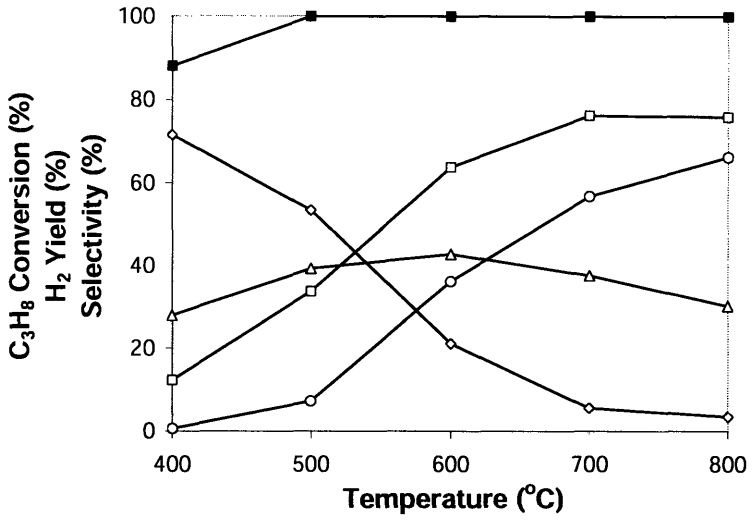

Figure 3.18 (□) H_2 yield, selectivities for (◊) CH_4, (○) CO and (Δ) CO_2, and (■) C_3H_8 conversion over nickel aluminate with Ni/Al = 1.10 in propane steam reforming at the reaction temperatures specified. Catalytic testing was performed with a feed of 10% C_3H_8 in N_2 and H_2O at 70,000 h^{-1} and $H_2O/C = 2$.

The steam reforming reaction over nickel aluminate with Ni/Al = 1.10 was held for 12 h at various reaction temperatures. Some decrease in propane conversion was noted over time at 400°C, but the selectivities and hydrogen yield remained essentially unchanged over 12 h (Figure 3.19(a)). The catalytic activity, selectivities and hydrogen yield were stable for 12 h at 600°C and 800°C (Figures 3.19(b) and (c)). This high stability would be very attractive for industrial applications, and illustrated the excellent coke resistance of nickel aluminate with Ni/Al = 1.10.

Figure 3.20 compares the equilibrium calculation of product composition in propane steam reforming and the experimental data obtained over 700°C-calcined nickel aluminate with Ni/Al = 1.10. Equilibrium calculation showed complete propane conversion even at temperatures as low as 200°C. Experimentally, full propane conversion was only achieved at ≥ 430°C. The equilibrium calculation and experimental data became quite consistent at temperatures above 430°C. The major differences at low temperatures could be attributed to incomplete propane conversion, which altered the product composition significantly below 430°C.

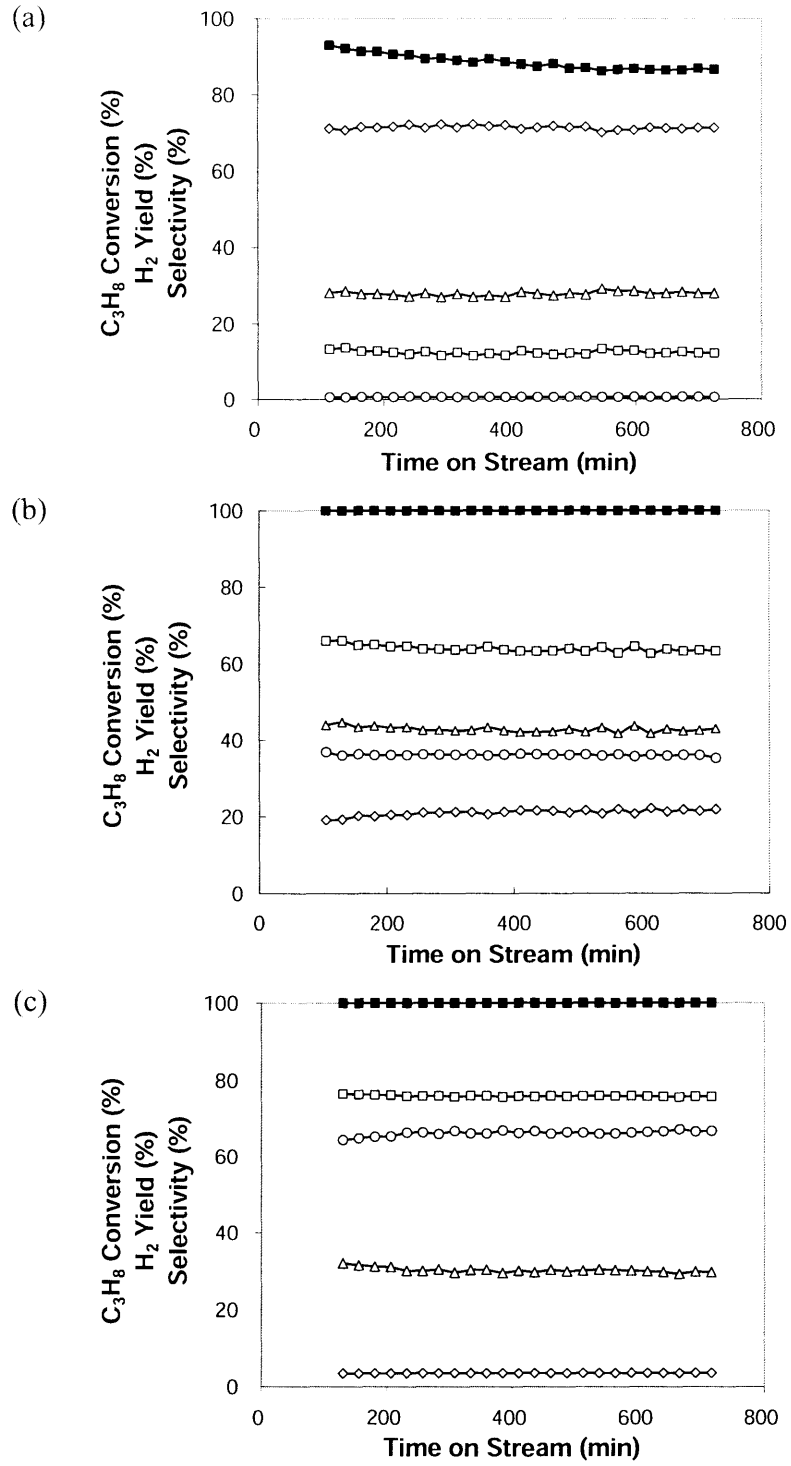

Figure 3.19 (□) H_2 yield, selectivities for (◊) CH_4, (○) CO and (Δ) CO_2, and (■) C_3H_8 conversion as a function of time over nickel aluminate with Ni/Al = 1.10 in propane steam reforming at (a) 400°C, (b) 600°C and (c) 800°C. Catalytic testing was performed with a feed of 10% C_3H_8 in N_2 and H_2O at 70,000 h^{-1} and $H_2O/C = 2$.

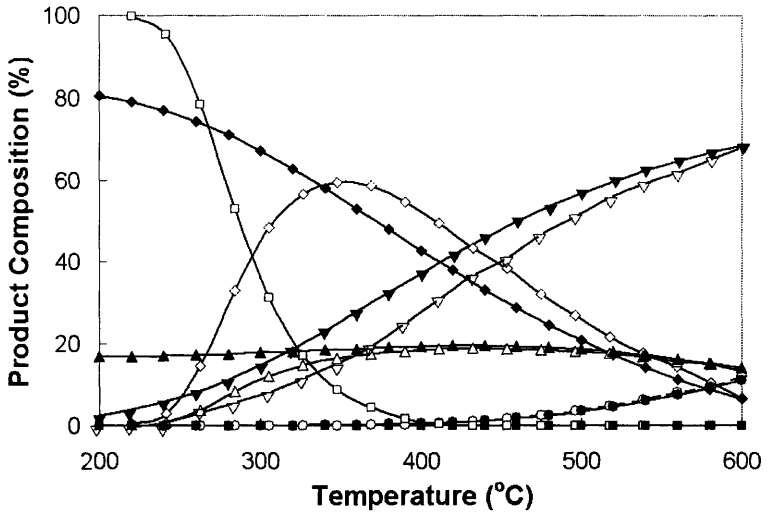

Figure 3.20 (Close symbols) Equilibrium and (open symbols) experimental product composition achieved over nickel aluminate with Ni/Al = 1.10 in propane steam reforming. The products were (▽) H_2, (◊) CH_4, (○) CO, (Δ) CO_2 and (□) C_3H_8. Catalytic testing was performed with a feed of 10% C_3H_8 in N_2 and H_2O at 70,000 h^{-1} and H_2O/C = 2.

The mechanism of propane steam reforming over nickel aluminates will be discussed later in detail. Briefly, the dissociative adsorption of C_3H_8 resulted in CH_x, which then underwent either H extraction to produce H_2, CO or carbon deposit on the catalyst surface or H adsorption to produce CH_4. Next, CO would react with H_2O to further produce CO_2. Therefore, more H_2 would be extracted from both C_3H_8 and H_2O with increasing reaction temperature. CO would only begin to appear at temperatures above 400°C as the exothermic water-gas shift reaction would convert CO to CO_2 at low temperatures. Therefore, CO production would increase with increasing temperature, while CO_2 production would first increased with temperature and then decreased when the temperature was raised beyond 400°C. Below 348°C, increasing CH_4 was produced with increasing temperature due to the dissociative adsorption of C_3H_8. However, CH_4 production decreased above 348°C as the dissociative adsorption of C_3H_8 progressed further with H extraction. We note that the equilibrium value for CH_4 composition was much higher at low temperatures than that experimentally obtained. This was because the reaction was too slow to achieve the equilibrium values at low temperatures.

The XRD patterns of nickel aluminate with Ni/Al = 1.10 after propane steam reforming at different reaction temperatures are shown in Figure 3.21. Only metallic Ni phase was detected in all samples, illustrating that the reduction of NiO and $NiAl_2O_4$ phases could be achieved even at relatively low temperatures. This was likely due to the fact that nanocrystals of NiO and $NiAl_2O_4$ were derived in our nickel aluminate synthesis, which facilitated the reduction process. Table 3.4 shows the grain sizes after calcination, reduction and reaction. The reduction temperature and reaction temperature were 50°C and 100°C below the calcination temperature, respectively. In each case, the Ni grain size after the reduction was not significantly different from the NiO grain size before the reduction. However, the Ni grains underwent significant grain growth during the reaction, especially when the reaction temperature was high.

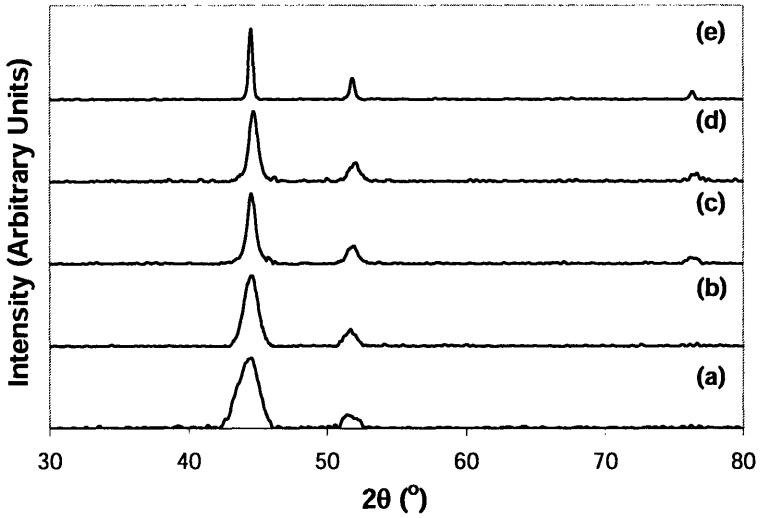

Figure 3.21 XRD patterns of nickel aluminate with Ni/Al = 1.10 after propane steam reforming reaction at (a) 400°C, (b) 500°C, (c) 600°C, (d) 700°C and (e) 800°C. All XRD peaks are associated with Ni.

Table 3.4 NiO and Ni grain sizes of nickel aluminate with Ni/Al = 1.10 after calcination, reduction and reaction.

Calcination Temperature (°C)	NiO Grain Size After Calcination (nm)	Ni Grain Size After Reduction (nm)	Ni Grain Size After Reaction (nm)
500	6.3	5.2	8.3
600	7.7	6.2	9.4
700	8.5	7.5	13.6
800	10.0	9.7	14.0
900	12.8	13.8	27.4

3.3.3 Effect of Catalyst Pretreatment

To investigate the effect of catalyst pretreatment on catalytic activity, 700°C-calcined nickel aluminate with Ni/Al = 1.10 was reduced in 5% H_2 in He at 650°C for 2–16 h. Figure 3.22 shows that only Ni phase was detected in all samples. This study indicated that 2 h was sufficient for reducing the NiO and $NiAl_2O_4$ phases at 650°C.

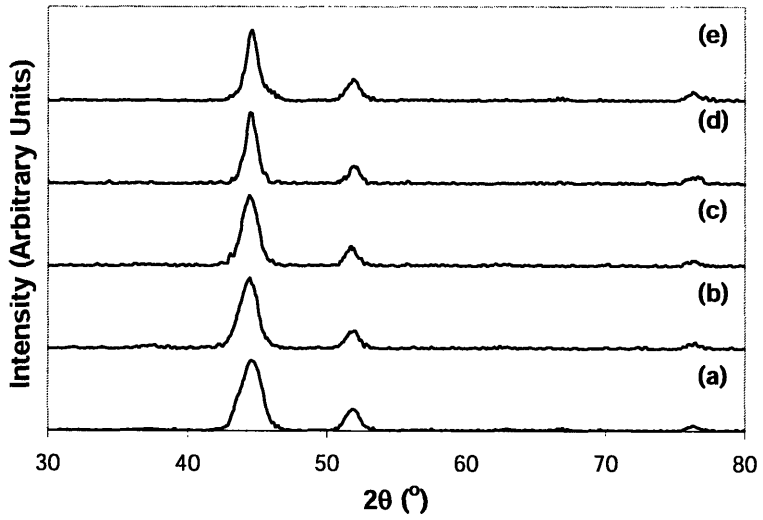

Figure 3.22 XRD patterns of nickel aluminate with Ni/Al = 1.10 after reduction at 650°C for (a) 2 h, (b) 6 h, (c) 10 h, (d) 12 h and (e) 16 h. All XRD peaks are associated with Ni.

The catalysts pretreated for different time periods were applied to steam reforming of propane. Figure 3.23 shows that the catalytic activity increased slightly with increasing reduction time, which could be attributed to the higher Ni surface area. H_2 chemisorption indicated the Ni surface area of samples reduced for 2 h and 12 h to be 7.1 m^2/g and 8.0

m^2/g, respectively. Since the effect of reduction period on catalytic activity was minor, a short reduction period of 2 h was used in subsequent studies.

The average values of H_2 yield, selectivities for CH_4, CO and CO_2, and C_3H_8 conversion at 600°C are shown in Figure 3.24 as a function of reduction period. Propane was converted completely in all cases. H_2 yield increased from 60% to 64% with increasing reduction period from 2 h to 10 h; only minor increase was observed with longer reduction time. The selectivity for CH_4 decreased slightly with increased reduction period, possibly because slightly more active sites were available for H extraction from CH_4. Selectivities for CO and CO_2 did not vary much with reduction time.

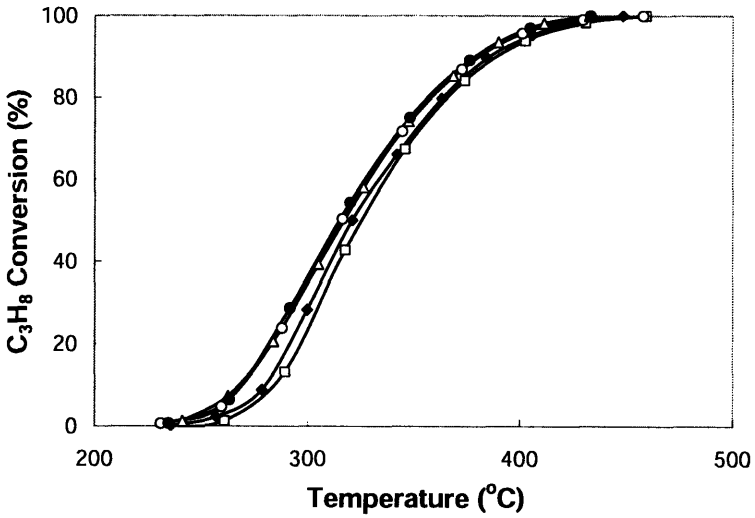

Figure 3.23 Propane conversion over nickel aluminate with Ni/Al = 1.10 after reduction at 650°C for (□) 2 h, (♦) 6 h, (○) 10 h, (Δ) 12 h and (●) 16 h. Catalytic testing was performed with a feed of 10% C_3H_8 in N_2 and H_2O at 70,000 h^{-1} and $H_2O/C = 2$.

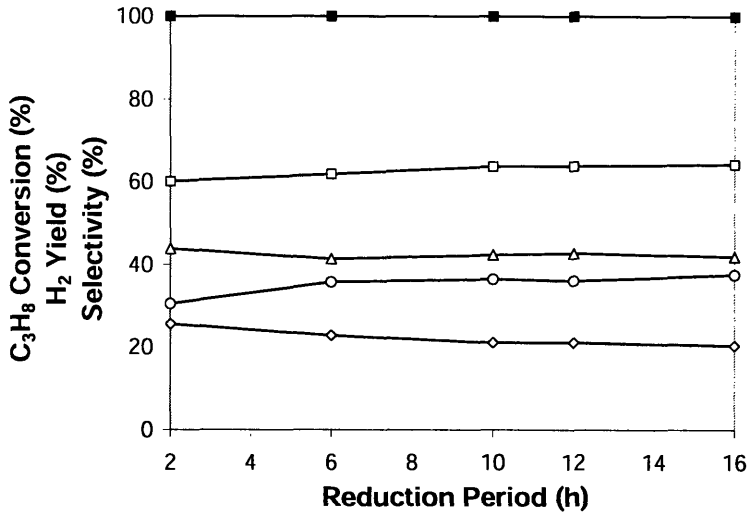

Figure 3.24 (□) H_2 yield, selectivities for (◊) CH_4, (○) CO and (Δ) CO_2, and (■) C_3H_8 conversion over nickel aluminate with Ni/Al = 1.10 in propane steam reforming at 600°C after reduction for different periods at 650°C. Catalytic testing was performed with a feed of 10% C_3H_8 in N_2 and H_2O at 70,000 h^{-1} and $H_2O/C = 2$.

Figure 3.25 shows the XRD patterns of reacted catalysts that had been reduced at 650°C for different periods. In all cases, metallic Ni was the only phase present. Table 3.5 shows that the samples underwent substantial grain growth during the steam reforming reaction. The reduction period only had very minor effects on the grain size of the samples.

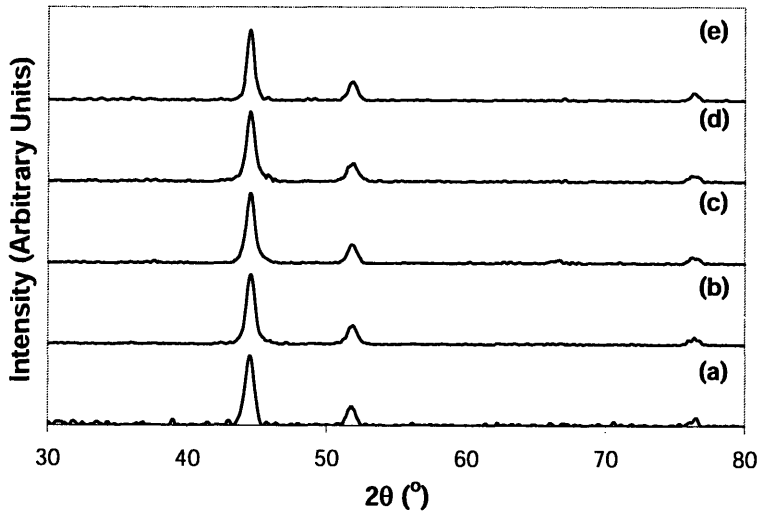

Figure 3.25 XRD patterns of nickel aluminate with Ni/Al = 1.10 after reaction at 600°C. Catalytic testing was performed with 50 mg of catalyst after reduction at 650°C for (a) 2 h, (b) 6 h, (c) 10 h, (d) 12 h and (e) 16 h. All XRD peaks are associated with Ni.

Table 3.5 Ni grain size of nickel aluminate with Ni/Al = 1.10 after reduction at 650°C and after reaction at 600°C.

Reduction Period (h)	Ni Grain Size (nm) After Reduction	Ni Grain Size (nm) After Reaction
2	7.3	12.7
6	7.4	13.1
10	7.5	13.5
12	7.5	13.6
16	7.8	14.1

3.3.4 Effect of H_2O/C Ratio

Figure 3.26 shows the effect of H_2O/C ratio on propane steam reforming over 700°C-calcined nickel aluminate with Ni/Al = 1.10. Complete conversion of propane was achieved even at a low H_2O/C ratio of 1. More water introduction enhanced the C oxidation, and decreased the selectivity for CH_4. Increasing H_2O/C ratio led to increased and decreased selectivities for CO_2 and CO, respectively, as driven by the water-gas shift reaction. H_2 yield increased with increasing H_2O/C ratio as more H could be extracted from C_3H_8 and H_2O.

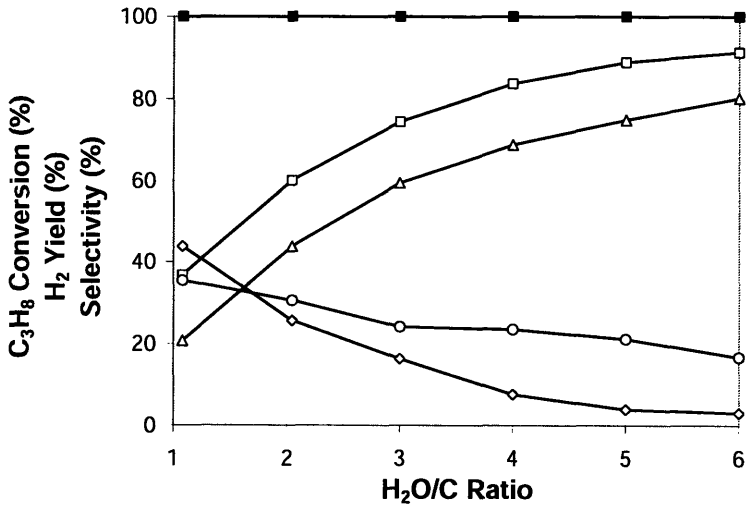

Figure 3.26 (□) H_2 yield, selectivities for (◊) CH_4, (○) CO and (Δ) CO_2, and (■) C_3H_8 conversion over nickel aluminate with Ni/Al = 1.10 in propane steam reforming at 600°C. Catalytic testing was performed with a feed of 10% C_3H_8 in N_2 and H_2O at 70,000 h^{-1} and the H_2O/C ratio specified.

The catalysts reacted at various H_2O/C ratios all showed a metallic Ni phase (Figure 3.27). Table 3.6 shows that propane steam reforming led to grain growth, the extent of which depended on H_2O/C ratios. Larger grain size was obtained at a high H_2O/C ratio, as water vapor facilitated sintering and grain growth.

The coke formation rate during propane steam reforming at 600°C was examined. When a higher H_2O/C ratio was employed, much less coke was deposited on the catalyst (Figure 3.28). This was because water introduction improved the oxygen transfer to the adsorbed carbon species on the catalyst surface, enhancing the oxidation of carbon atoms.

Severe coke formation on nickel surface has been the major challenge for nickel-based catalysts. The mechanism of coke formation has been investigated by various researchers [11, 12]. It is believed that coke formation on nickel surface is due mainly to the dissociation of hydrocarbons to produce highly reactive monatomic carbon C_α [12]. C_α is easily combined with adsorbed oxygen or hydroxyl group to produce carbon monoxide. However, excess C_α could lead to polymerization to form C_β, which is much less active, and accumulates on the nickel surface or diffuses into the crystal structure. Three types of coke have been reported in the steam reforming of hydrocarbons over supported catalysts: pyrolytic, encapsulating and whisker coke [12, 13]. Pyrolytic coke is due to the decomposition of hydrocarbons in the gas phase, while encapsulating and whisker coke are formed on metallic sites. Typically, whisker carbon is detected in nickel-based catalysts, and is initiated from nickel carbide formation [12, 14]. Carbonaceous species are dissolved and diffuses through the nickel particle to the grain boundary, precipitating at the end of the nickel particle. This process continues over time, forming a carbon filament at the edge of the nickel particle. In this study, whisker carbon was deposited on the nickel aluminate catalysts during propane steam reforming. The elemental maps showed that a high dispersion of Ni on the aluminate support was retained during the reaction (Figure 3.29). The non-homogeneous dispersion of carbon was associated with coke deposition on the catalyst surface during steam reforming. Figure 3.30 also shows the increase in catalyst grain size after reaction.

Although a high H_2O/C ratio helped to inhibit coke formation, the energy cost associated with the introduction of large quantities of H_2O would made it impractical for industrial applications. Various promoters have been developed for nickel-based catalysts

in attempt to improve the coke resistance [11, 12, 14-16]. To enhance the coke resistance of nickel aluminates, metal promoters were investigated in detail in Chapter 4 [17].

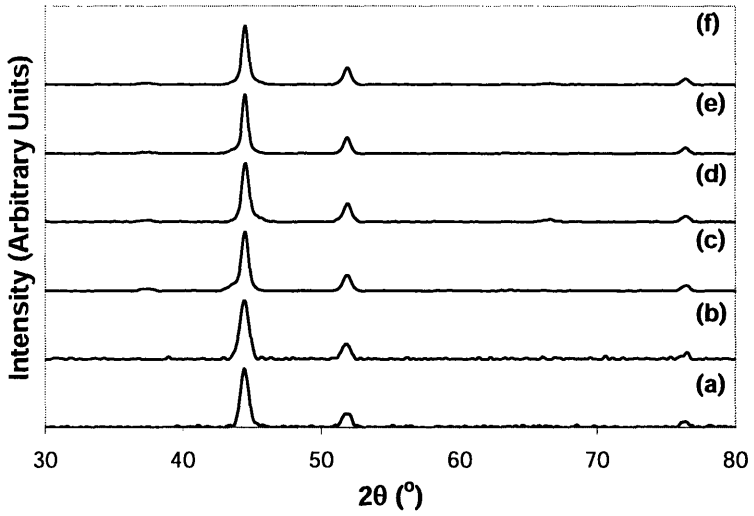

Figure 3.27 XRD patterns of nickel aluminate with Ni/Al = 1.10 after reaction at 600°C at a H_2O/C ratio of (a) 1, (b) 2, (c) 3, (d) 4, (e) 5 and (f) 6. All XRD peaks are associated with Ni.

Table 3.6 Ni grain size of nickel aluminate with Ni/Al = 1.10 after reduction at 650°C and after reaction at 600°C at the H_2O/C ratio specified.

H_2O/C Ratio	Ni Grain Size (nm) After Reduction	Ni Grain Size (nm) After Reaction
1	7.3	11.6
2	7.3	12.7
3	7.3	14.1
4	7.3	15.2
5	7.3	15.9
6	7.3	16.1

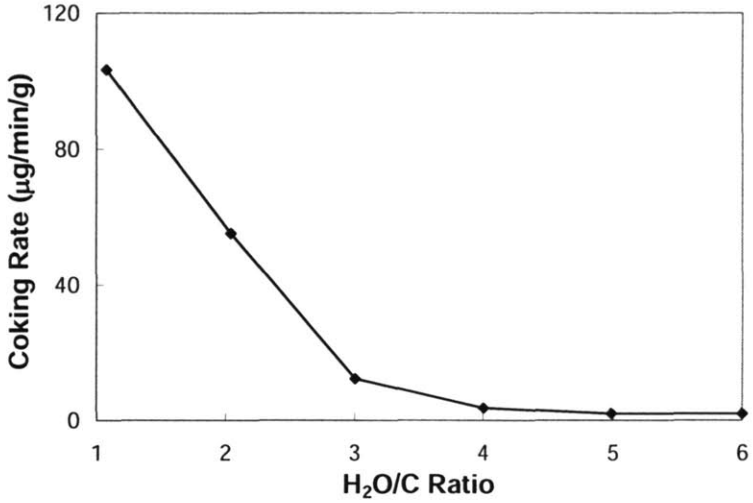

Figure 3.28 Coking rate over nickel aluminate with Ni/Al = 1.10 in propane steam reforming at 600°C. Catalytic testing was performed with a feed of 10% C_3H_8 in N_2 and H_2O at 70,000 h^{-1} and the H_2O/C ratio specified.

(a)

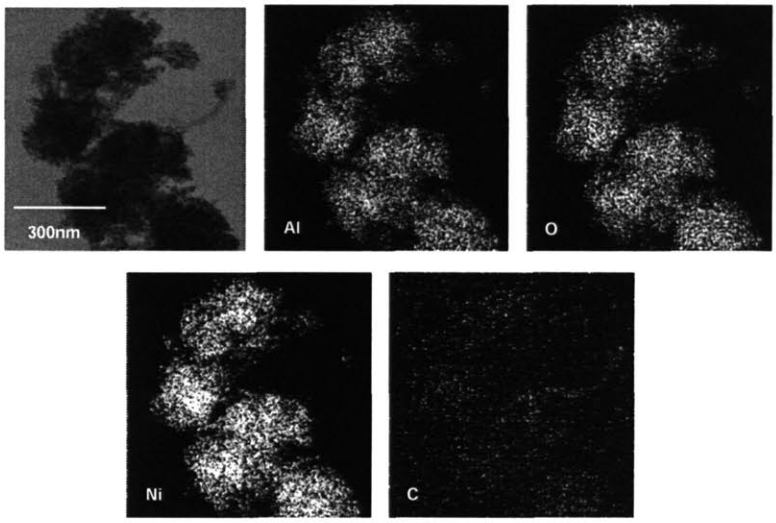

Figure 3.29 STEM/EDX image and elemental maps of 700°C-calcined nickel aluminate with Ni/Al = 1.10, after reaction at 600°C. Catalytic testing was performed with a feed of 10% C_3H_8 in N_2 and H_2O at 70,000 h^{-1} and $H_2O/C = 2$.

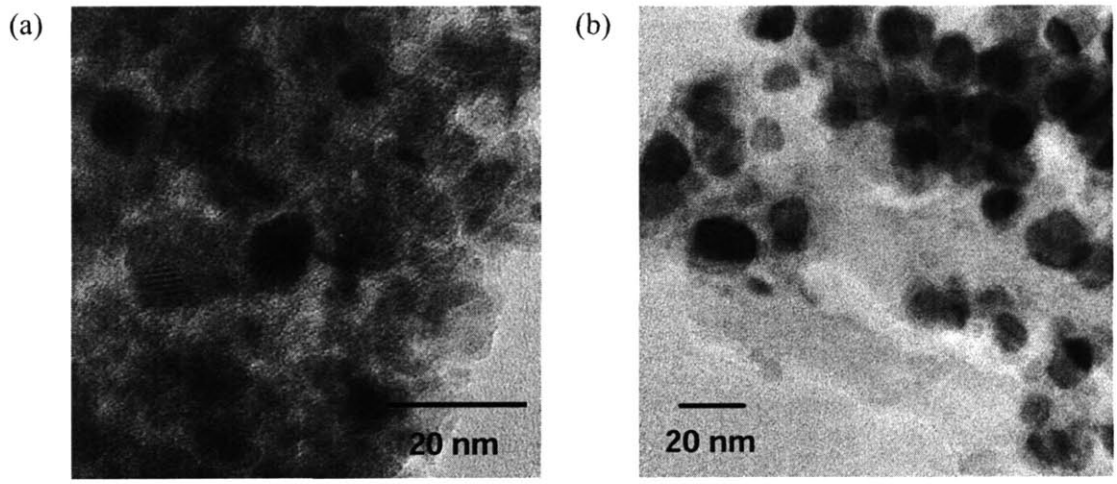

Figure 3.30 TEM images of nickel aluminate with Ni/Al = 1.10 (a) before and (b) after reaction at 600°C. Catalytic testing was performed with a feed of 10% C_3H_8 in N_2 and H_2O at 70,000 h^{-1} and $H_2O/C = 1$.

3.3.5 Mechanistic Analysis of Propane Steam Reforming

The kinetics and mechanism of steam reforming of hydrocarbons over various catalysts have been discussed in the literature [7, 10, 18-27]. Murthy's research [24] found that calcined $NiAl_2O_4$ showed only dehydration activity in the decomposition of 2-propanol, with Al^{3+} acting as a Lewis acid center. The reduced catalyst promoted dehydrogenation reaction instead, which was catalyzed by metallic Ni. The mechanistic study on methane steam reforming over nickel aluminates showed that the dissociative adsorption of both water and methane occurred on the same Ni site [1].

Since only C_1 products were detected in propane steam reforming over nickel aluminates, the first step of the reaction should be C_3H_8 dissociation to adsorbed CH_x. The mechanism for C_1 species formation was proposed to be selective attack by Ni on the terminal carbon by means of successive α-scission steps [10]. In addition, H_2O was adsorbed on the surface to form hydrogen and hydroxyl groups, then three different reactions could occur to generate the final products. First, H was derived from CH_x to produce H_2 and form carbon on the nickel surface. Secondly, CH_x would combine with the adsorbed H on another active site to produce CH_4. Thirdly, CO and H_2 were generated through the reaction between CH_x and adsorbed OH. CO could be further converted to CO_2 by water-gas shift reaction. Figure 3.31 illustrates the proposed reaction scheme.

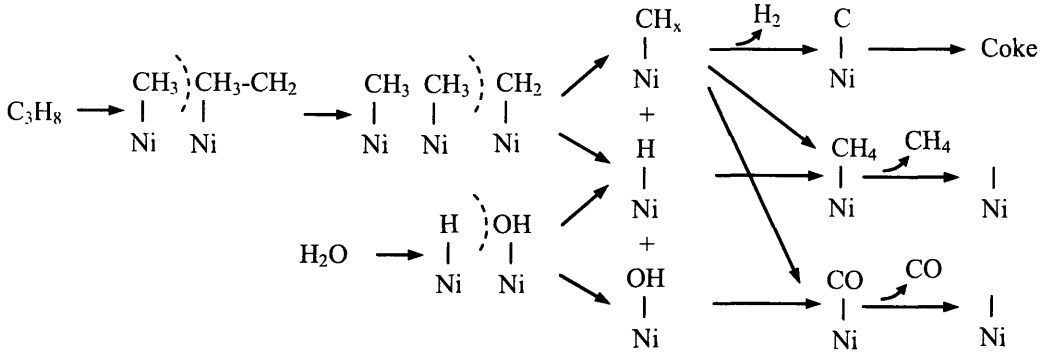

Figure 3.31 Proposed reaction scheme for propane steam reforming.

Besides the reactions discussed above, side-reactions such as propane dehydrogenation, CO and CO_2 methanation, CO disproportionation, and CH_4 and CO_2 decomposition could occur under certain conditions. Thus, the proposed scheme represented a simplified model, and more details on reaction intermediates are necessary to complete the mechanistic study.

Neither CO nor CO_2 concentration has been reported to affect the reaction rate [28, 29]. In this study, it was found that propane steam reforming was positively impacted by the introduction of CO at low temperatures (Figure 3.32). More CH_4 was formed, and more CO_2 and H_2 were produced at low temperatures (from the water-gas shift reaction) with CO introduction. The resulting H_2 helped to prevent the active sites from being oxidized, thus increasing the propane conversion at low temperatures.

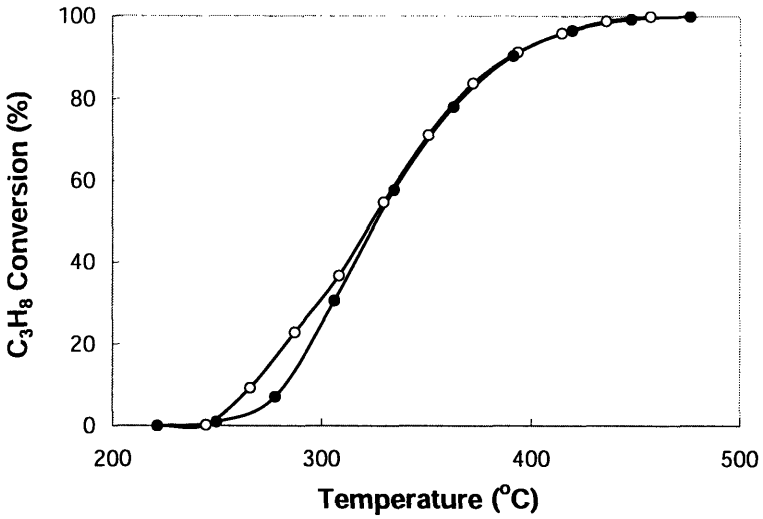

Figure 3.32 Propane conversion over 700°C-calcined nickel aluminate (Ni/Al = 1.10) (○) with and (●) without the introduction of CO (3 ml/min). Catalytic testing was performed with a feed of 10% C_3H_8 in N_2, CO and H_2O at 70,000 h^{-1} and $H_2O/C = 2$.

The introduction of H_2 (3 ml/min) improved the propane conversion rate at low temperatures (Figure 3.33). More CH_4 and less H_2 were produced at low temperatures with H_2 introduction (Figure 3.34).

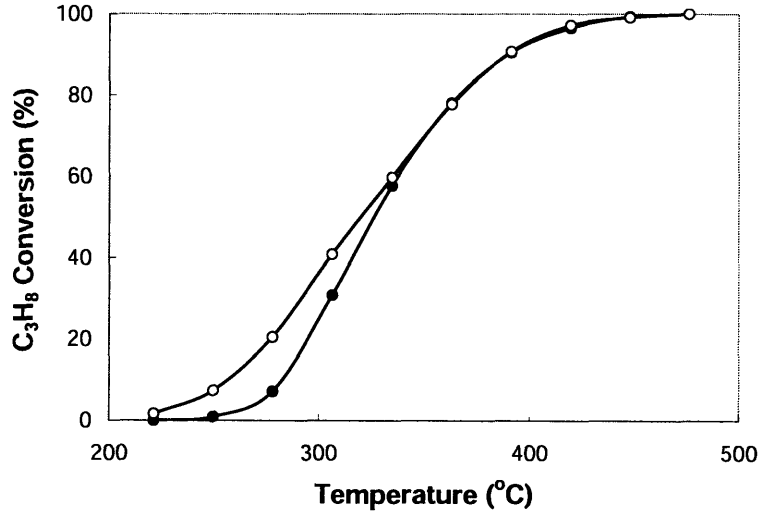

Figure 3.33 Propane conversion over 700°C-calcined nickel aluminate (Ni/Al = 1.10) (○) with and (●) without the introduction of H_2 (3 ml/min). Catalytic testing was performed with a feed of 10% C_3H_8 in N_2, H_2 and H_2O at 70,000 h^{-1} and $H_2O/C = 2$.

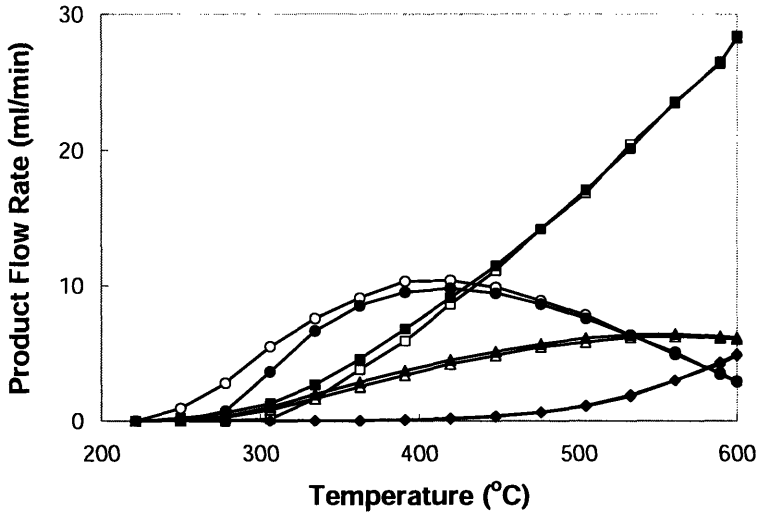

Figure 3.34 Flow rates of (■) H_2, (●) CH_4, (♦) CO and (▲) CO_2 in the steam reforming of propane (open symbols) with and (close symbols) without the introduction of H_2 (3 ml/min). Catalytic testing was performed over 700°C-calcined nickel aluminate (Ni/Al = 1.10) with a feed of 10% C_3H_8 in N_2, H_2 and H_2O at 70,000 h^{-1} and $H_2O/C = 2$.

Nickel aluminate catalyst (Ni/Al = 1.10) was also applied to the steam reforming of methane. Not surprisingly, it showed excellent activity for this reaction (see Figure 3.35). This suggested that the methane produced from the steam reforming of propane might further react over the catalytically active sites to form CO, CO_2 and H_2. The competition between the various reactions further complicated the reaction mechanism for steam reforming reaction.

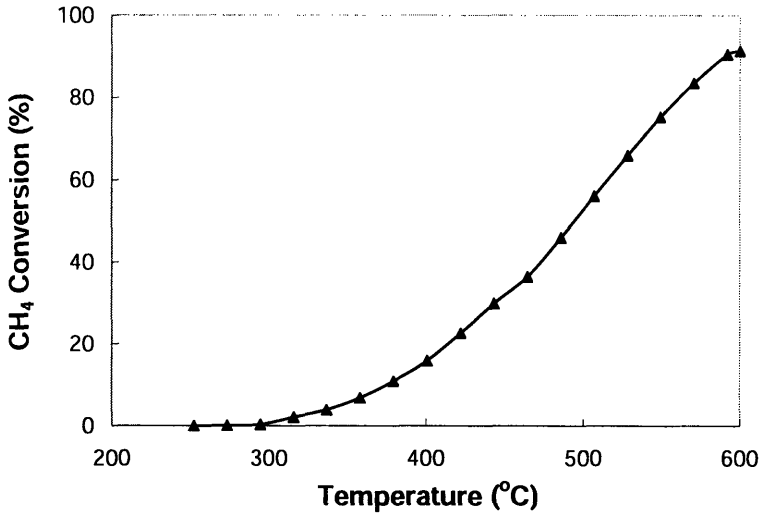

Figure 3.35 Methane conversion over 700°C-calcined nickel aluminate (Ni/Al = 1.10). Catalytic testing was performed with a feed of 35% of CH_4 in N_2 and H_2O at 130,000 h^{-1} and H_2O/C = 5.4.

3.4 Summary

Nickel aluminates showed excellent catalytic activity for propane steam reforming. Compared to Ni-poor and stoichiometric systems, Ni-rich materials provided higher catalytic activity and H_2 yield. The optimal material has a Ni/Al molar ratio of 1.10, which demonstrated the highest reducibility and Ni surface area. Active Ni nanocrystals were obtained from the reduction of nickel aluminates. Unlike conventional nickel-based systems, our catalyst was highly resistant against coke formation in the steam reforming reaction.

The optimal nickel aluminate was calcined at various temperatures. The best catalytic activity was achieved by the sample calcined at 700°C, which led to the highest Ni surface area. H_2 yield increased with increasing reaction temperature up to 700°C. The selectivity for CH_4 decreased significantly with increasing reaction temperature. The exothermic water-gas shift reaction resulted in increased selectivity for CO and decreased selectivity for CO_2 at high reaction temperatures. The H_2 yield was stably maintained over 12 h at various reaction temperatures.

The catalytic activity and H_2 yield increased slightly with increasing reduction period from 2 h to 16 h. Higher H_2O/C ratio resulted in higher H_2 yield and lower selectivity for CH_4. Coke formation was inhibited especially at high H_2O/C ratios.

3.5 References

[1] Al-Ubaid, A., Wolf, E. E., *Appl. Catal.* **40**, 73 (1988).
[2] Li, G. H., Hu, L. J., Hill, J. M., *Appl. Catal. A: Gen.* **301**, 16 (2006).
[3] Myers, D. B., "Steam Reforming of Methane with Nickel Aluminate-based Catalysts," M.S. Thesis, Massachusetts Institute of Technology, 2000.
[4] Scheffer, B., Molhoek, P., Moulijn, J. A., *Appl. Catal.* **46**, 11 (1989).
[5] Vargas, A., Maldonado, C., Montoya, J. A., Noreña, L., Morales, J., *Appl. Catal. A: Gen.* **273**, 269 (2004).
[6] Borowiecki, T., Gac, W., Denis, A., *Appl. Catal. A: Gen.* **270**, 27 (2004).
[7] Natesakhawat, S., Oktar, O., Ozkan, U. S., *J. Mol. Catal. A: Chem.* **241**, 133 (2005).
[8] Scheffer, B., Molhoek, P., Mouljin, J. A., *Appl. Catal.* **46**, 11 (1989).
[9] Ishihara, A., Qian, E. W., Finahari, I. M., Sutrisna, I. P., Kabe, T., *Fuel* **84**, 1462 (2005).
[10] Melo, F., Morlanés, N., *Catal. Today* **107–108**, 458 (2005).
[11] Rostrup-Nielsen, J. A., *J. Catal.* **33**, 184 (1974).
[12] Trimm, D. L., *Catal. Today* **49**, 3 (1999).
[13] Shamsi, A., Baltrus, J. P., Spivey, J. J., *Appl. Catal. A: Gen.* **293**, 145 (2005).
[14] Natesakhawat, S., Watson, R. B., Wang, X. Q., Ozkan, U. S., *J. Catal.* **234**, 496 (2005).
[15] Huang, T. J., Lin, H. J., Yu, T. C., *Catal. Lett.* **105**, 239 (2005).
[16] Ul-Haque, I., Trimm, D. L., US Patent 5,595,719 (1997).
[17] He, H., Ying, J.Y., to be submitted to *J. Catal.*
[18] Kolb, G., Zapf, R., Hessel, W., Löwe, H., *Appl. Catal. A: Gen.* **277**, 155 (2004).
[19] Hardiman, K. M., Ying, T. T., Adesina, A. A., Kennedy, E. M., Dlugogorski, B. Z., *Chem. Eng. J.* **102**, 119 (2004).
[20] Kasza, R. V., Griffiths, G., Shapter, J. G., Norton, P. R., Harrington, D. A., *Surf. Sci.* **356**, 195 (1996).
[21] Laosiripojana, N., Assabumrungrat, S., *Appl. Catal. A: Gen.* **290**, 200 (2005).
[22] Berman, A., Karn, P. K., Epstein, M., *Appl. Catal. A: Gen.* **282**, 73 (2005).
[23] Laosiripojana, N., Assabumrungrat, S., *Appl. Catal. B: Environ.* **60**, 107 (2005).
[24] Murthy, I. A. P. S., Swamy, C. S., *J. Mater. Sci.* **28**, 1194 (1993).
[25] Adesina, P. A. A., Trimm, D. L., Cant, N. W., *Chem. Eng. J.* **99**, 131 (2004).
[26] Ramírez-Cabrera, E., Laosiripojana, N., Atkinson, A., Chadwick, D., *Catal. Today* **78**, 433 (2003).
[27] Ramírez-Cabrera, E., Atkinson, A., Chadwick, D., *Appl. Catal. B: Environ.* **47**, 127 (2004).
[28] Rostrup-Nielsen, J. R., *J. Catal.* **31**, 173 (1973).
[29] Rostrup-Nielsen, J. R., Alstrup, I., *Catal. Today* **53**, 311 (1999).

Chapter 4. Propane Steam Reforming over Modified Nickel Aluminates

4.1 Introduction

Nickel-based catalysts are the most widely used industrial catalysts in steam reforming reactions because of their high activity and low cost. However, the coke formation on the catalysts surface can block the gas pathway, and increase the pressure drop in catalysts bed. Compared to nickel-based catalysts, noble metal systems, such as Ru, Rh, Pd and Pt, possess higher activities without coking problems, but their highly expensive nature prohibits broad industrial applications. Thus, significant efforts have been devoted towards improving the catalytic activity and coke resistance of nickel-based systems by the introduction of metal promoters. Alkaline and alkaline-earth metals are known for inhibiting coke formation by improving water adsorption [1, 2]. Group IVA and VA elements, such as Ge, Sn, Pb, As, Sb and Bi, and rare earth metals can significantly reduce coking in steam reforming reactions [2-5]. Higher catalytic activity can be achieved with the addition of Ce, Re and noble metals [6-9].

Compared to NiO/Al_2O_3, nickel aluminates have to be reduced at higher temperatures, but they possess superior coke resistance (see Chapter 3) [10]. To further improve the low-temperature activity and the coke resistance of nickel aluminates, various metal promoters were examined in this study. The effects of reaction temperature, feed composition and space velocity on the catalytic activity were investigated for nickel aluminates with selected promoters.

4.2 Experimental

4.2.1 Catalyst Synthesis

The metal promoters were introduced onto the nickel aluminate with Ni/Al = 1.10 by wet impregnation. In this research, $Sr(NO_3)_2$, VCl_3, $NbCl_5$, $TaCl_5$, $Cr(NO_3)_3{\cdot}9H_2O$, $(NH_4)_6Mo_7O_{24}$, WCl_6, $Mn(NO_3)_3$, NH_4ReO_4, $Fe(NO_3)_3{\cdot}9H_2O$, $RuCl_3$, $OsCl_3$, $Co(NO_3)_2{\cdot}6H_2O$, $Rh(NO_3)_3{\cdot}2H_2O$, $IrCl_3{\cdot}3H_2O$, $Pd(NO_3)_2$, H_2PtCl_6, $Cu(NO_3)_2{\cdot}3H_2O$, $AgNO_3$, $AuCl_3$, $SnCl_2$, $SnCl_4{\cdot}3H_2O$, $La(NO_3)_3{\cdot}6H_2O$, $Ce(NO_3)_3{\cdot}6H_2O$, and $Sm(NO_3)_3{\cdot}6H_2O$ (Alfa Aesar) were used as precursors for various promoters. Typically, 100 mg of nanocrystalline nickel aluminate with Ni/Al = 1.10 (see Chapter 3) [10] were

first dispersed in 200 ml of deionized water with stirring. The desired amount of promoter precursor was dissolved in a small amount of deionized water, and introduced to the nickel aluminate suspension. The impregnated system was heated to 50°C, and aged for 24 h. After drying at 110°C for 24 h, the powder was ground with a mortar-and-pestle, sieved to 230 mesh, and calcined at the temperatures specified.

Besides impregnation, Ru was also introduced onto nickel aluminate by vapor grafting [11]. Vapor grafting has been applied by Mehnert *et al.* to introduce highly dispersed Pd nanoclusters onto MCM-41 mesoporous silica as catalysts for the Heck reaction [12, 13]. This approach could be used for grafting various metals onto supports using the appropriate volatile organometallic complex precursor. In this work, bis(2,2,6,6-tetramethyl-3,5-heptanedionato) (1,5,-cyclo-octadiene) ruthenium(II) ($(C_{11}O_{19}O_2)_2(C_8H_{12})$Ru, 99.9%, Strem) was selected as the Ru precursor as it has a sublimation temperature as low as 100°C at 0.05 torr. Excess Ru precursor and calcined nickel aluminate were loaded at a weight ratio of 1:10 to obtain a final Ru loading of ~ 1 wt%. During the vapor grafting process, the apparatus containing Ru precursor and nickel aluminate was kept at < 0.1 torr in an oil bath at 145°C. The nickel aluminate vapor-grafted (VG) with Ru was then subjected to calcination.

4.2.2 Catalyst Characterization

The BET surface area of the catalysts was determined by nitrogen adsorption with a Micromeritics ASAP 2000 instrument. The active surface area of metal was analyzed by hydrogen chemisorption using a Micromeritics ASAP 2010 chemisorption system. Powder X-ray diffraction (XRD) was performed on a Siemens D5000 θ-θ diffractometer (45 kV, 40 mA, Cu-Kα). High-resolution transmission electron microscopy (HR-TEM) was carried out on a JEOL 2010 microscope (200 kV) equipped with a high-performance X-ray detector for energy-dispersive X-ray (EDX) spectroscopy. The catalyst composition and elemental dispersion were examined by scanning transmission electron microscopy (STEM) (Vacuum Generators HB603) and energy-dispersive X-ray (EDX) spectroscopy. For temperature-programmed reduction (TPR) studies, catalysts were pretreated in air at 500°C, and reduced by a stream of 5% H_2 in He at 30–900°C (ramp = 5°C/min). The

weight change was recorded with a Perkin Elmer System 7HT Thermal Gravimetric Analyzer (TGA).

Catalytic activity was evaluated at atmospheric pressure under steady-state in a packed-bed reactor. Typically, 50 mg of catalysts were loaded into a 1/4"-O.D. quartz reactor tube, and placed between two quartz wool plugs. Following reduction in 5% H_2 in He for 2 h at a temperature that was 50°C lower than the sample calcination temperature, 10% C_3H_8 in N_2 was introduced with H_2O at a specified H_2O/C ratio, and the reaction took place at a temperature that was 100°C lower than the sample calcination temperature. Reactants were introduced at space velocities of 70,000 h^{-1}, 120,000 h^{-1} and 350,000 h^{-1}. The product stream was analyzed by a Hewlett-Packard 6890 Gas Chromatograph (GC) equipped with molecular sieve 5A and Porapak Q chromatographic columns, which allowed CO, CO_2, CH_4, C_2H_4, C_2H_6, C_3H_6, C_3H_8, H_2 and N_2 to be separated and quantified.

4.2.3 Coking Studies

Coking studies were performed with a Perkin Elmer System 7HT TGA. The catalysts were first reduced at 650°C for 2 h, and subjected to coking under 10% C_3H_8 in N_2 at 600°C for 1 h. The coked catalysts were exposed to 5%, 10% and 20% H_2O in N_2 in a packed bed reactor at 100–800°C (ramp = 0.8°C/min). A Hewlett-Packard 6890 GC equipped with molecular sieve 5A and Porapak Q chromatographic columns was used to analyze the product stream. The coke remnants on the catalysts after gasification was evaluated by TGA with temperature-programmed oxidation (TPO) in air at 30–800°C (ramp = 5°C/min).

4.3 Results and Discussion

4.3.1 Effect of Promoters

4.3.1.1 Screening for Catalytic Activity

The effect of promoters on the reducibility of nickel oxide has been investigated by various researchers [14-18]. Additives could be incorporated into NiO surface layers to affect the stability of Ni-O bonds, the interaction with support materials, the dissociation rate of hydrogen, and the desorption rate of H_2O.

In this study, various metals were introduced at ~ 1 wt% loading onto nickel aluminate with Ni/Al = 1.10 by wet impregnation or vapor grafting, and calcined at 700°C. The first group of promoters, Re, Rh, Pt, Ir, Pd, Ru and V, gave rise to improved reducibility (see Figure 4.1), allowing the modified catalysts to be reduced at a temperature of ~ 50°C lower than the unmodified nickel aluminate with Ni/Al = 1.10. Their low-temperature peak was more intense, and shifted to a lower temperature.

In contrast, the second group of promoters, Fe, La, Co, Mn, Os, Sr and Ce, showed less impact on the reducibility of nickel aluminate (see Figure 4.2). The modified catalysts were reduced at a temperature of ~ 20°C lower than the unmodified nickel aluminate. Their low-temperature peak was similar to that of the unmodified catalyst. The third group of promoters, Ta, Mo, Cr, Au, Sm, Nb, Cu, W, Sn and Ag, showed either negligible or negative impact on the catalyst reducibility (Figure 4.3).

Figure 4.4 compares the steam reforming light-off temperatures (corresponding to 10% propane conversion) over nickel aluminate (with Ni/Al = 1.10) with the first group of promoters. The decreased light-off temperature was consistent with the increased active surface area due to the improved reducibility associated with this group of additives. Compared to the unmodified catalyst, Re-promoted catalyst lowered the light-off temperature by 20°C. The catalysts with the first group of promoters also offered higher H_2 yield and lower CH_4 selectivity compared to unmodified nickel aluminate (see Figure 4.5), as the higher active surface area facilitated carbon oxidation to generate more H_2.

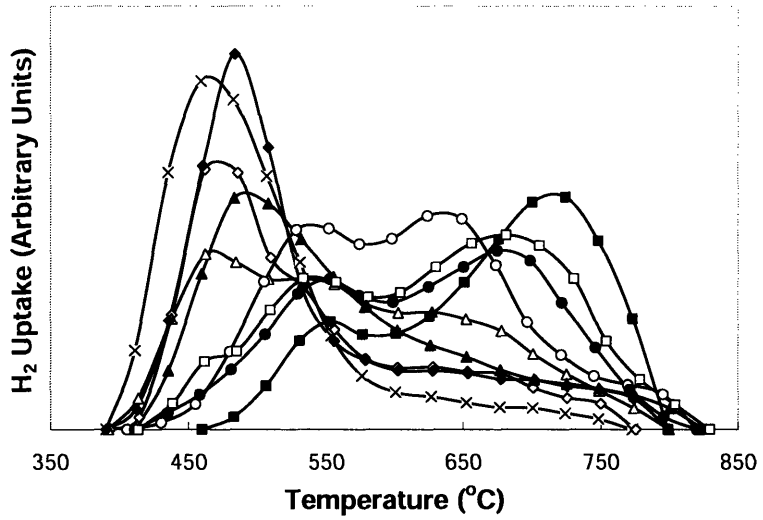

Figure 4.1 TPR profiles of nickel aluminate with Ni/Al = 1.10 and (■) no promoter, and 1 wt% of (×) Re, (Δ) Rh, (♦) Pt, (▲) Ir, (◊) Pd, (●) vapor-grafted Ru, (○) Ru and (□) V, after calcination at 700°C in air.

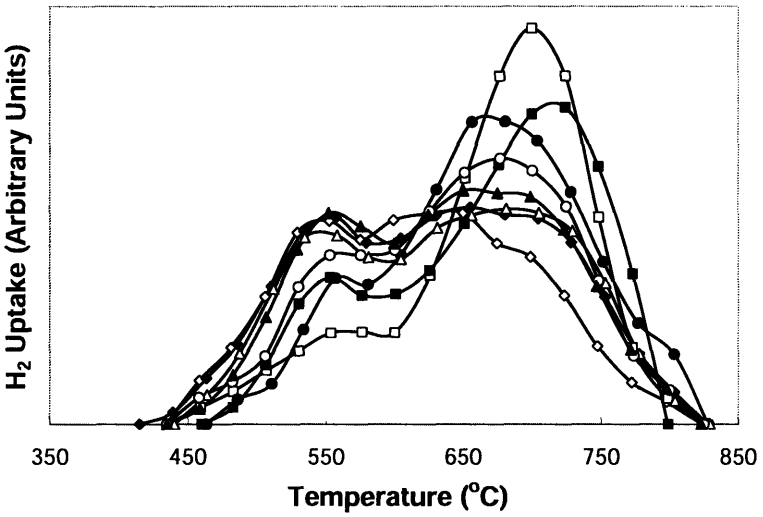

Figure 4.2 TPR profiles of nickel aluminate with Ni/Al = 1.10 and (■) no promoter, and 1 wt% of (◊) Fe, (□) La, (○) Co, (♦) Mn, (●) Os, (Δ) Sr and (▲) Ce, after calcination at 700°C in air.

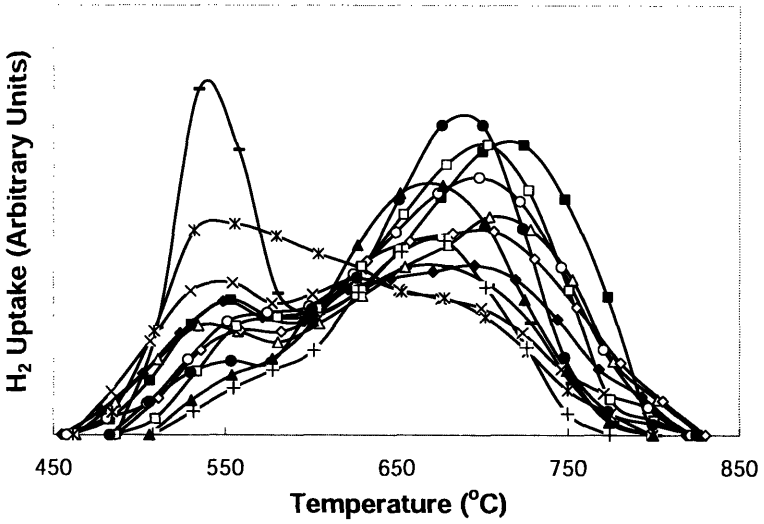

Figure 4.3 TPR profiles of nickel aluminate with Ni/Al = 1.10 and (■) no promoter, and 1 wt% of (×) Ta, (□) Mo, (○) Cr, (◊) Au, (▲) Sm, (♦) Nb, (*) Cu, (●) W, (Δ) Sn(II), (+) Sn(IV) and (–) Ag, after calcination at 700°C in air.

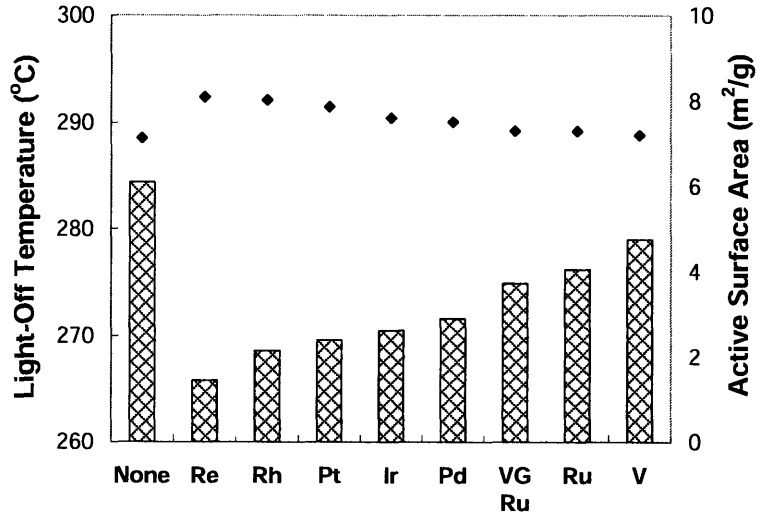

Figure 4.4 (▩) Light-off temperature in propane steam reforming and (♦) active surface area of nickel aluminate with Ni/Al = 1.10 and 1 wt% of the promoter specified, after calcination at 700°C in air. Catalytic testing was performed with a feed of 10% C_3H_8 in N_2 and H_2O at 70,000 h^{-1} and $H_2O/C = 2$.

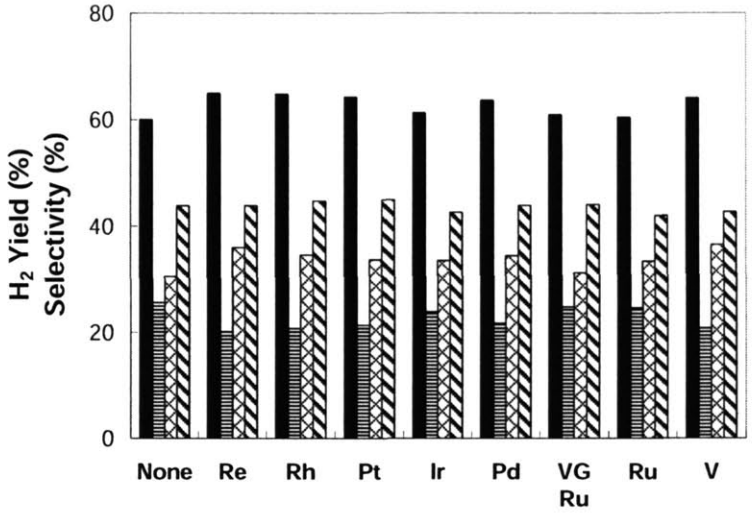

Figure 4.5 (■) H_2 yield, and selectivities for (▤) CH_4, (▩) CO and (▨) CO_2 over nickel aluminate with Ni/Al = 1.10 and 1 wt% of the promoter specified. Propane steam reforming was performed with a feed of 10% C_3H_8 in N_2 and H_2O at 600°C, 70,000 h^{-1} and $H_2O/C = 2$.

The second group of promoters showed minor effect on the active surface area and catalytic activity in propane steam reforming (Figure 4.6). The third group of promoters led to lower catalytic activity compared to the unmodified nickel aluminate (Figure 4.7).

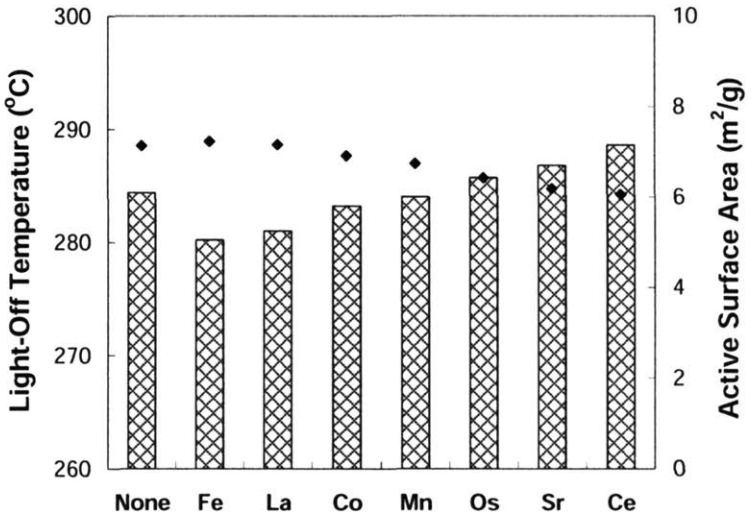

Figure 4.6 (▩) Light-off temperature in propane steam reforming and (♦) active surface area of nickel aluminate with Ni/Al = 1.10 and 1 wt% of the promoter specified, after calcination at 700°C in air. Catalytic testing was performed with a feed of 10% C_3H_8 in N_2 and H_2O at 70,000 h^{-1} and $H_2O/C = 2$.

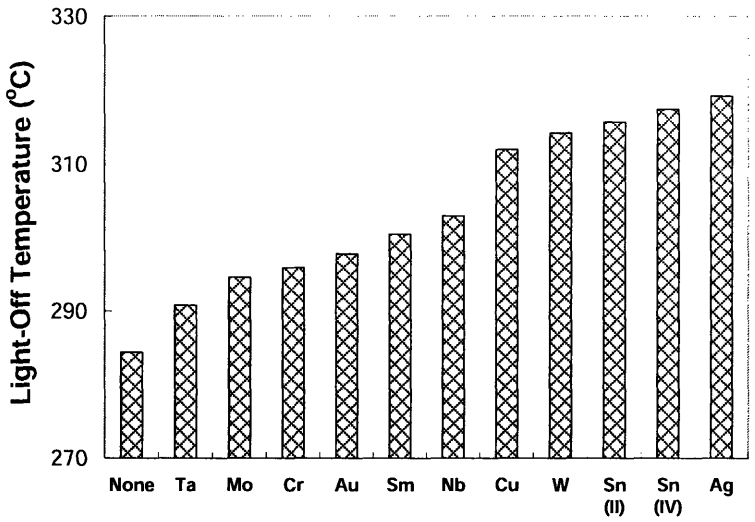

Figure 4.7 Light-off temperature in propane steam reforming over nickel aluminate with Ni/Al = 1.10 and 1 wt% of the promoter specified, after calcination at 700°C in air. Catalytic testing was performed with a feed of 10% C_3H_8 in N_2 and H_2O at 70,000 h^{-1} and $H_2O/C = 2$.

4.3.1.2 Effect of Selected Promoters on Catalytic Activity

The first group of promoters gave rise to some improvement in catalytic activity. This benefit was not significant in the 700°C-calcined catalysts. To examine the modified catalysts in more detail, they were calcined at 600°C and tested for propane steam reforming. Figure 4.8 shows that only the Ru-modified catalyst formed a detectable separate phase, RuO_2, especially when the Ru was vapor-grafted. Other modified catalysts only showed similar XRD peaks as the nickel aluminate with Ni/Al = 1.10, due to the high dispersion of their metal additives. Table 4.1 illustrates that the grain size of NiO was not significantly affected by the impregnation or vapor grafting of promoters, and the subsequent calcination process.

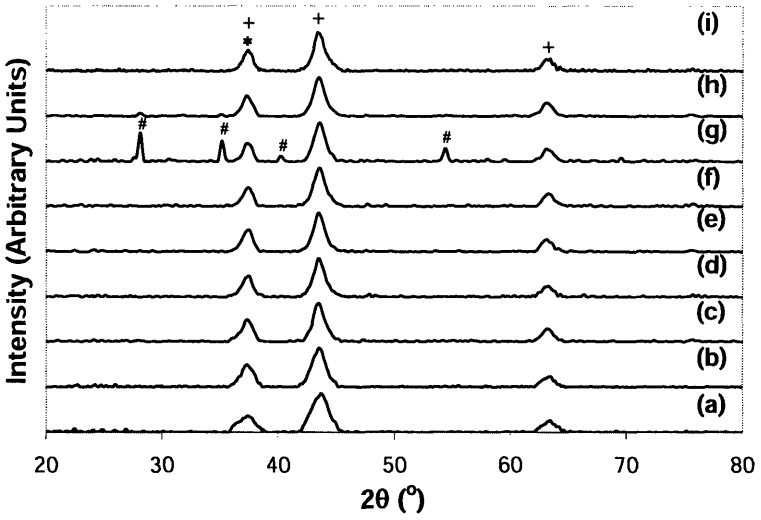

Figure 4.8 XRD patterns of nickel aluminate with Ni/Al = 1.10 and (a) no promoter, and 1 wt% of (b) Re, (c) Rh, (d) Pt, (e) Ir, (f) Pd, (g) vapor-grafted Ru, (h) Ru and (i) V, after calcination at 600°C in air. XRD peaks of $NiAl_2O_4$, NiO and RuO_2 are denoted by *, + and #, respectively.

Table 4.1 NiO grain size of nickel aluminate with Ni/Al = 1.10 and 1 wt% of the promoter specified, after calcination at 600°C.

Promoter	NiO Grain Size (nm)
—	7.7
Re	7.8
Rh	8.5
Pt	8.9
Ir	8.8
Pd	9.2
VG Ru	8.6
Ru	10.1
V	8.9

Figure 4.9 indicates that the reducibility was improved significantly by the introduction of promoters, especially Re. The modified catalysts were reduced at a temperature of 50–100°C lower than the unmodified nickel aluminate with Ni/Al = 1.10. Their low-temperature peak was substantially more intense, and shifted to a lower temperature. Compared to the 700°C-calcined catalysts (Figure 4.1), the 600°C-calcined catalysts showed greater reducibility.

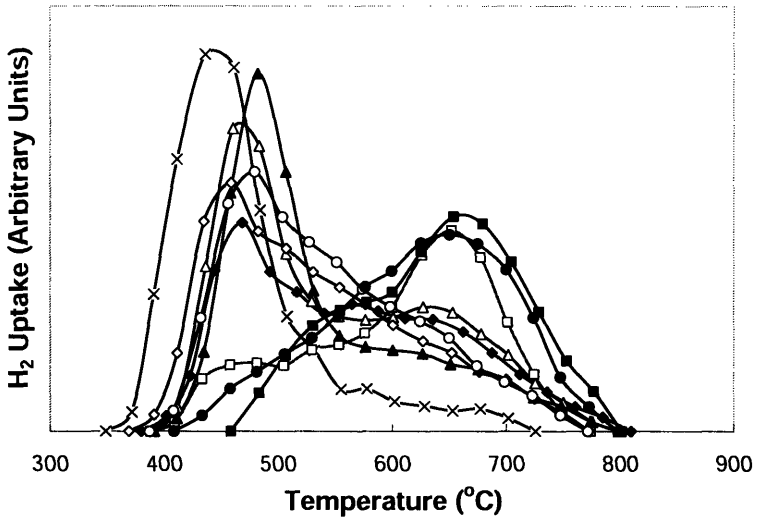

Figure 4.9 TPR profiles of nickel aluminate with Ni/Al = 1.10 and (■) no promoter, and 1 wt% of (×) Re, (◊) Rh, (▲) Pt, (○) Ir, (Δ) Pd, (□) vapor-grafted Ru, (♦) Ru and (●) V, after calcination at 600°C.

Figure 4.10 showed that the promoters resulted in modified catalysts with a substantially higher active surface area, especially in the case of Re. For the Re-modified catalyst, the 600°C-calcined sample showed a higher active surface area than the 700°C-calcined sample (Figure 4.4).

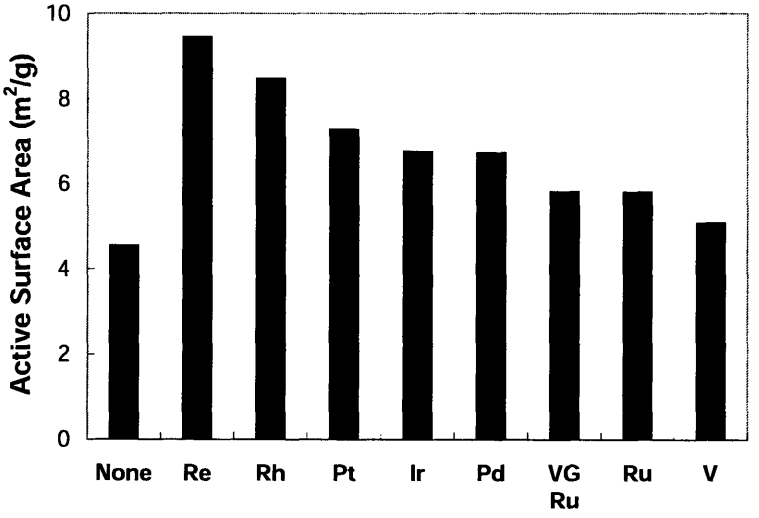

Figure 4.10 Active surface area of nickel aluminate with Ni/Al = 1.10 and 1 wt% of the promoter specified, after calcination at 600°C in air.

Due to the increased active surface area, both the catalytic activity and H_2 yield were enhanced significantly by introducing the promoters, in the order of Re > Rh > Pt > Ir > Pd > vapor-grafted Ru > Ru > V (see Figures 4.11 and 4.12). In particular, the light-off temperature was decreased by over 50°C and the H_2 yield was increased by 6.4% with the addition of Re.

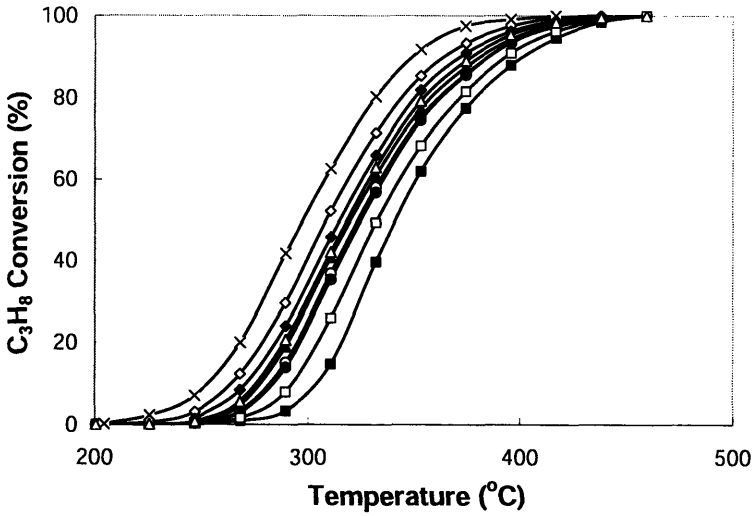

Figure 4.11 Propane conversion over nickel aluminate with Ni/Al = 1.10 and (■) no promoter, and 1 wt% of (×) Re, (◊) Rh, (♦) Pt, (Δ) Ir, (▲) Pd, (○) vapor-grafted Ru, (●) Ru and (□) V, after calcination at 600°C in air. Catalytic testing was performed with a feed of 10% C_3H_8 in N_2 and H_2O at 70,000 h^{-1} and $H_2O/C = 2$.

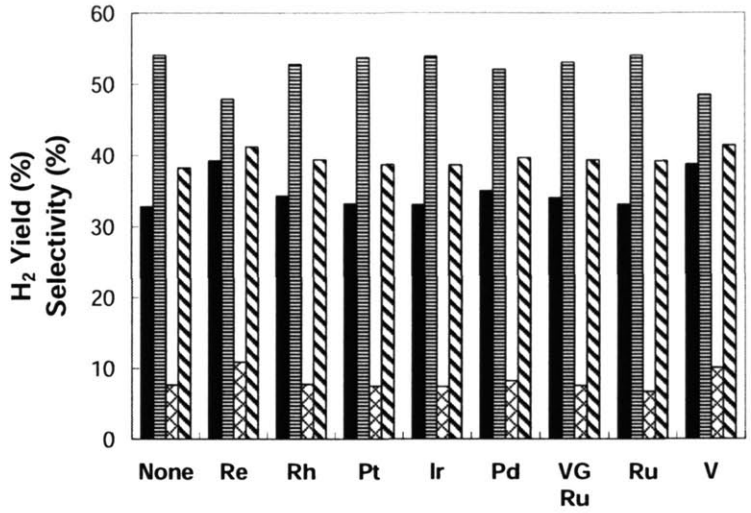

Figure 4.12 (■) H_2 yield, and selectivities for (▤) CH_4, (▩) CO and (▨) CO_2 over nickel aluminate with Ni/Al = 1.10 and 1 wt% of the promoter specified. Propane steam reforming was performed with a feed of 10% C_3H_8 in N_2 and H_2O at 500°C, 70,000 h^{-1} and $H_2O/C = 2$.

To investigate the effect of promoter loading, 2 wt% of metal additives were introduced to nickel aluminate with Ni/Al = 1.10. Figures 4.13 and 4.14 show that 1 wt% Re-promoted catalyst gave superior propane conversion and H_2 yield, compared to the various catalysts with 2 wt% promoters.

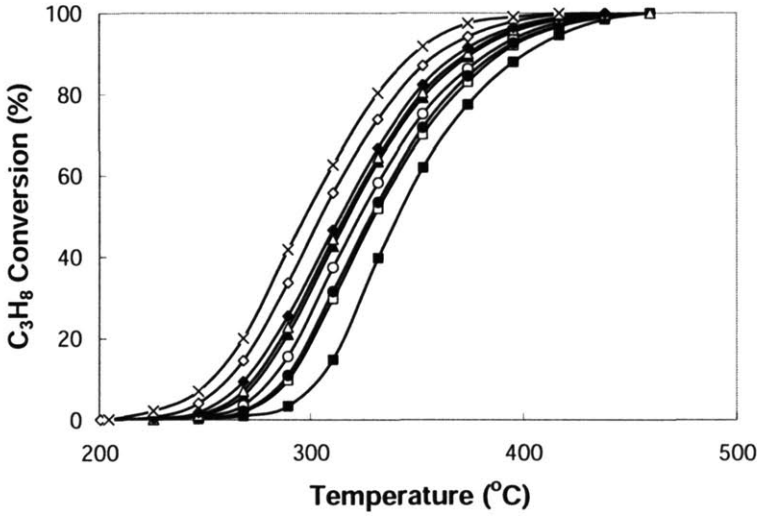

Figure 4.13 Propane conversion over nickel aluminate with Ni/Al = 1.10 and (■) no promoter, (×) 1 wt% of Re, and 2 wt% of (◊) Re, (♦) Ru, (Δ) Ir, (▲) Rh, (○) Pt, (●) V and (□) Pd, after calcination at 600°C in air. Catalytic testing was performed with a feed of 10% C_3H_8 in N_2 and H_2O at 70,000 h^{-1} and $H_2O/C = 2$.

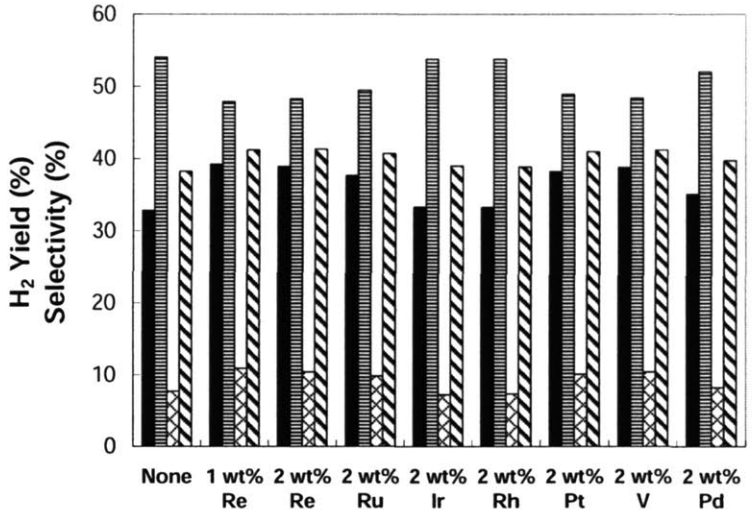

Figure 4.14 (■) H_2 yield, and selectivities for (▤) CH_4, (▩) CO and (▨) CO_2 over nickel aluminate with Ni/Al = 1.10 and the promoter specified. Propane steam reforming was performed with a feed of 10% C_3H_8 in N_2 and H_2O at 500°C, 70,000 h^{-1} and $H_2O/C = 2$.

To further improve the catalytic activity, 1 wt% of a second promoter was introduced to 1 wt% Re-promoted nickel aluminate. The results showed that Re,Ru-promoted system provided the highest catalytic activity of the systems examined. The Re,Ru-modified nickel aluminate (Ni/Al = 1.10) was then further optimized, and the results showed that 2 wt% Re,2 wt% Ru-promoted system had the highest catalytic activity. Therefore, 2 wt% of various second promoters were introduced to 2 wt% Re-modified nickel aluminate (Ni/Al = 1.10). Of the various metals examined as the second promoter, Ru was confirmed to possess superior catalytic activity (Figure 4.15). However, 2 wt% Re,2 wt% Ru-promoted nickel aluminate was still not competitive with 1 wt% Re-promoted nickel aluminate in catalytic activity and H_2 yield (see Figures 4.15 and 4.16).

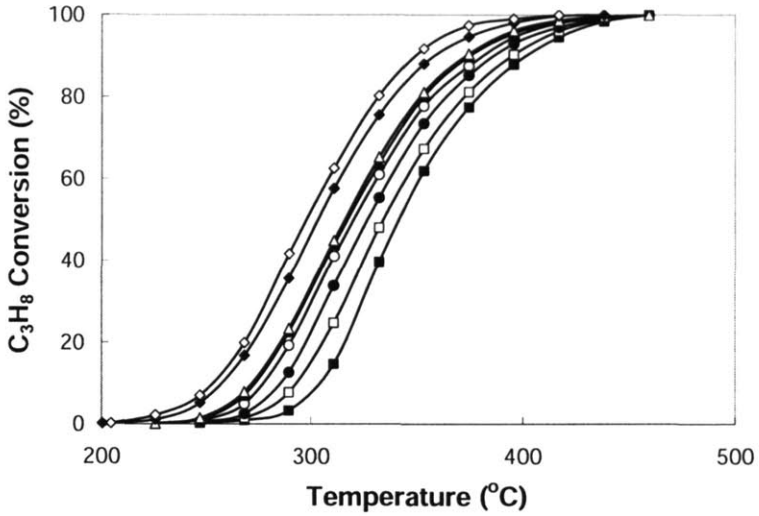

Figure 4.15 Propane conversion over nickel aluminate with Ni/Al = 1.10 and (■) no promoter, (◊) 1 wt% of Re, and 2 wt% of Re + 2 wt% of (♦) Ru, (Δ) Ir, (▲) V, (○) Rh, (●) Pd and (□) Pt, after calcination at 600°C in air. Catalytic testing was performed with a feed of 10% C_3H_8 in N_2 and H_2O at 70,000 h^{-1} and $H_2O/C = 2$.

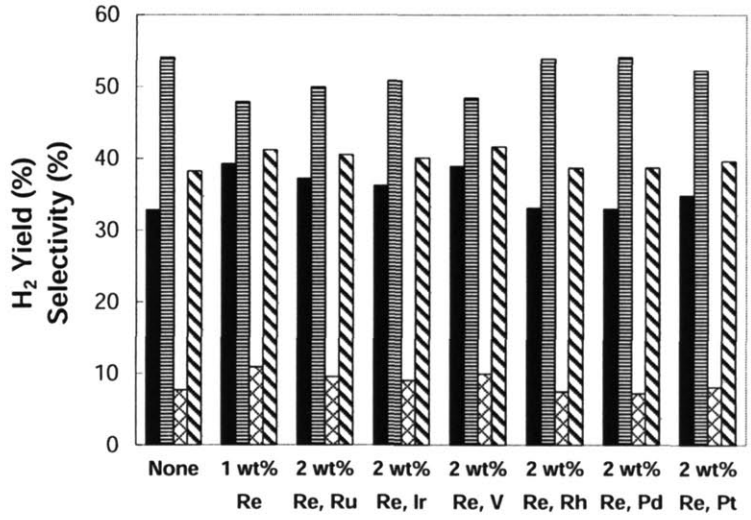

Figure 4.16 (■) H_2 yield, and selectivities for (▤) CH_4, (▩) CO and (▧) CO_2 over nickel aluminate with Ni/Al = 1.10 and the promoter(s) specified. Propane steam reforming was performed with a feed of 10% C_3H_8 in N_2 and H_2O at 500°C, 70,000 h^{-1} and $H_2O/C = 2$.

4.3.1.3 Screening for Coke Resistance

Figure 4.17 shows the coking rate during propane steam reforming at 600°C over modified nickel aluminates. Re and Rh additives had almost no effect on coking rate,

while Pt, Ir, Pd and Ru additives led to more severe coking. Coke formation was significantly inhibited with the addition of V, Mo, and W. However, we note that Mo and W showed negative impact on the catalytic activity of nickel aluminate (Figure 4.7), so they were not suitable as additives. In contrast, V successfully promoted coke resistance and catalytic activity simultaneously. Thus, V was added as a second metal to suppress coke formation in Re-modified nickel aluminate (see Section 4.3.3).

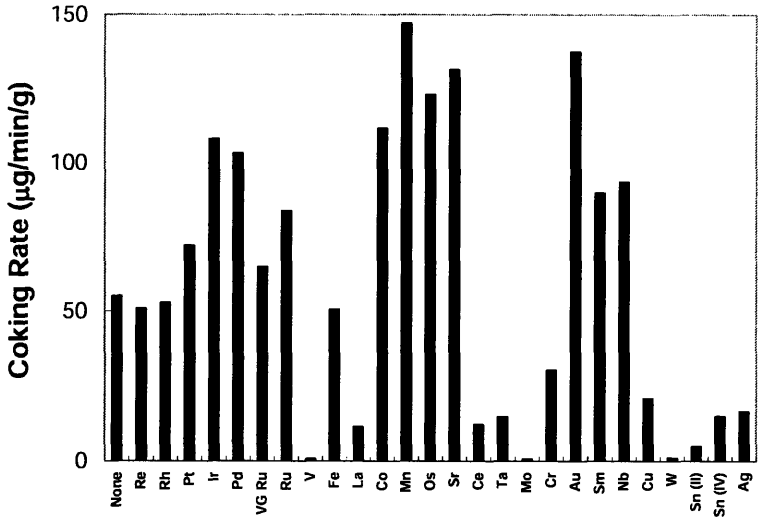

Figure 4.17 Coking rate over nickel aluminate with Ni/Al = 1.10 and 1 wt% of the promoter specified. Propane steam reforming was performed with a feed of 10% C_3H_8 in N_2 and H_2O at 600°C, 70,000 h^{-1} and $H_2O/C = 2$.

4.3.2 Re-Promoted Catalysts

4.3.2.1 Effect of Re Loading

Various loadings of Re were introduced to nickel aluminate with Ni/Al = 1.10, and calcined at 600°C to investigate the optimal Re loading. Figure 4.18 indicates that the XRD pattern of nickel aluminate was not significantly altered by Re loadings of $\leq$ 5 wt%. No separate Re-related phases were formed after the Re impregnation and subsequent calcination processes, illustrating the uniform dispersion of Re on the nickel aluminate support.

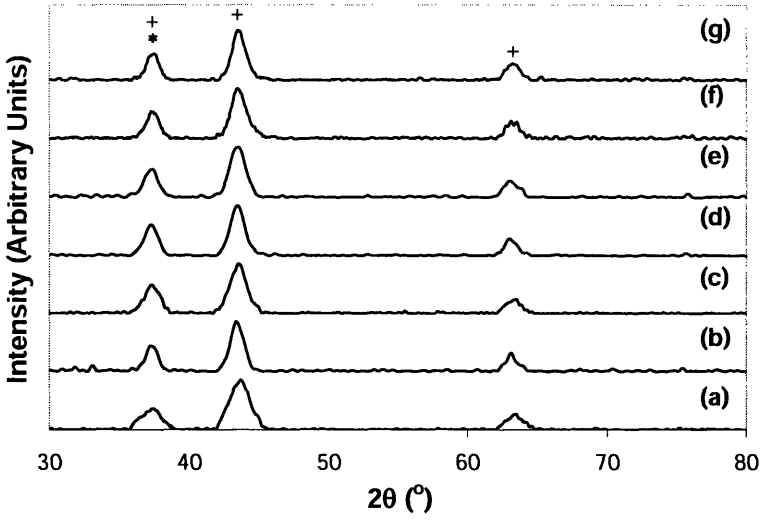

Figure 4.18 XRD patterns of nickel aluminate with Ni/Al = 1.10 and (a) 0, (b) 0.5, (c) 1, (d) 2, (e) 3, (f) 4 and (g) 5 wt% of Re, after calcination at 600°C in air. XRD peaks of $NiAl_2O_4$ and NiO are denoted by * and +, respectively.

Figure 4.19 shows that the reducibility of 600°C-calcined nickel aluminate (Ni/Al = 1.10) was improved significantly by Re introduction. However, the TPR profile was quite similar for nickel aluminates with Re loadings of 1–5 wt%. Re-promoted catalysts provided higher active surface areas than unmodified nickel aluminate (Figure 4.20). The highest active surface area was achieved at 1 wt% Re loading. Further increase in Re loading actually led to decreasing active surface area, suggesting that agglomeration might have led to reduced metal dispersion.

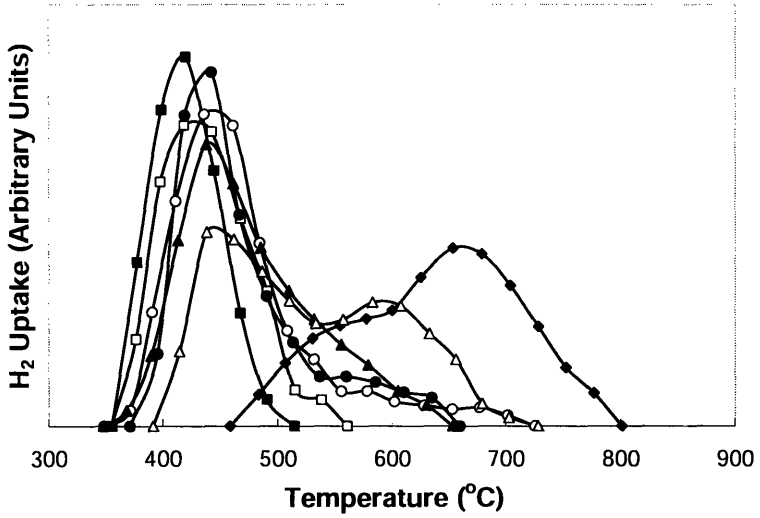

Figure 4.19 TPR profiles of nickel aluminate with Ni/Al = 1.10 and (♦) 0, (Δ) 0.5, (○) 1, (●) 2, (▲) 3, (□) 4 and (■) 5 wt% of Re, after calcination at 600°C in air.

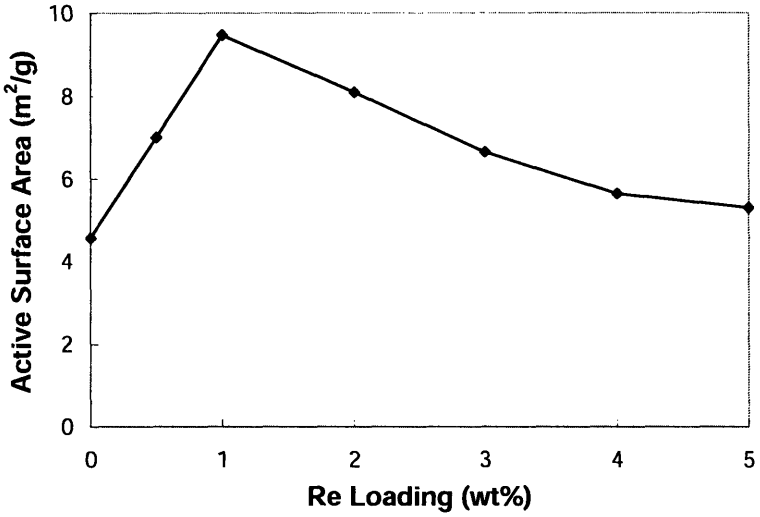

Figure 4.20 Active surface area of nickel aluminate with Ni/Al = 1.10 and the Re loading specified, after calcination at 600°C in air.

Figure 4.21 shows that 1 wt% Re-promoted catalyst provided the highest catalytic activity, with complete propane conversion at ~ 410°C. The highest H_2 yield at 500°C was also achieved by 1 wt% Re-promoted nickel aluminate (Figure 4.22). The trends of both catalytic activity and H_2 yield matched that of the active surface area shown in Figure 4.20.

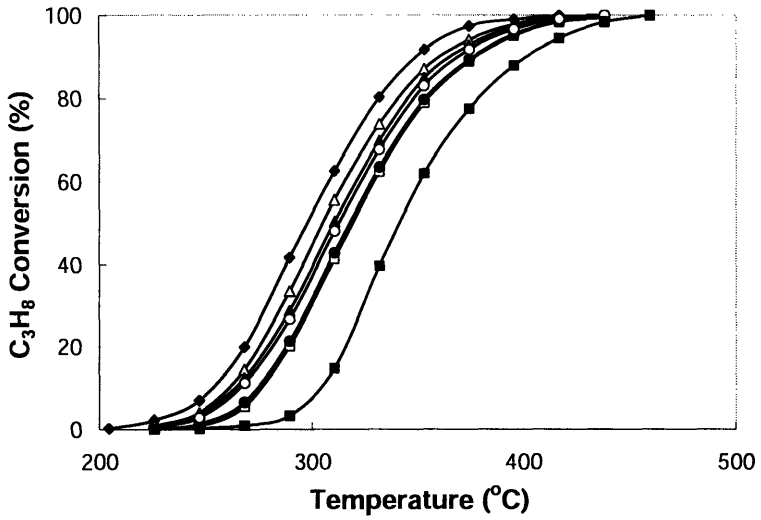

Figure 4.21 Propane conversion over nickel aluminate with Ni/Al = 1.10 and (■) 0, (▲) 0.5, (♦) 1, (Δ) 2, (○) 3, (●) 4 and (□) 5 wt% of Re, after calcination at 600°C in air. Catalytic testing was performed with a feed of 10% C_3H_8 in N_2 and H_2O at 70,000 h^{-1} and $H_2O/C = 2$.

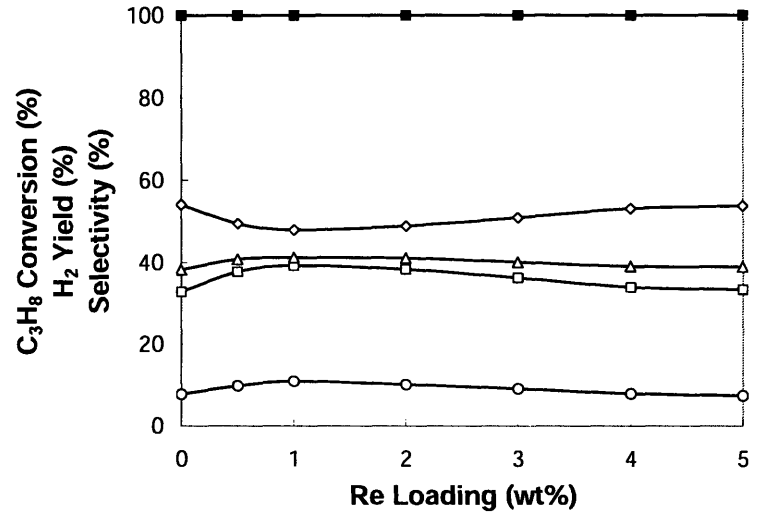

Figure 4.22 (□) H_2 yield, and selectivities for (◊) CH_4, (○) CO and (Δ) CO_2, and (■) C_3H_8 conversion over nickel aluminate with Ni/Al = 1.10 and the Re loading specified. Propane steam reforming was performed with a feed of 10% C_3H_8 in N_2 and H_2O at 500°C, 70,000 h^{-1} and $H_2O/C = 2$.

Figure 4.23 illustrates the effects of reduction, reaction and re-oxidation processes on the XRD pattern of 1 wt% Re-promoted nickel aluminate. Overlapping $NiAl_2O_4$ and NiO peaks were observed after calcination at 600°C. However, these peaks were replaced

by Ni peaks after reduction at 550°C. The Ni peaks were retained after the steam reforming reaction with minor increase in grain size (Table 4.2). The Ni phase disappeared upon re-oxidation at 800°C, which brought back $NiAl_2O_4$ and NiO phases with minor grain growth.

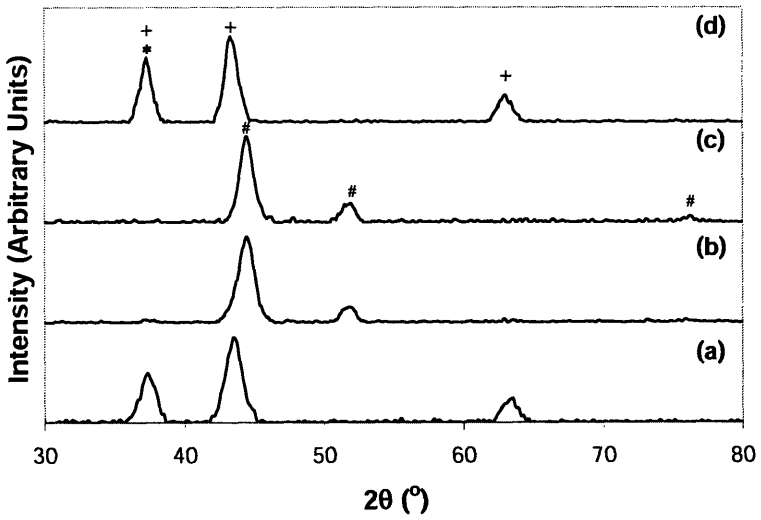

Figure 4.23 XRD patterns of 1 wt% Re-promoted nickel aluminate (Ni/Al = 1.10) after (a) calcination at 600°C, (b) reduction at 550°C, (c) reaction at 500°C, and (d) re-oxidation at 800°C. XRD peaks of $NiAl_2O_4$, NiO and Ni are denoted by *, + and #, respectively.

Table 4.2 NiO and Ni grain sizes of 1 wt% Re-promoted nickel aluminate (Ni/Al = 1.10) after calcination, reduction, reaction and re-oxidation.

Catalyst	NiO Grain Size (nm)	Ni Grain Size (nm)
Calcined at 600°C	7.8	—
Reduced at 550°C	—	6.9
Reacted at 500°C	—	8.8
Re-oxidized at 800°C	9.2	—

4.3.2.2 Effect of Calcination Temperature

In order to investigate the effect of calcination temperature, 1 wt% Re-promoted nickel aluminate (Ni/Al = 1.10) was calcined at 500–700°C. Similar XRD patterns with overlapping $NiAl_2O_4$ and NiO peaks were obtained for the catalysts calcined at different temperatures (Figure 4.24), while the grain size increased from 7.0 nm to 9.5 nm with increasing calcination temperature from 500°C to 700°C (Table 4.3).

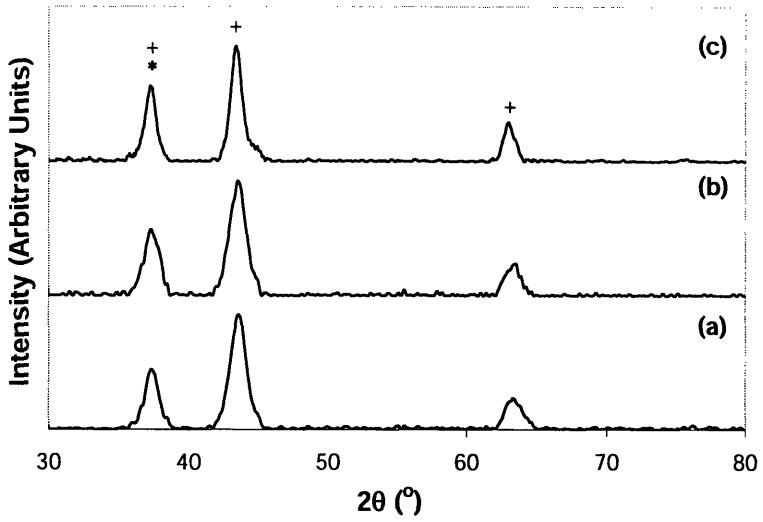

Figure 4.24 XRD patterns of 1 wt% Re-promoted nickel aluminate (Ni/Al = 1.10) after calcination at (a) 500°C, (b) 600°C and (c) 700°C. XRD peaks of $NiAl_2O_4$ and NiO and are denoted by * and +, respectively.

Table 4.3 NiO grain sizes of 1 wt% Re-promoted nickel aluminate (Ni/Al = 1.10) after calcination at various temperatures.

Calcination Temperature (°C)	NiO Grain Size (nm)
500	7.0
600	7.8
700	9.5

Figure 4.25 shows that both unmodified and 1 wt% Re-promoted nickel aluminates exhibited improved reducibility when calcined at a lower temperature. Greater reducibility was achieved with Re promoter at a given calcination temperature. This could be attributed to the increase in active surface area with 1 wt% Re addition (see Figure 4.26). The highest active surface area was achieved with the Re-promoted catalyst calcined at 600°C. The effect of Re addition on active surface area was particularly significant for samples calcined at 500°C. The presence of Re has promoted reducibility and metal dispersion, so that high temperatures were not necessary to attain those desired characteristics.

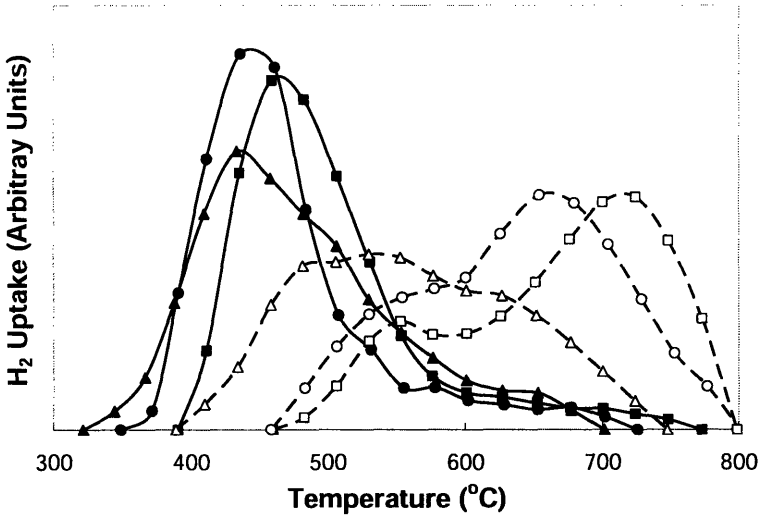

Figure 4.25 TPR profiles of nickel aluminate (Ni/Al = 1.10) with (open symbols) no promoter and (closed symbols) 1 wt% of Re, after calcination at (▲) 500°C, (●) 600°C and (■) 700°C in air.

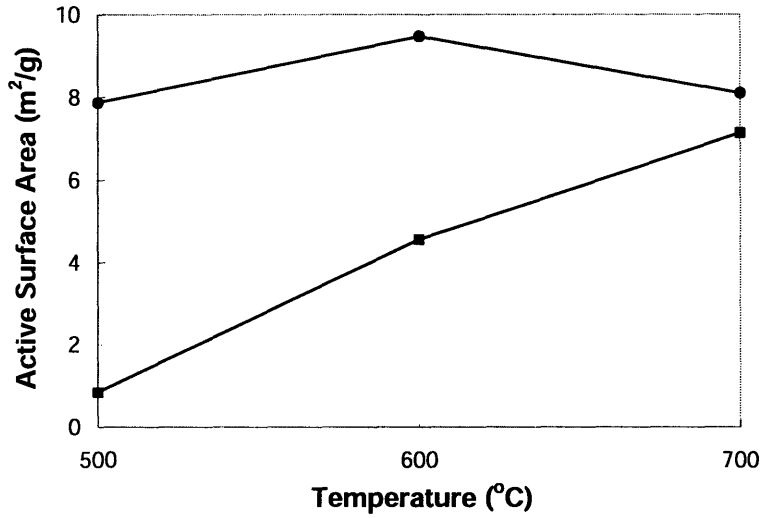

Figure 4.26 Active surface area of nickel aluminate (Ni/Al = 1.10) with (■) no promoter and (●) 1 wt% of Re, after calcination at various temperatures.

Following calcination, the nickel aluminate catalysts with and without 1 wt% of Re was reduced at a temperature that was 50°C lower than the calcination temperature. Figure 4.27 shows that Re-promoted catalyst outperformed the unmodified nickel aluminate. The trend in catalytic activity matched that of the active surface area in Figure 4.26. The Re-promoted nickel aluminate calcined at 600°C gave rise to the highest catalytic activity as it

possessed the highest active surface area. Figure 4.28 shows the effect of Re on the product compositions at various reaction temperatures. Not surprisingly, Re addition improved the production of H_2, especially at lower temperatures.

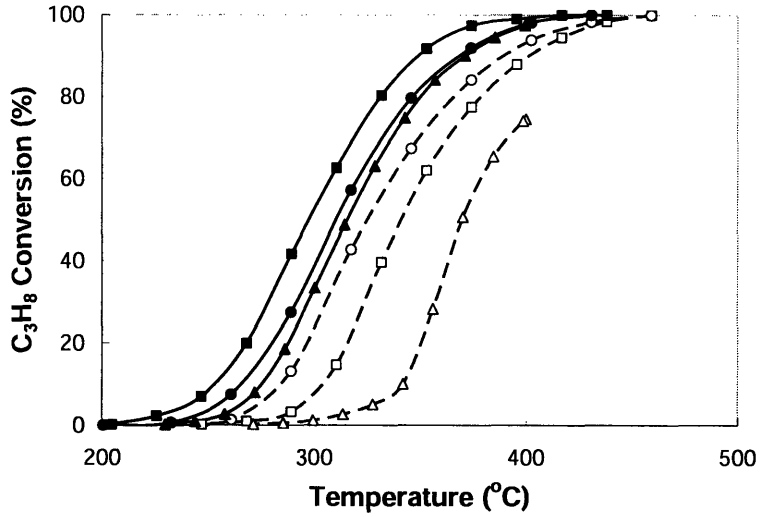

Figure 4.27 Propane conversion over nickel aluminate (Ni/Al = 1.10) with (open symbols) no promoter and (closed symbols) 1 wt% of Re, after calcination at (▲) 500°C, (■) 600°C and (●) 700°C in air. Catalytic testing was performed with a feed of 10% C_3H_8 in N_2 and H_2O at 70,000 h^{-1} and $H_2O/C = 2$.

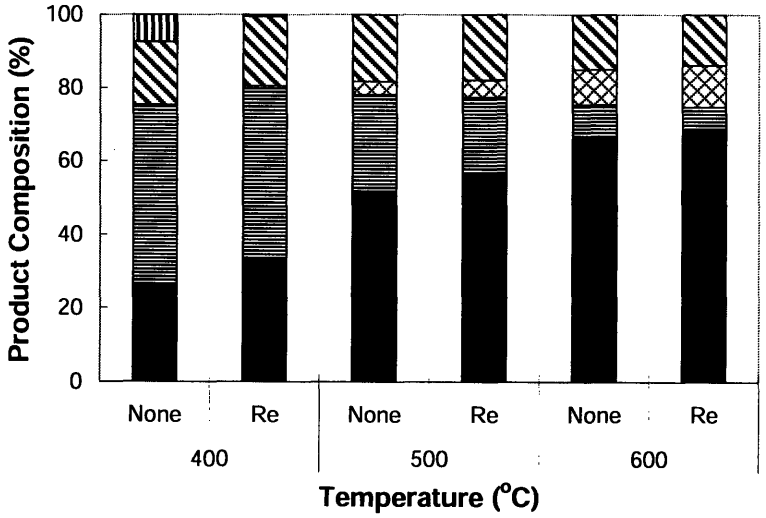

Figure 4.28 (■) H_2, (▤) CH_4, (▩) CO, (▧) CO_2 and (▥) C_3H_8 composition in the product stream of propane steam reforming over nickel aluminate (Ni/Al = 1.10) with no promoter or 1 wt% of Re. Catalytic testing was performed with a feed of 10% C_3H_8 in N_2 and H_2O at the temperature specified, 70,000 h^{-1} and $H_2O/C = 2$.

The stability of 1 wt% Re-promoted nickel aluminate in propane steam reforming was examined at 500°C. Figure 4.29 illustrates that the catalytic performance of this system was successfully maintained over 12 h.

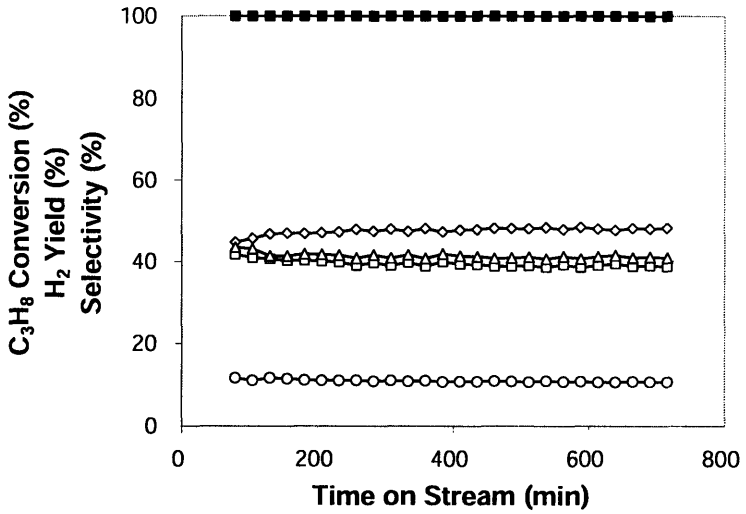

Figure 4.29 (□) H_2 yield, selectivities for (◊) CH_4, (○) CO and (Δ) CO_2, and (■) C_3H_8 conversion as a function of time over 1 wt% Re-promoted nickel aluminate (Ni/Al = 1.10). Propane steam reforming was performed with a feed of 10% C_3H_8 in N_2 and H_2O at 500°C, 70,000 h^{-1} and $H_2O/C = 2$.

Figure 4.30 compares the equilibrium calculation of product composition in propane steam reforming and the experimental data obtained over 1 wt% Re-promoted nickel aluminate. Equilibrium calculation showed complete propane conversion even at temperatures as low as 200°C. Experimentally, full propane conversion was only achieved at ≥ 380°C. The equilibrium calculation and experimental data became quite consistent at temperatures above 380°C. The major differences at low temperatures could be attributed to incomplete propane conversion, which altered the product composition significantly below 380°C.

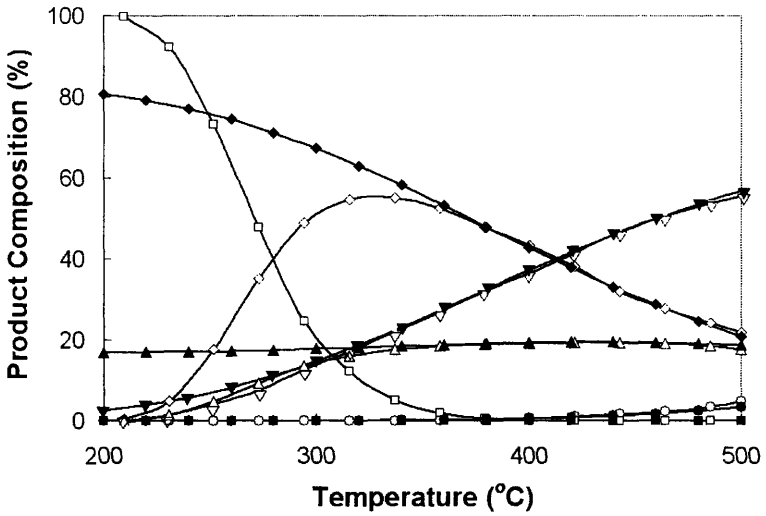

Figure 4.30 (Close symbols) Equilibrium and (open symbols) experimental product composition achieved over 1 wt% Re-promoted nickel aluminate (Ni/Al = 1.10) in propane steam reforming. The products were (▽) H_2, (◊) CH_4, (○) CO, (Δ) CO_2 and (□) C_3H_8. Catalytic testing was performed with a feed of 10% C_3H_8 in N_2 and H_2O at 70,000 h^{-1} and $H_2O/C = 2$.

4.3.2.3 Effect of Space Velocity

Figure 4.31 compares the effect of space velocity on the catalytic activity of unmodified and Re-promoted nickel aluminate in propane steam reforming. For both systems, the catalytic activity decreased with increasing space velocity due to shorter contact time. At each space velocity, the Re-promoted catalyst always provided a higher catalytic activity than the unmodified catalyst. Figure 4.32 shows the H_2 yield, selectivity for CH_4, and C_3H_8 conversion as a function of space velocity. The selectivities for CO and CO_2 were not presented in this figure as similar values were obtained at different space velocities. A higher H_2 yield was achieved with Re addition and at a lower space velocity, which corresponded to a lower selectivity for CH_4.

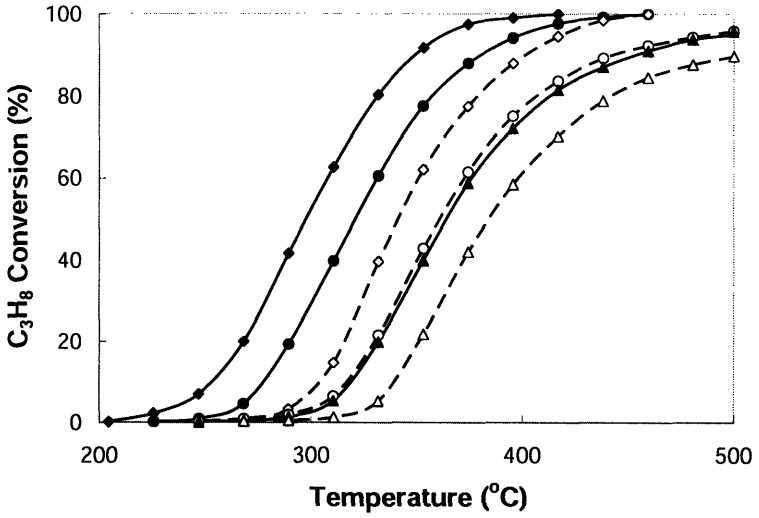

Figure 4.31 Propane conversion over nickel aluminate (Ni/Al = 1.10) with (open symbols) no promoter and (close symbols) 1 wt% of Re, after calcination at 600°C in air. Catalytic testing was performed with a feed of 10% C_3H_8 in N_2 and H_2O at (♦) 70,000 h^{-1}, (●) 120,000 h^{-1} and (▲) 350,000 h^{-1}, and $H_2O/C = 2$.

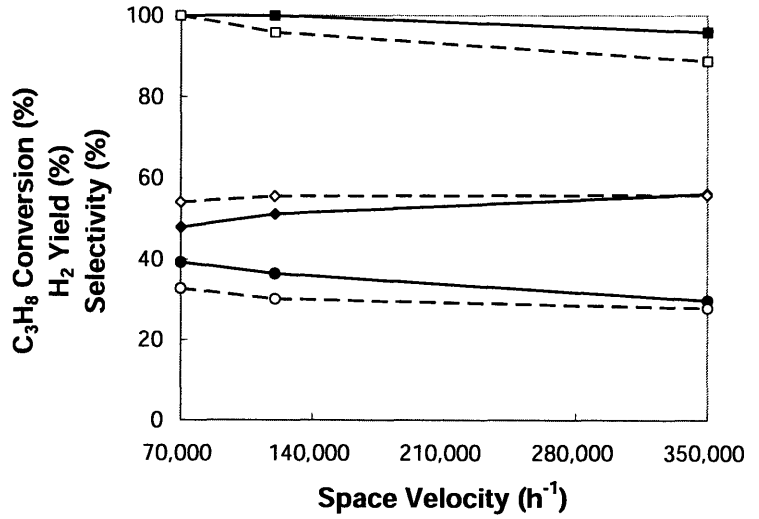

Figure 4.32 (●) H_2 yield, (♦) selectivity for CH_4, and (■) C_3H_8 conversion as a function of space velocity over nickel aluminate (Ni/Al = 1.10) with (open symbols) no promoter and (close symbols) 1 wt% of Re in propane steam reforming at 500°C. Catalytic testing was performed with a feed of 10% C_3H_8 in N_2 and H_2O at $H_2O/C = 2$.

4.3.2.4 Effect of H_2O/C Ratio

1 wt% Re-promoted nickel aluminate was examined for propane steam reforming under H_2O/C ratios of 1–6 at different temperatures. The H_2 yield obtained experimentally

was compared with the equilibrium calculations in Figure 4.33. At a H_2O/C ratio higher than 2, the experimental results matched the equilibrium calculations. The experimental values were lower than the equilibrium calculations at a low H_2O/C ratio of 1, mainly due to the significant coke formation on the catalyst surface under such condition (Figure 4.34). We note that the coking rate of Re-promoted catalyst was lower than the unmodified nickel aluminate at H_2O/C ratio = 1. The coking rate decreased significantly with increasing H_2O/C ratio. While a high H_2O/C ratio helped to inhibit coke formation, the energy cost associated with the introduction of large quantities of H_2O would make it prohibitive for industrial applications. To further improve the coke resistance of Re-promoted nickel aluminate at a low H_2O/C ratio, V was introduced and studied in propane steam reforming (Section 4.3.3).

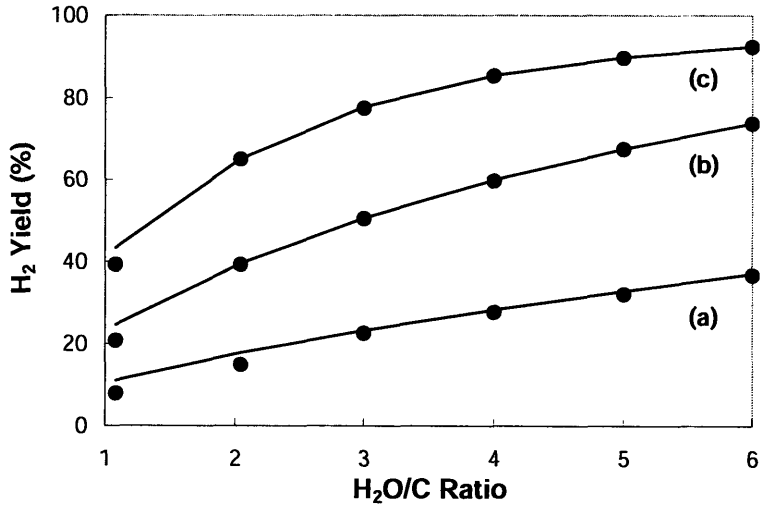

Figure 4.33 H_2 yield as a function of H_2O/C ratio in propane steam reforming over (•) 1 wt% Re-promoted nickel aluminate (Ni/Al = 1.10) at (a) 400°C, (b) 500°C and (c) 600°C. The solid lines represent the equilibrium calculation results. Catalytic testing was performed with a feed of 10% C_3H_8 in N_2 and H_2O at 70,000 h^{-1}.

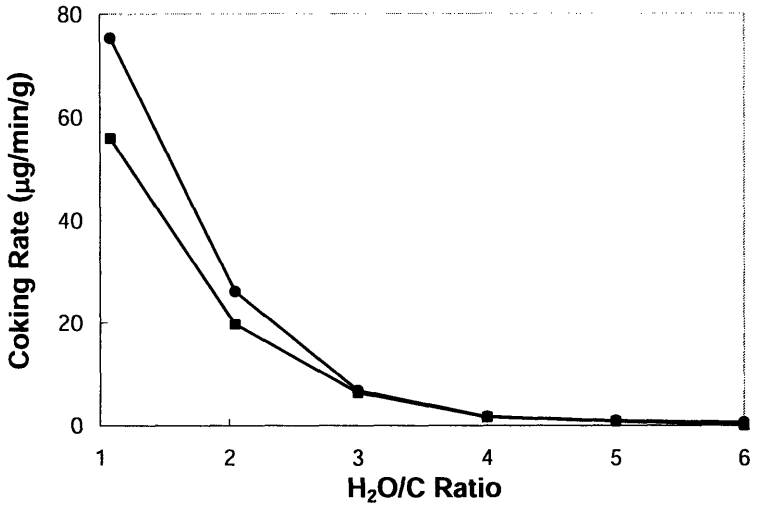

Figure 4.34 Coking rate over nickel aluminate (Ni/Al = 1.10) with (●) no promoter and (■) 1 wt% of Re. Propane steam reforming was performed with a feed of 10% C_3H_8 in N_2 and H_2O at 500°C, 70,000 h^{-1} and the H_2O/C ratio specified.

4.3.3 V-Promoted Catalysts

4.3.3.1 Optimization of V-Promoted Catalysts

Re,V-promoted nickel aluminates were examined to provide high catalytic activity and coke resistance at a low H_2O/C ratio of 1. Before optimizing the Re,V-promoted nickel aluminate system, V-promoted nickel aluminates (Ni/Al = 1.10) were studied to determine the practical range for V loading. Figure 4.35 shows the catalytic activity was not substantially affected by V loadings of 1–5 wt%. The V-promoted nickel aluminates outperformed the unmodified catalyst in propane conversion and H_2 yield, especially for the sample containing 3 wt% V (Figure 4.36). TPR studies showed that the catalyst reducibility improved with increasing V loading (Figure 4.37).

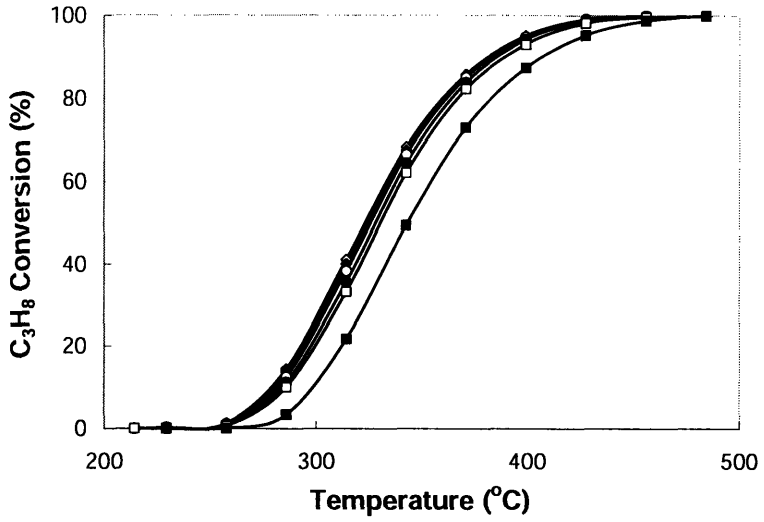

Figure 4.35 Propane conversion over nickel aluminate with Ni/Al = 1.10 and (■) 0, (□) 1, (♦) 2, (◊) 3, (○) 4 and (●) 5 wt% of V, after calcination at 700°C in air. Catalytic testing was performed with a feed of 10% C_3H_8 in N_2 and H_2O at 70,000 h^{-1} and $H_2O/C = 1$.

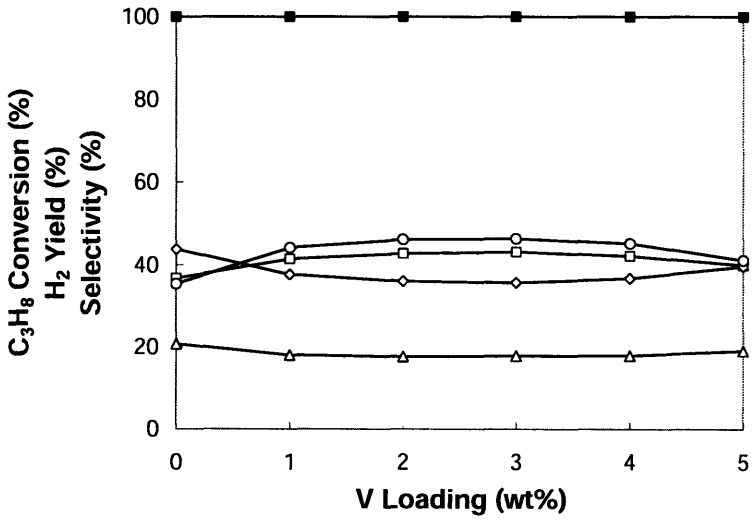

Figure 4.36 (□) H_2 yield, selectivities for (◊) CH_4, (○) CO and (Δ) CO_2, and (■) C_3H_8 conversion over nickel aluminate with Ni/Al = 1.10 and the V loading specified. Propane steam reforming was performed with a feed of 10% C_3H_8 in N_2 and H_2O at 600°C, 70,000 h^{-1} and $H_2O/C = 1$.

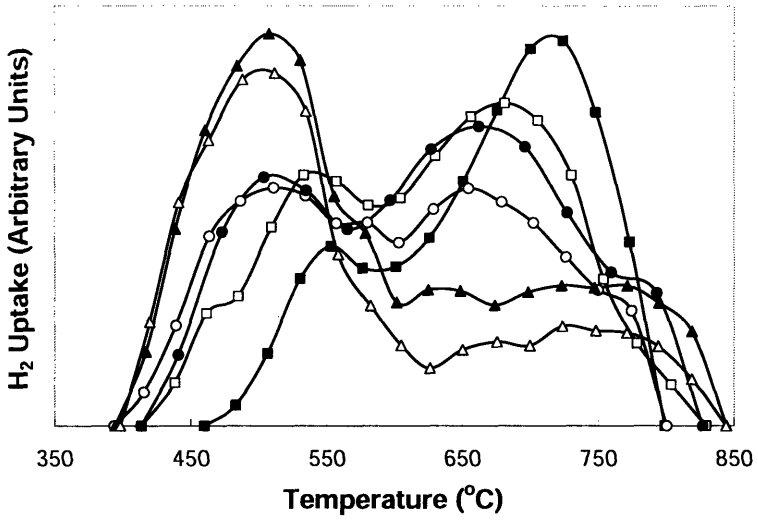

Figure 4.37 TPR profiles of nickel aluminate (Ni/Al = 1.10) with (■) 0, (□) 1, (●) 2, (○) 3, (▲) 4 and (Δ) 5 wt% of V, after calcination at 700°C in air.

The XRD patterns of 3 wt% V-promoted nickel aluminate after calcination, reduction, reaction and re-oxidation are shown in Figure 4.38. Both $NiAl_2O_4$ and NiO phases formed during calcination at 700°C were replaced by the Ni phase after reduction. Minor grain growth was observed after reaction at 600°C. Upon re-oxidation in air at 800°C, both $NiAl_2O_4$ and NiO phases re-emerged with a slightly larger grain size. Table 4.4 confirmed that the presence of V suppressed the grain growth of the nickel aluminate support and the active nickel nanocrystals during the reduction/reaction/re-oxidation processes.

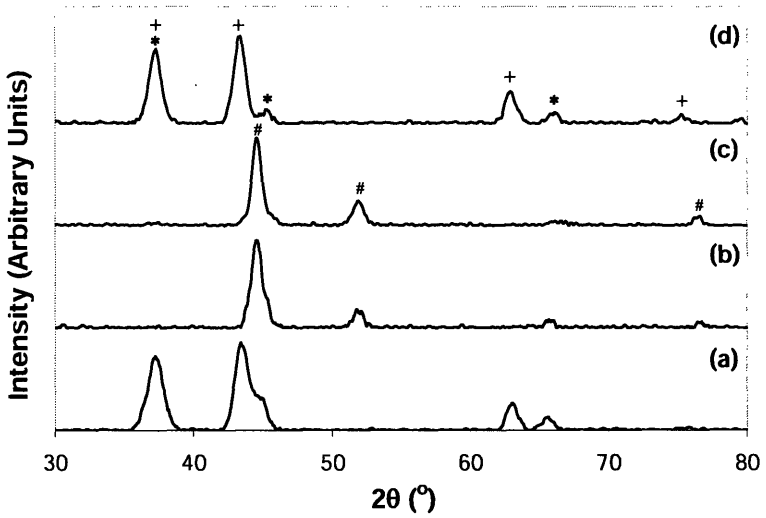

Figure 4.38 XRD patterns of 3 wt% V-promoted nickel aluminate (Ni/Al = 1.10) after (a) calcination at 700°C, (b) reduction at 650°C, (c) reaction at 600°C, and (d) re-oxidation at 800°C. XRD peaks of $NiAl_2O_4$, NiO and Ni are denoted by *, + and #, respectively.

Table 4.4 NiO and Ni grain sizes of 3 wt% V-promoted nickel aluminate (Ni/Al = 1.10) after calcination, reduction, reaction and re-oxidation.

Catalyst	NiO Grain Size (nm)	Ni Grain Size (nm)
Calcined at 700°C	11.2	—
Reduced at 650°C	—	10.8
Reacted at 600°C	—	11.8
Re-oxidized at 800°C	11.9	—

4.3.3.2 Effect of Calcination Temperature

The 3 wt% V-promoted catalyst was calcined at 600–800°C, and compared to the unmodified nickel aluminate for catalytic activity. Higher catalytic activities were always achieved over the V-promoted catalyst (see Figure 4.39). The benefit of the V promoter in improving H_2 yield was significant at lower reaction temperatures. The unmodified and V-promoted catalysts provided similarly high H_2 yield at a high reaction temperature of 700°C (Figure 4.40).

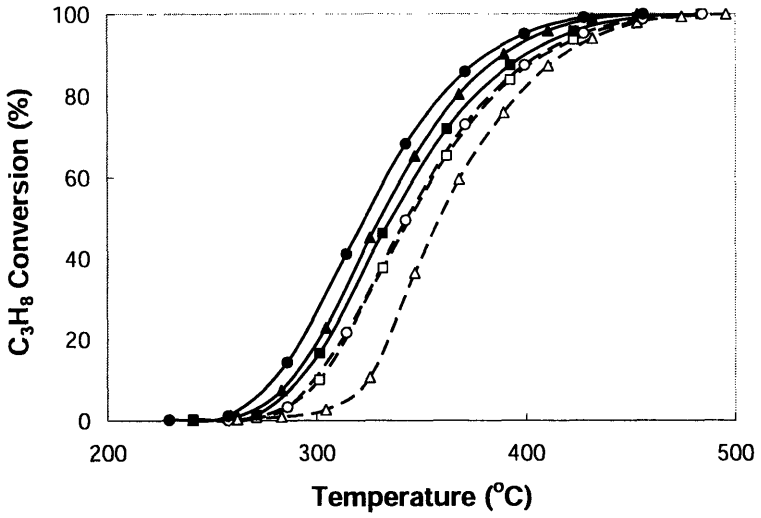

Figure 4.39 Propane conversion over nickel aluminate (Ni/Al = 1.10) with (open symbols) no promoter and (close symbols) 3 wt% of V, after calcination at (▲) 600°C, (●) 700°C and (■) 800°C in air. Catalytic testing was performed with a feed of 10% C_3H_8 in N_2 and H_2O at 70,000 h^{-1} and $H_2O/C = 1$.

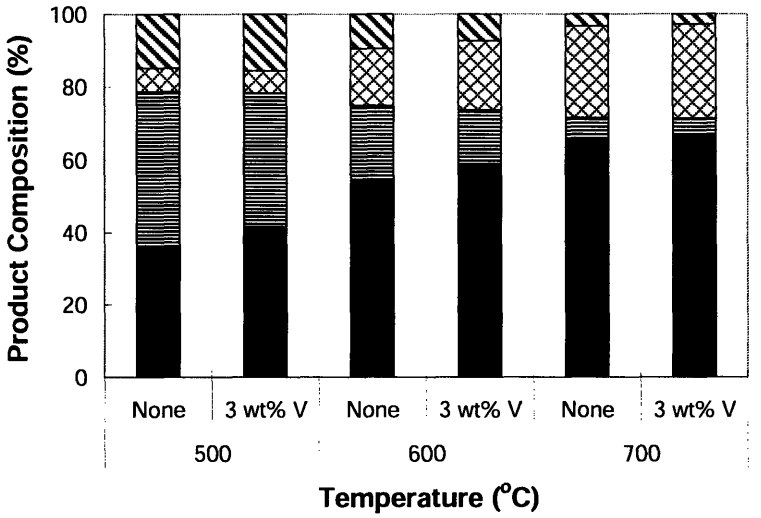

Figure 4.40 (■) H_2, (▤) CH_4, (▩) CO and (▨) CO_2 composition in the product stream of propane steam reforming over nickel aluminate (Ni/Al = 1.10) with no promoter or 3 wt% of V. Catalytic testing was performed with a feed of 10% C_3H_8 in N_2 and H_2O at the temperature specified, 70,000 h^{-1} and $H_2O/C = 1$.

Propane steam reforming was conducted over 3 wt% V-promoted nickel aluminate at 600°C and H_2O/C ratio of 1. Figure 4.41 shows that excellent catalytic activity and selectivities were stably maintained over 12 h. Remarkably, this V-promoted system was

able to achieve and maintain equilibrium H_2 yield at the low H_2O/C ratio of 1, which confirmed the superior coke resistance of the V-promoted nickel aluminate.

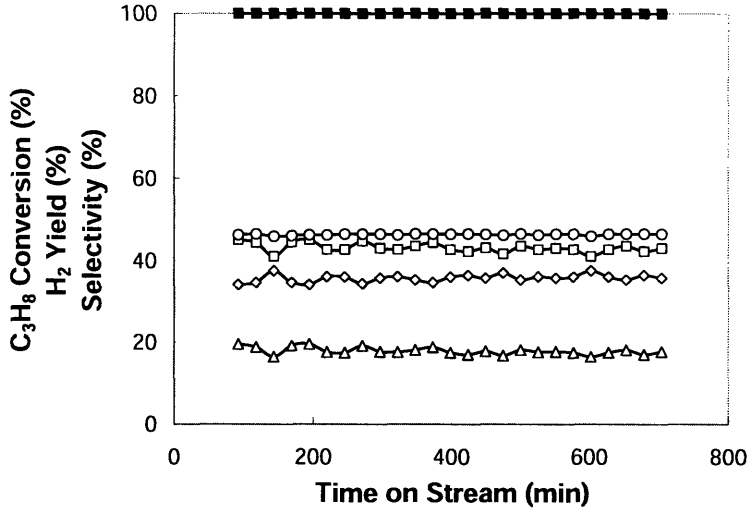

Figure 4.41 (□) H_2 yield, selectivities for (◊) CH_4, (○) CO and (Δ) CO_2, and (■) C_3H_8 conversion as a function of time over 3 wt% V-promoted nickel aluminate (Ni/Al = 1.10). Propane steam reforming was performed with a feed of 10% C_3H_8 in N_2 and H_2O at 600°C, 70,000 h^{-1} and $H_2O/C = 1$.

Figure 4.42 compares the equilibrium calculation of product composition in propane steam reforming and the experimental data obtained over 3 wt% V-promoted nickel aluminate at a H_2O/C ratio of 1. Equilibrium calculation showed that complete propane conversion could be achieved at a temperature as low as 200°C. Experimentally, however, full propane conversion was only achieved above 400°C. The equilibrium calculation and experimental data became quite similar at temperatures above 400°C. The major discrepancies at low temperatures could be attributed to incomplete propane conversion, which altered the product composition significantly below 400°C.

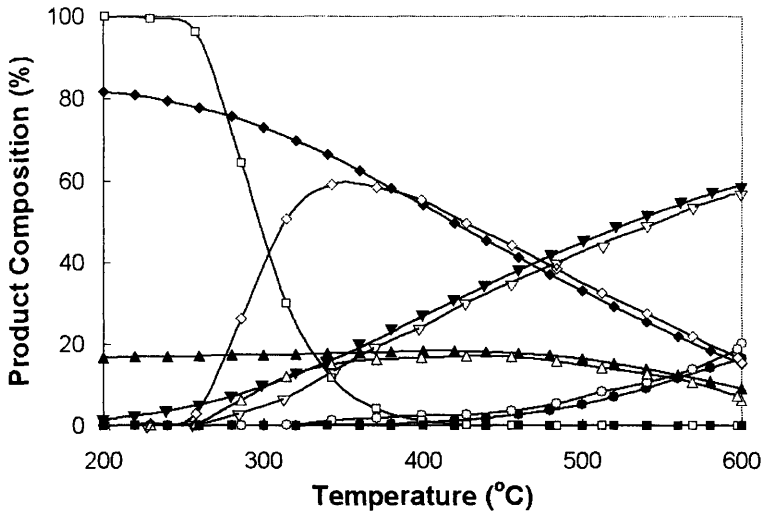

Figure 4.42 (Close symbols) Equilibrium and (open symbols) experimental product composition achieved over 3 wt% V-promoted nickel aluminate (Ni/Al = 1.10) in propane steam reforming. The products were (▽) H_2, (◊) CH_4, (○) CO, (Δ) CO_2 and (□) C_3H_8. Catalytic testing was performed with a feed of 10% C_3H_8 in N_2 and H_2O at 70,000 h^{-1} and $H_2O/C = 1$.

4.3.3.3 Effect of Space Velocity

Figure 4.43 shows that even at a high space velocity of 120,000 h^{-1}, complete propane conversion could be achieved at 485°C over the highly active, 3 wt% V-promoted nickel aluminate. Higher space velocity led to slightly lower propane conversion and H_2 yield at 600°C (Figure 4.44).

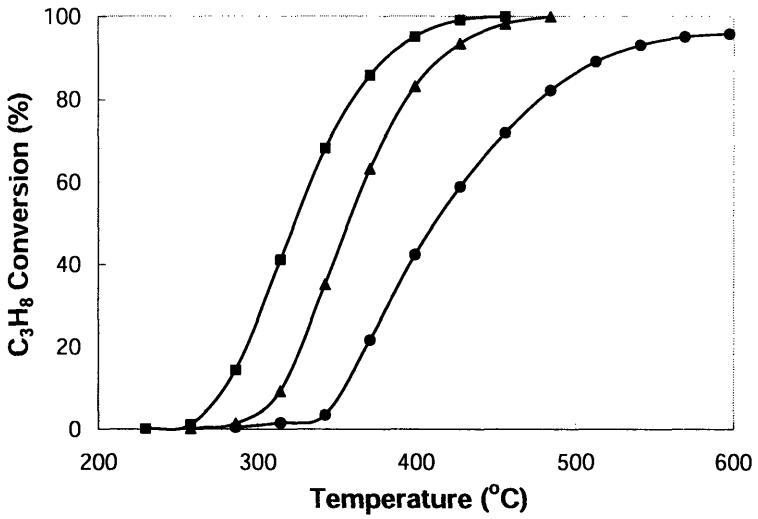

Figure 4.43 Propane conversion over 3 wt% V-promoted nickel aluminate (Ni/Al = 1.10), after calcination at 700°C in air. Catalytic testing was performed with a feed of 10% C_3H_8 in N_2 and H_2O at (■) 70,000 h^{-1}, (▲) 120,000 h^{-1} and (●) 350,000 h^{-1}, and $H_2O/C = 1$.

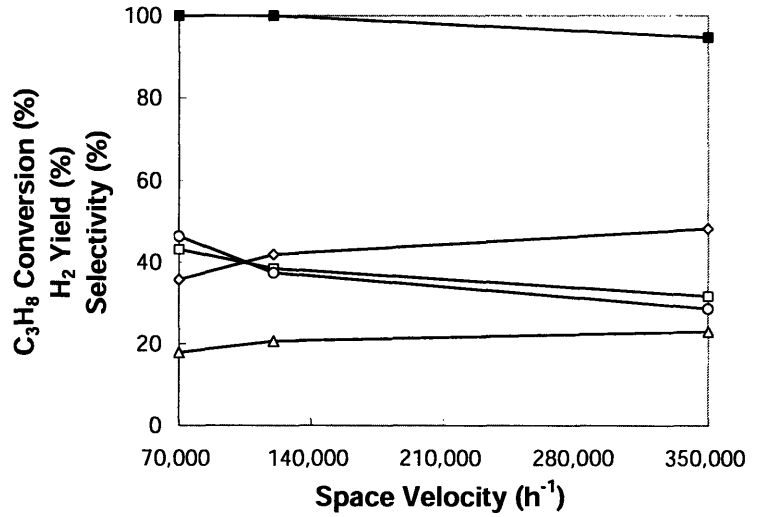

Figure 4.44 (□) H_2 yield, selectivities for (◊) CH_4, (○) CO and (Δ) CO_2, and (■) C_3H_8 conversion as a function of space velocity over 3 wt% V-promoted nickel aluminate (Ni/Al = 1.10) in propane steam reforming at 600°C. Catalytic testing was performed with a feed of 10% C_3H_8 in N_2 and H_2O, and $H_2O/C = 1$.

4.3.3.4 Effect of H_2O/C Ratio

3 wt% V-promoted and unmodified nickel aluminate catalysts were examined for propane steam reforming at H_2O/C ratios of 1–6 and various temperatures. The H_2 yield obtained experimentally was compared to the equilibrium calculations in Figure 4.45. At

temperatures higher than 600°C, the experimental results matched the equilibrium calculations. Compared to unmodified nickel aluminate, the catalyst with V promoter provided higher H_2 yield under all conditions, especially at a low H_2O/C ratio of 1, due to the greatly improved coking resistance (Figure 4.46).

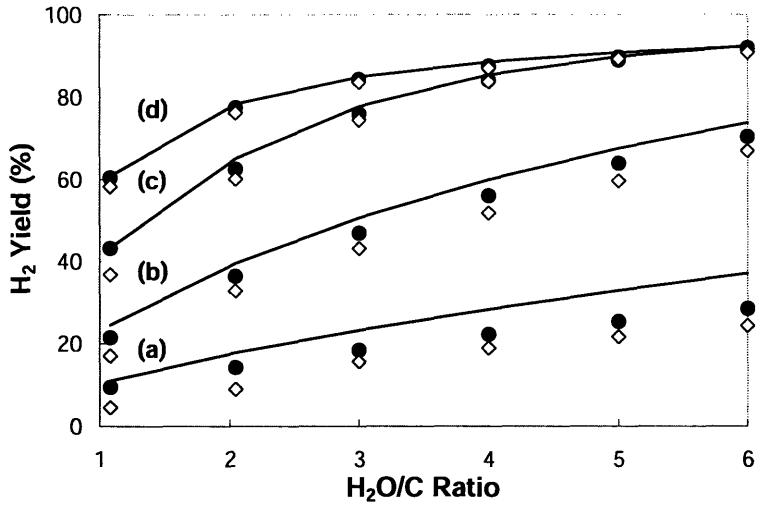

Figure 4.45 H_2 yield as a function of H_2O/C ratio in propane steam reforming over nickel aluminate (Ni/Al = 1.10) with (◊) no promoter and (●) 3 wt% of V. The solid lines represent equilibrium calculation results. Catalytic testing was performed with a feed of 10% C_3H_8 in N_2 and H_2O at (a) 400°C, (b) 500°C, (c) 600°C and (d) 700°C and 70,000 h^{-1}.

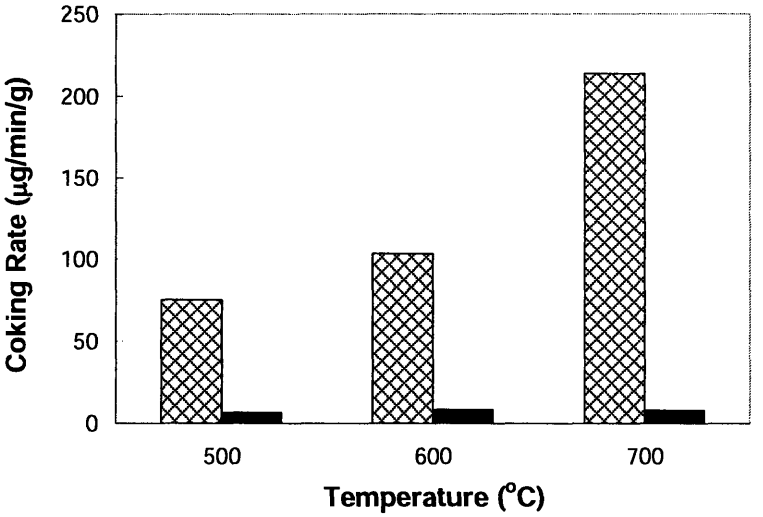

Figure 4.46 Coking rate over nickel aluminate (Ni/Al = 1.10) with (▩) no promoter and (■) 3 wt% of V in propane steam reforming at the temperature specified. Catalytic testing was performed with a feed of 10% C_3H_8 in N_2 and H_2O at 70,000 h^{-1} and $H_2O/C = 1$.

4.3.4 Re,V-Promoted Catalysts

4.3.4.1 Optimization of Re,V-Promoted Catalysts

To optimize the Re,V-promoted nickel aluminate system, various loadings of Re and V were introduced onto nickel aluminate (Ni/Al = 1.10). Figure 4.47 shows that the introduction of Re and V promoters helped to reduce the light-off temperature of nickel aluminate in propane steam reforming. It was interesting to note that the second promoter, V, further decreased the light-off temperature of Re-promoted nickel aluminate. Nickel aluminate with 2 wt% Re, 2 wt% V provided the lowest light-off temperature. Compared to unmodified and 1 wt% Re-promoted nickel aluminate, 3 wt% V-promoted nickel aluminate and 2 wt% Re,2 wt% V-promoted nickel aluminate provided higher H_2 yield (Figure 4.48). This was because V could improve carbon gasification [19-25], facilitating the generation of H_2.

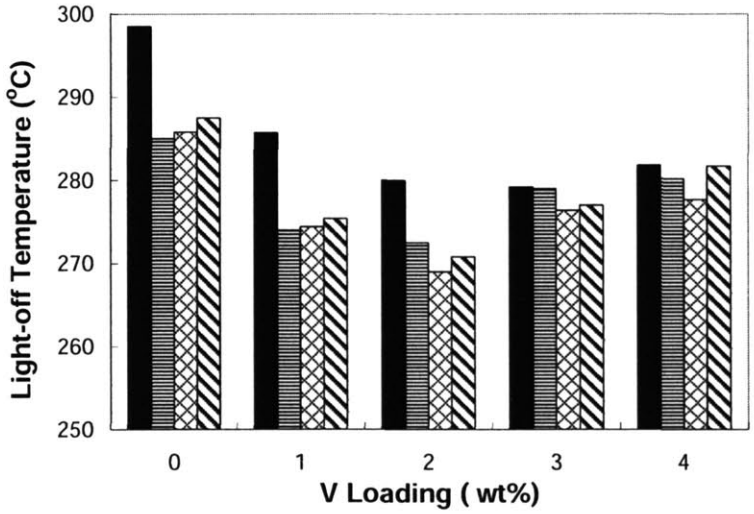

Figure 4.47 Light-off temperature in propane steam reforming over nickel aluminate (Ni/Al = 1.10) promoted with (■) 0, (▤) 1, (▩) 2 and (▧) 3 wt% of Re and the V loading specified, after calcination at 700°C in air. Catalytic testing was performed with a feed of 10% C_3H_8 in N_2 and H_2O at 70,000 h^{-1} and $H_2O/C = 1$.

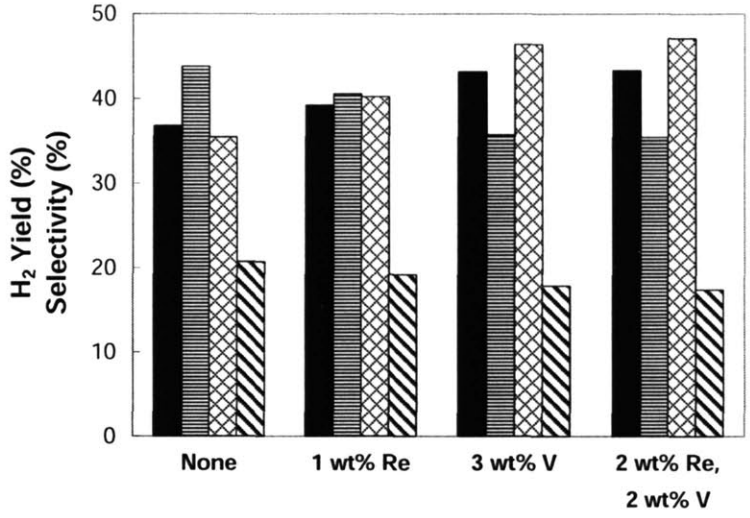

Figure 4.48 (■) H_2 yield, and selectivities for (▤) CH_4, (▩) CO and (▧) CO_2 over nickel aluminate (Ni/Al = 1.10) with the promoter(s) specified. Propane steam reforming was performed with a feed of 10% C_3H_8 in N_2 and H_2O at 600°C, 70,000 h^{-1} and H_2O/C = 1.

The TPR profiles in Figure 4.49 shows that reducibility was initiated at a much lower temperature of 390°C for 1 wt% Re-promoted, 3 wt% V-promoted, and 2 wt% Re,2 wt% V-promoted nickel aluminates, compared to the unmodified catalyst (460°C). The TPR profile of 2 wt% Re,2 wt% V-promoted nickel aluminate was similar to that of 1 wt% Re-promoted nickel aluminate, illustrating a significantly enhanced low-temperature TPR peak centered at 460°C. These two catalysts also showed comparable active surface area of 7.8 m^2/g and 8.1 m^2/g, respectively. This suggested that the excellent reducibility and metal dispersion of Re,V-promoted nickel aluminate were mainly governed by the presence of the Re promoter. This study also illustrated that the second promoter, V, did not negatively impacted the reducibility and metal dispersion of Re-promoted nickel aluminate, while enhancing coke resistance. It was postulated that the presence of V inhibited the blockage of active site by carbon deposition. Consequently, the V addition further increased the catalytic activity of Re-promoted nickel aluminate, especially at a low H_2O/C ratio.

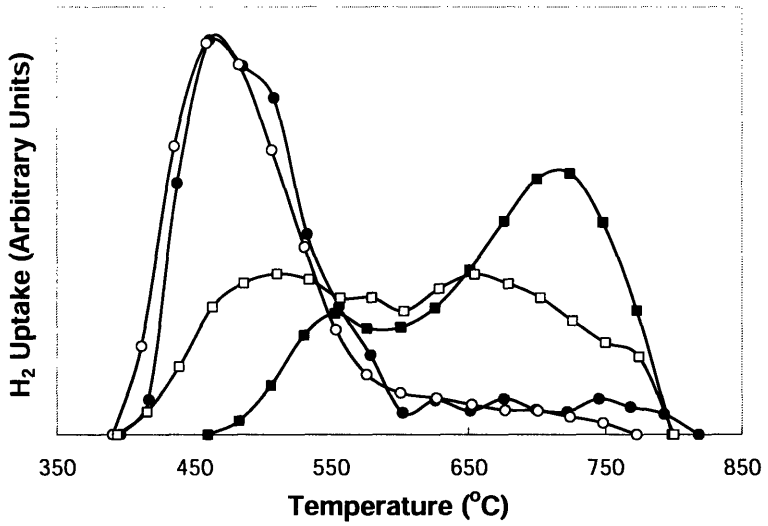

Figure 4.49 TPR profiles of nickel aluminate (Ni/Al = 1.10) with (■) no promoter, (○) 1 wt% Re, (□) 3 wt% V, and (●) 2 wt% Re + 2 wt% V, after calcination at 700°C in air.

The XRD patterns of 2 wt% Re,2 wt% V-promoted nickel aluminate after calcination, reduction, reaction and re-oxidation are shown in Figure 4.50. Both $NiAl_2O_4$ and NiO phases were detected after sample calcination at 700°C. These phases were replaced by the Ni phase after sample reduction. The Ni phase was retained with some grain growth to 9.9 nm after the steam reforming reaction. Upon re-oxidation in air at 800°C, both $NiAl_2O_4$ and NiO phases re-emerged with minor grain growth (NiO grain size = 10.9 nm). In contrast, the unmodified nickel aluminate underwent substantial grain growth after reaction (Ni grain size = 13.6 nm) and re-oxidation (NiO grain size = 14.6 nm) (Table 3.2) [10]. Thus, we could conclude that the presence of Re and V suppressed the grain growth of the nickel aluminate support and the active nickel nanocrystals.

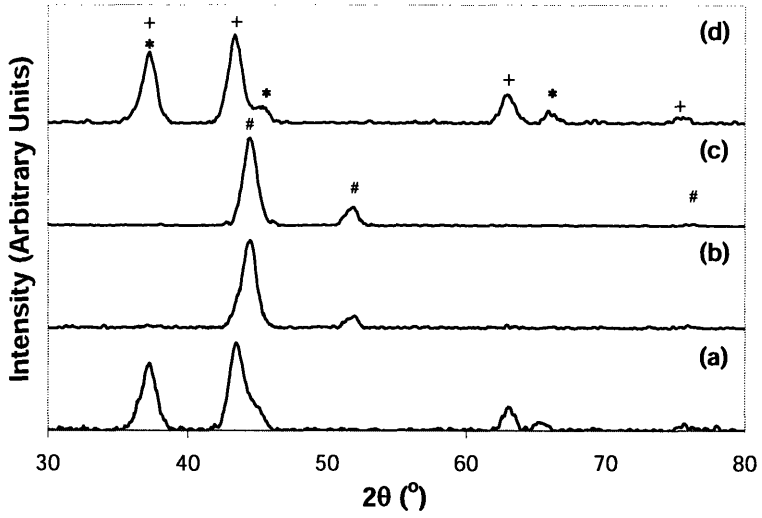

Figure 4.50 XRD patterns of 2 wt% Re,2 wt% V-promoted nickel aluminate (Ni/Al = 1.10) after (a) calcination at 700°C, (b) reduction at 650°C, (c) reaction at 600°C, and (d) re-oxidation at 800°C. XRD peaks of $NiAl_2O_4$, NiO and Ni are denoted by *, + and #, respectively.

Table 4.5 NiO and Ni grain sizes of 2 wt% Re,2 wt% V-promoted nickel aluminate (Ni/Al = 1.10) after calcination, reduction, reaction and re-oxidation.

Catalyst	NiO Grain Size (nm)	Ni Grain Size (nm)
Calcined at 700°C	9.2	—
Reduced at 650°C	—	8.3
Reacted at 600°C	—	9.9
Re-oxidized at 800°C	10.9	—

4.3.4.2 Effect of Calcination Temperature

The Re,V-promoted catalyst was calcined at 600–800°C, and compared to unmodified nickel aluminate for catalytic activity. Figure 4.51 shows that higher catalytic activities were achieved over the catalyst with Re and V promoters, and that calcination temperature did not have a significant effect on the catalytic activity. The unmodified and Re,V-promoted catalysts provided similarly high H_2 yield at a high reaction temperature of 700°C. The benefit of the Re and V promoters in improving H_2 yield was significant at lower reaction temperatures.

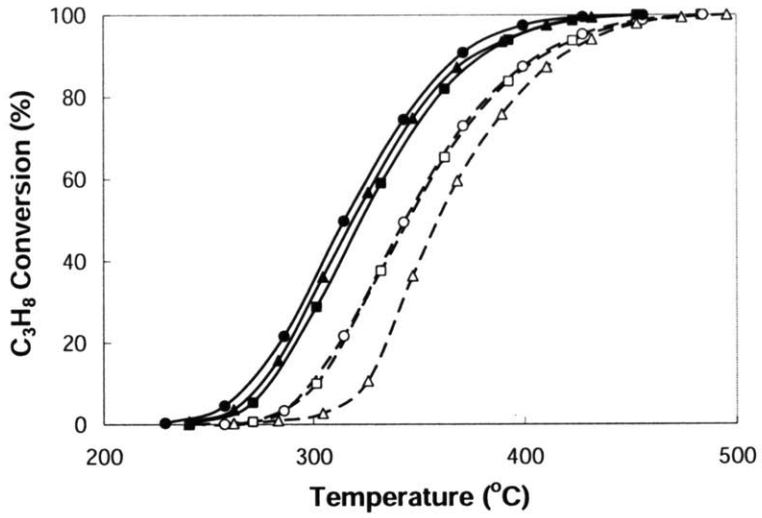

Figure 4.51 Propane conversion over nickel aluminate (Ni/Al = 1.10) with (open symbols) no promoter and (close symbols) 2 wt% Re + 2 wt% V, after calcination at (▲) 600°C, (●) 700°C and (■) 800°C in air. Catalytic testing was performed with a feed of 10% C_3H_8 in N_2 and H_2O at 70,000 h^{-1} and $H_2O/C = 1$.

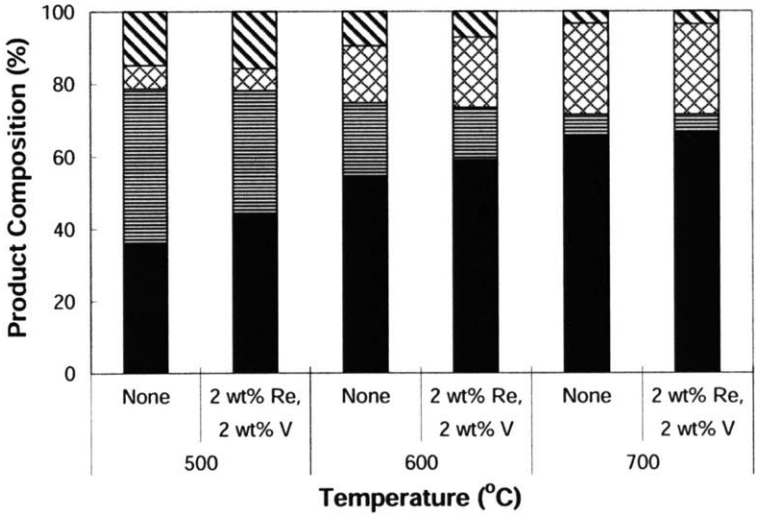

Figure 4.52 (■) H_2, (▤) CH_4, (▩) CO and (▨) CO_2 composition in the product stream of propane steam reforming over nickel aluminate (Ni/Al = 1.10) with no promoter or 2 wt% Re + 2 wt% V. Catalytic testing was performed with a feed of 10% C_3H_8 in N_2 and H_2O at the temperature specified, 70,000 h^{-1} and $H_2O/C = 1$.

Propane steam reforming was conducted over 2 wt% Re,2 wt% V-promoted nickel aluminate at 600°C and $H_2O/C = 1$. Figure 4.53 demonstrates that the excellent catalytic activity and selectivities of this system were stably retained for over 12 h. Remarkably,

this Re,V-promoted system was able to achieve and maintain the equilibrium H_2 yield at a low H_2O/C = 1, unlike the 1 wt% Re-promoted nickel aluminate. This confirmed the superior catalytic performance and coke resistance of the Re,V-promoted nickel aluminate.

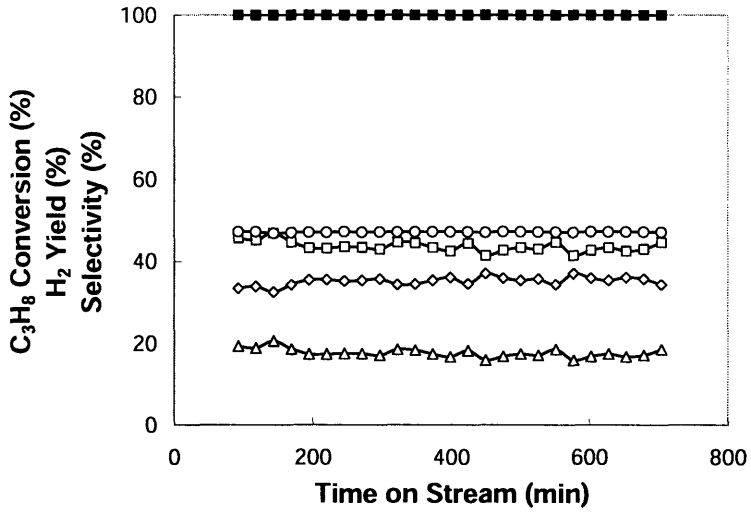

Figure 4.53 (□) H_2 yield, selectivities for (◊) CH_4, (○) CO and (Δ) CO_2, and (■) C_3H_8 conversion as a function of time over 2 wt% Re,2 wt% V-promoted nickel aluminate (Ni/Al = 1.10). Propane steam reforming was performed with a feed of 10% C_3H_8 in N_2 and H_2O at 600°C, 70,000 h^{-1} and H_2O/C = 1.

Figure 4.54 compares the equilibrium calculation of product composition in propane steam reforming and the experimental data obtained over 2 wt% Re,2 wt% V-promoted nickel aluminate at a H_2O/C ratio of 1. Equilibrium calculation showed complete propane conversion at a temperature as low as 200°C. Experimentally, full propane conversion was only achieved by 400°C. The equilibrium calculation and experimental data became quite consistent at temperatures above 400°C. The major differences at low temperatures could be attributed to incomplete propane conversion, which altered the product composition significantly below 400°C.

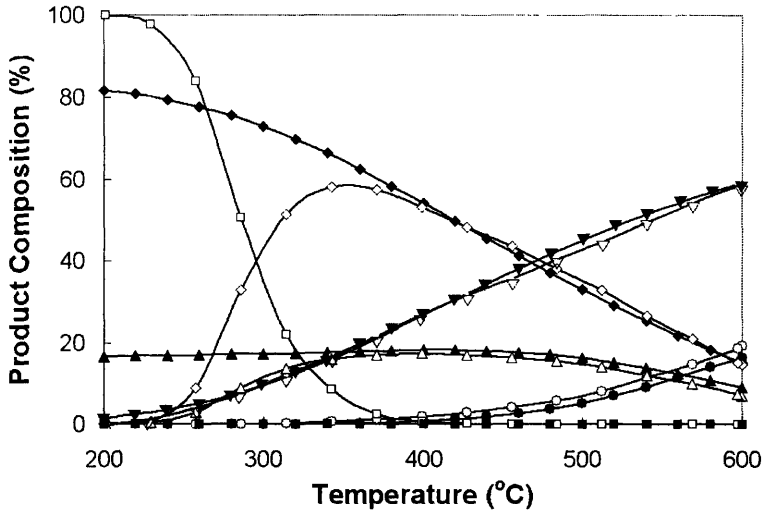

Figure 4.54 (Close symbols) Equilibrium and (open symbols) experimental product composition achieved over 2 wt% Re,2 wt% V-promoted nickel aluminate (Ni/Al = 1.10) in propane steam reforming. The products were (▽) H_2, (◊) CH_4, (○) CO, (Δ) CO_2 and (□) C_3H_8. Catalytic testing was performed with a feed of 10% C_3H_8 in N_2 and H_2O at 70,000 h^{-1} and $H_2O/C = 1$.

4.3.4.3 Effect of Space Velocity

Figure 4.55 shows that even at a high space velocity of 120,000 h^{-1}, complete propane conversion could be achieved at 480°C over the highly active, 2 wt% Re,2 wt% V-promoted nickel aluminate. Higher space velocity led to slightly lower propane conversion and H_2 yield at 600°C (Figure 4.56).

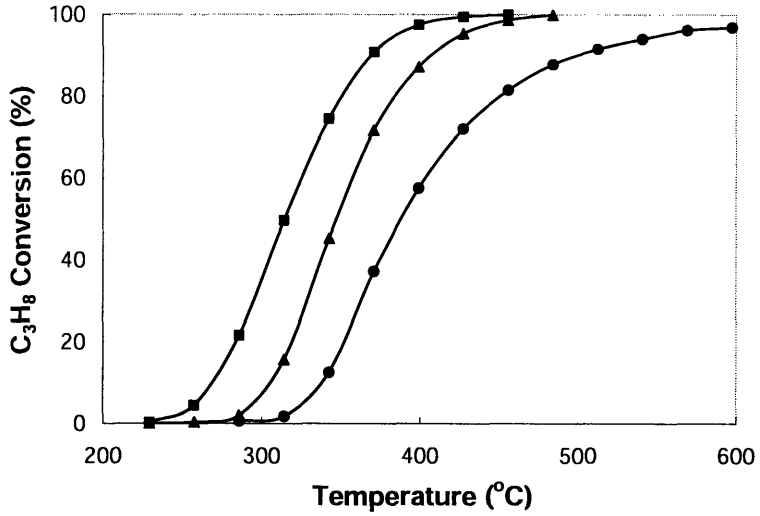

Figure 4.55 Propane conversion over 2 wt% Re,2 wt% V-promoted nickel aluminate (Ni/Al = 1.10), after calcination at 700°C in air. Catalytic testing was performed with a feed of 10% C_3H_8 in N_2 and H_2O at (■) 70,000 h^{-1}, (▲) 120,000 h^{-1} and (●) 350,000 h^{-1}, and $H_2O/C = 1$.

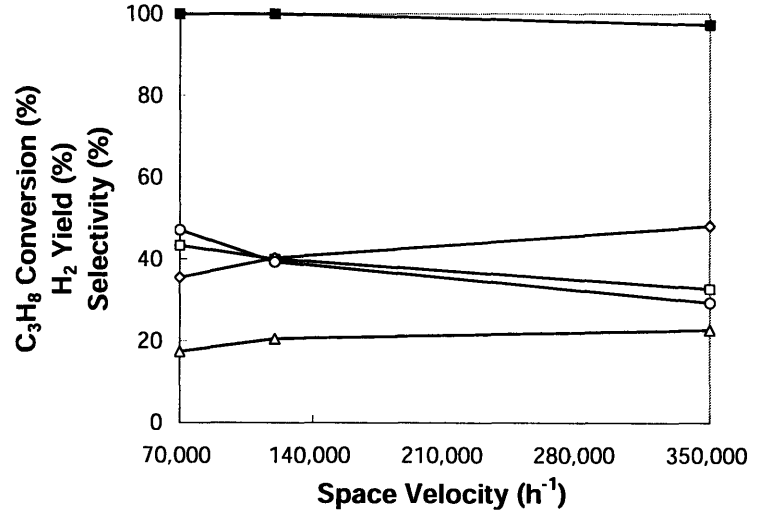

Figure 4.56 (□) H_2 yield, selectivities for (◊) CH_4, (○) CO and (Δ) CO_2, and (■) C_3H_8 conversion as a function of space velocity over 2 wt% Re,2 wt% V-promoted nickel aluminate (Ni/Al = 1.10) in propane steam reforming at 600°C. Catalytic testing was performed with a feed of 10% C_3H_8 in N_2 and H_2O and $H_2O/C = 1$.

4.3.4.4 Effect of H_2O/C Ratio

H_2 yield was examined as a function of H_2O/C for unmodified nickel aluminate, 1 wt% Re-promoted nickel aluminate, and 2 wt% Re,2 wt% V-promoted nickel aluminate.

In all cases, the catalysts with promoter(s) provided higher H_2 yields than unmodified catalyst, especially at low temperatures. The Re-promoted catalyst showed the best results at a low temperature of 400°C and H_2O/C ratios of ≥ 2. At temperatures of $\geq$ 500°C and H_2O/C ratios of ≥ 2, similar H_2 yields were achieved by the Re-promoted and Re,V-promoted catalysts. At a low H_2O/C ratio of 1, the Re,V-promoted catalyst attained the highest H_2 yield at all temperatures examined. This system successfully acquired the equilibrium H_2 yield at $\geq$ 600°C, illustrating its effectiveness at suppressing coke formation and its thermal/hydrothermal stability over a broad range of H_2O/C ratios (1–6).

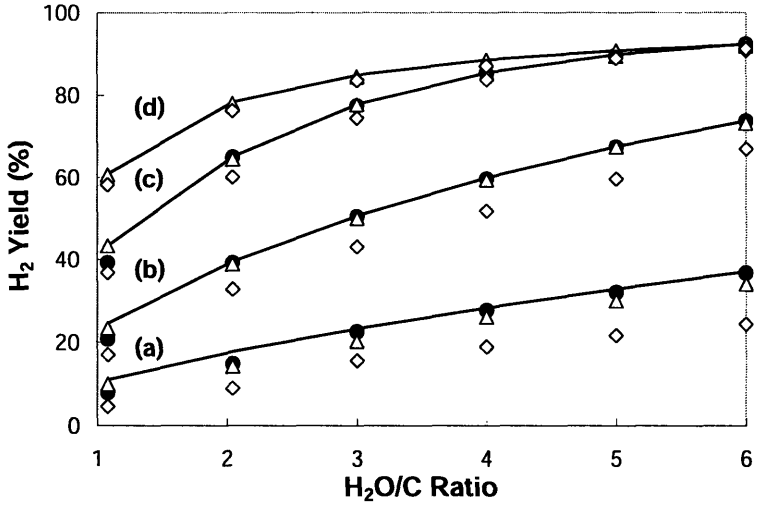

Figure 4.57 H_2 yield as a function of H_2O/C ratio in propane steam reforming over nickel aluminate catalyst (Ni/Al = 1.10) with (◊) no promoter, (●) 1 wt% Re, and (Δ) 2 wt% Re + 2 wt% V. The solid lines represent equilibrium calculation results. Catalytic testing was performed with a feed of 10% C_3H_8 in N_2 and H_2O at (a) 400°C, (b) 500°C, (c) 600°C and (d) 700°C, and 70,000 h^{-1}.

Figure 4.58 shows the XRD patterns of 2 wt% Re,2 wt% V-promoted nickel aluminate after propane steam reforming at various H_2O/C ratios. Nanocrystalline Ni was retained under all reaction conditions, indicating the hydrothermal stability of this catalyst. Compared to the results associated with unmodified nickel aluminate (Table 3.6 [10]), the relatively small increase in Ni grain size demonstrated that the presence of Re and V inhibited the grain growth of the active nickel nanocrystals (Table 4.6).

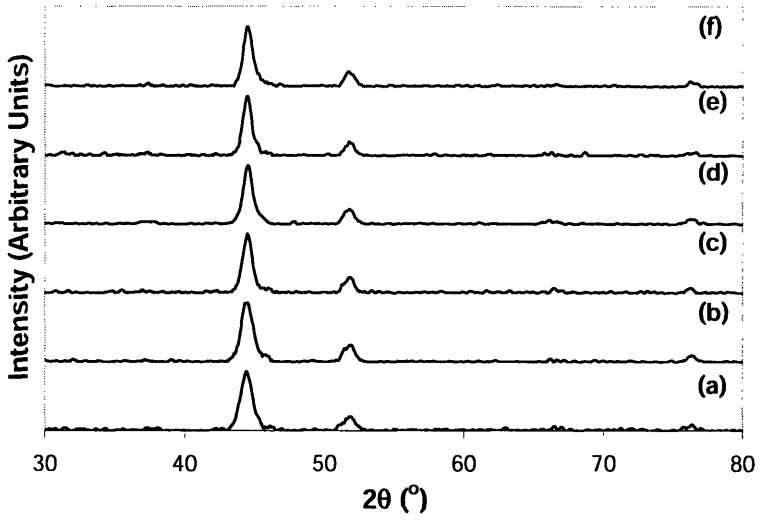

Figure 4.58 XRD patterns of 2 wt% Re,2 wt% V-promoted nickel aluminate (Ni/Al = 1.10) after propane steam reforming at 600°C, 70,000 h^{-1}, and H_2O/C = (a) 1, (b) 2, (c) 3, (d) 4, (e) 5 and (f) 6. All XRD peaks are associated with Ni.

Table 4.6 Ni grain sizes of 2 wt% Re,2 wt% V-promoted nickel aluminate (Ni/Al = 1.10) after reduction at 650°C and reaction at 600°C at the H_2O/C ratio specified.

H_2O/C Ratio	Ni Grain Size (nm) After Reduction	Ni Grain Size (nm) After Reaction
1	8.3	9.9
2	8.3	10.3
3	8.3	10.9
4	8.3	11.4
5	8.3	11.9
6	8.3	12.2

4.3.4.5 Coking Studies

The coke formation rates over unmodified and 2 wt% Re,2 wt% V-promoted nickel aluminates were compared at a low H_2O/C ratio of 1 (Figure 4.59). Re,V-promoted catalyst showed superior coke resistance at 500–700°C, dramatically reducing the coke formation rate. Coking became more severe with increasing reaction temperature over unmodified nickel aluminate, but was insignificant at all temperatures over the Re,V-promoted catalyst.

The elemental maps of Re,V-promoted nickel aluminate (Ni/Al = 1.10) after reduction and reaction are shown in Figure 4.60. Ni, Re and V were highly dispersed over

the oxide support after the reduction. Distinct nanocrystals of Ni were observed after the reaction, while Re and V remained highly dispersed over the support. C mapping was uniform for the entire image (including areas where no samples were present), indicating that the carbon was associated with the STEM sample grid. This suggested that the steam reforming reaction did not lead to significant carbon deposition on the sample surface. Unlike the unmodified nickel aluminate (Figure 3.29(b) [10]), no carbon filament were observed in the Re,V-promoted catalyst after reaction (Figure 4.61). The only structural change detected in the Re,V-promoted catalyst after reaction was a minor increase in grain size.

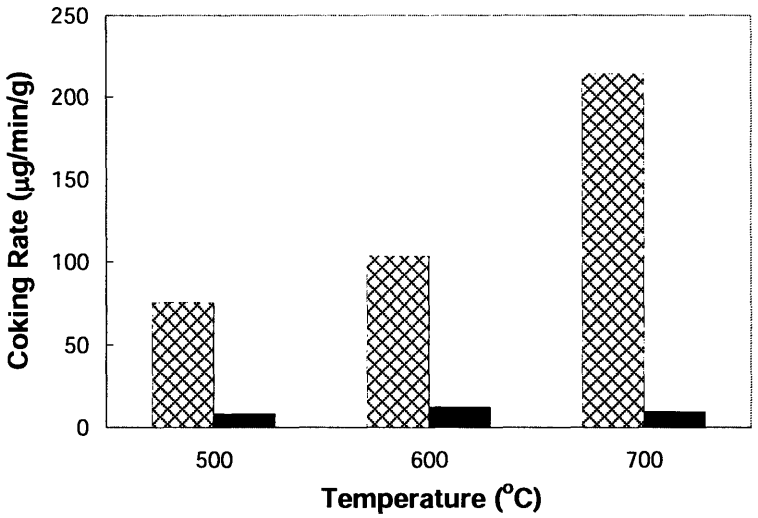

Figure 4.59 Coking rate over nickel aluminate (Ni/Al = 1.10) with (▨) no promoter and (■) 2 wt% Re + 2 wt% V in propane steam reforming at the temperature specified. Catalytic testing was performed with a feed of 10% C_3H_8 in N_2 and H_2O at 70,000 h^{-1} and $H_2O/C = 1$.

To demonstrate the ability of vanadium at improving carbon gasification, temperature-programmed coking and gasification were performed. The same amount of coke (1 g/g) was allowed to form on the reduced catalysts without promoter, with Re promoter and with Re and V promoters at 600°C over time. Following the coking process, coke gasification was undertaken with various concentrations of H_2O in N_2 at 100°C–800°C (ramp = 0.8°C/min). The catalysts were then oxidized in air to determine the coke remaining on the catalyst surface. Figure 4.62 shows that a low H_2O concentration in N_2 (5%) was sufficient to gasify most of the coke on 2 wt% Re,2 wt% V-promoted nickel

aluminate. In contrast, a large amount of coke was left on the surface of 1 wt% Re-promoted and unmodified nickel aluminate even after gasification with a high H_2O concentration in N_2 (20%). This confirmed that V favored the gasification of carbon, as mentioned in the literature [19-25].

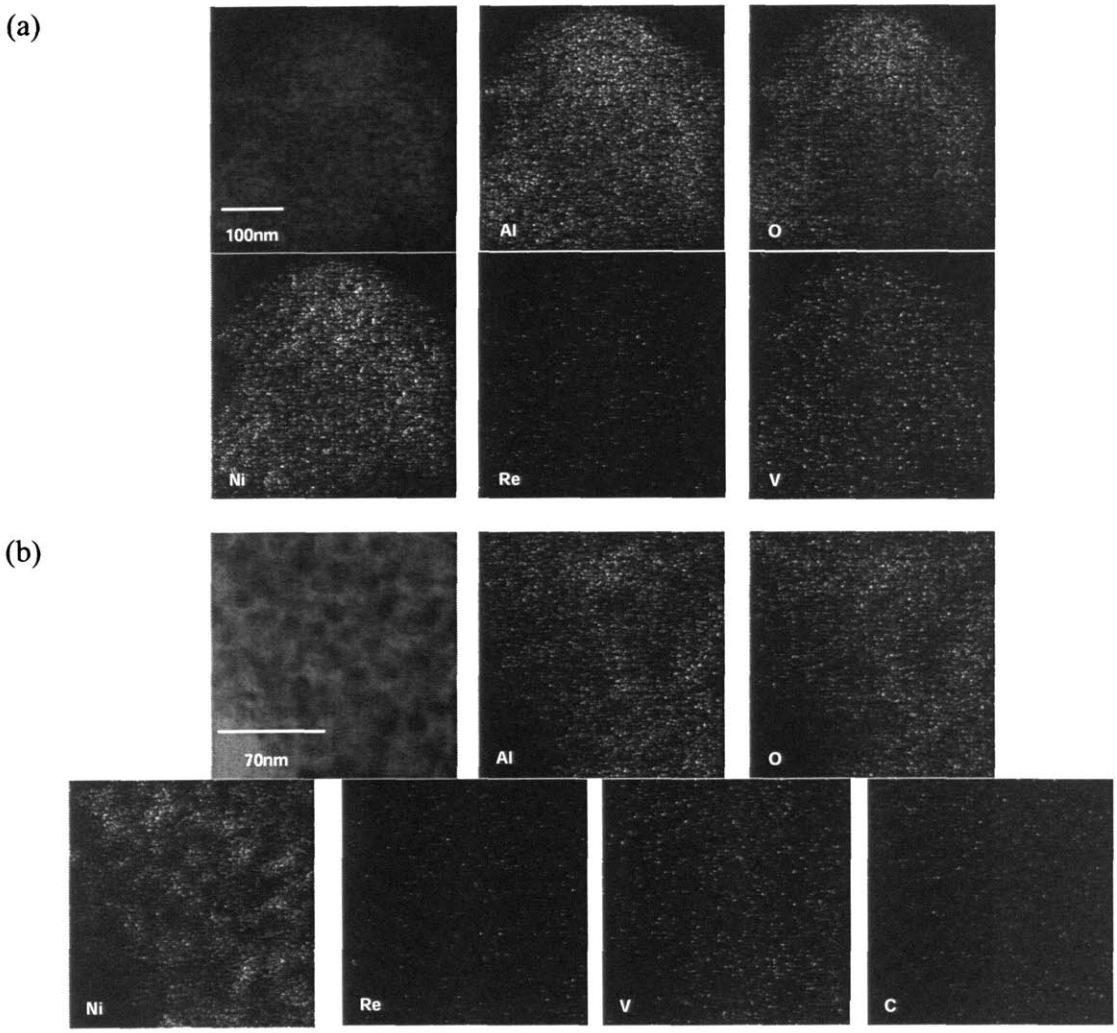

Figure 4.60 STEM/EDX image and elemental maps of 2 wt% Re,2 wt% V-promoted nickel aluminate after (a) reduction at 650°C, and (b) reaction at 600°C. Catalytic testing was performed with a feed of 10% C_3H_8 in N_2 and H_2O at 70,000 h^{-1} and $H_2O/C = 1$.

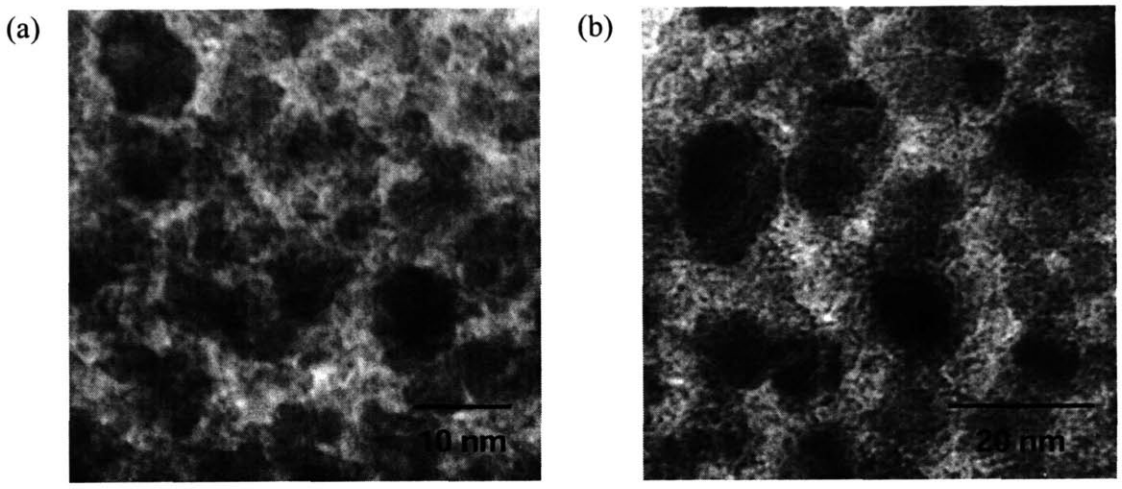

Figure 4.61 TEM images of 2 wt% Re,2 wt% V-promoted nickel aluminate (Ni/Al = 1.10) (a) before and (b) after propane steam reforming at 600°C. Catalytic testing was performed with a feed of 10% C_3H_8 in N_2 and H_2O at 70,000 h^{-1} and $H_2O/C = 1$.

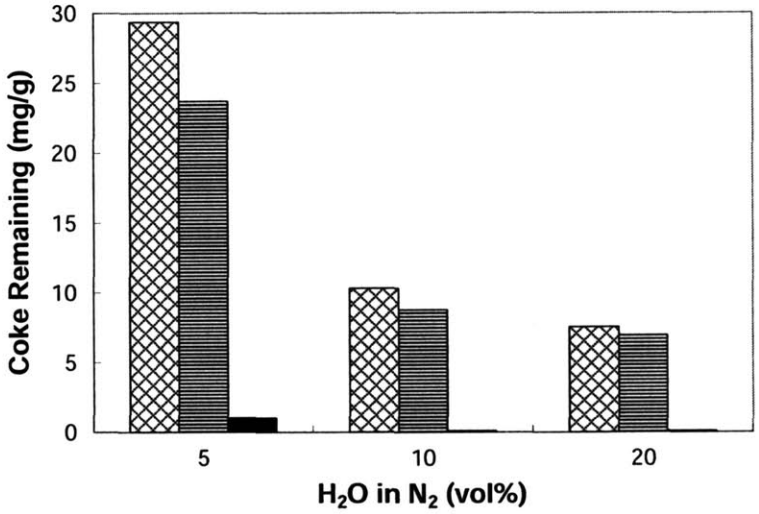

Figure 4.62 Coke remaining on nickel aluminate (Ni/Al = 1.10) with (▨) no promoter, (▤) 1 wt% Re and (■) 2 wt% Re + 2 wt% V, after coke gasification with the specified concentration of H_2O in N_2 at 100°C–800°C.

4.4 Summary

To further improve the catalytic activity and coke resistance, metal promoters were introduced to the optimized nickel aluminate system (Ni/Al = 1.10) for propane steam reforming. The catalytic activity and H_2 yield were increased with the addition of selected metals, in the order of Re > Rh > Pt > Ir > Pd > vapor-grafted Ru > Ru > V. The catalyst

promoted with Re showed the highest reducibility and active surface area. It enhanced the low-temperature catalytic activity most significantly. The optimal Re loading was 1 wt%. Re-promoted catalyst provided superior reaction rate to unmodified nickel aluminate at various temperatures due to its higher metal dispersion. This advantage was particularly noticeable at low calcination and pretreatment temperatures.

Promoters were also examined for improving the coke resistance of nickel aluminate. Coking was dramatically reduced with the addition of V, Mo and W. V was of particular interest as it showed a positive instead of negative impact on the catalytic activity of nickel aluminate.

To derive a steam reforming catalyst with both excellent catalytic activity and coke resistance, Re and V promoters were both introduced to nickel aluminate. The optimal combination involved 2 wt% Re and 2 wt% V, which provided superior catalytic activity and H_2 yield than unmodified, Re-promoted, and V-promoted nickel aluminates in propane steam reforming at a low H_2O/C ratio of 1. This could be attributed to the high reducibility and improved carbon gasification of Re,V-promoted catalyst due to Re addition and V introduction, respectively. The superb coke resistance and catalyst stability of the Re,V-promoted system was also demonstrated.

In conclusion, 2 wt% Re,2 wt% V-promoted nickel aluminate would be of great interest for applications at a low H_2O/C ratio (e.g. 1), while 1 wt% Re-promoted nickel aluminate would be most suitable for propane steam reforming at low temperatures (e.g. 400°C) and H_2O/C ratios $\geq$ 2. This study illustrated the successful tailoring of nanocomposite catalysts for the effective steam reforming of propane. The synergistic effects between the complex oxide support and the two metallic promoters in attaining high catalytic activity, selectivity, deactivation resistance and thermal/hydrothermal stability could be extended towards the design of catalytic systems for other challenging industrial processes.

4.5 References

[1] Rostrup-Nielsen, J. A., *J. Catal.* **33**, 184 (1974).
[2] Trimm, D. L., *Catal. Today* **49**, 3 (1999).
[3] Huang, T. J., Lin, H. J., Yu, T. C., *Catal. Lett.* **105**, 239 (2005).
[4] Natesakhawat, S., Watson, R. B., Wang, X. Q., Ozkan, U. S., *J. Catal.* **234**, 496 (2005).

[5] Ul-Haque, I., Trimm, D. L., US Patent 5,595,719 (1997).
[6] Natesakhawat, S., Oktar, O., Ozkan, U. S., *J. Mol. Catal. A: Chem.* **241**, 133 (2005).
[7] Wang, L. S., Murata, K., Inaba, M., *Appl. Catal. A: Gen.* **257**, 43 (2004).
[8] Kikuchi, R., Eguchi, K., *J. Jpn. Pet. Inst.* **47**, 225 (2004).
[9] Laosiripojana, N., Sangtongkitcharoen, W., Assabumrungrat, S., *Fuel* **85**, 323 (2006).
[10] He, H., Ying, J. Y., to be submitted to *J. Catal.*
[11] Myers, D. B., "Steam Reforming of Methane with Nickel Aluminate-based Catalysts," M.S. Thesis, Massachusetts Institute of Technology, 2000.
[12] Mehnert, C. P., Weaver, D. W., Ying, J. Y., *J. Am. Chem. Soc.* **120**, 12289 (1998).
[13] Mehnert, C. P., Ying, J. Y., *Chem. Commun.*, 2215 (1997).
[14] Borowiecki, T., Gac, W., Denis, A., *Appl. Catal. A: Gen.* **270**, 27 (2004).
[15] Richardson, J. T., Turk, B., Lei, M., Forster, K., *Appl. Catal. A: Gen.* **83**, 87 (1992).
[16] Richardson, J. T., Lei, M., Turk, B., Forster, K., Martyn, V., *Appl. Catal. A: Gen.* **110**, 217 (1994).
[17] Richardson, J. T., Turk, B., Twigg, M. V., *Appl. Catal. A: Gen.* **148**, 97 (1996).
[18] Borowiecki, T., Denis, A., Gac, W., Dziembaj, R., Piwowarska, Z., Drozdek, M., *Appl. Catal. A: Gen.* **274**, 259 (2004).
[19] Mul, G., Kapteijn, F., Doornkamp, C., Moulijn, J. A., *J. Catal.* **179**, 258 (1998).
[20] Gokarn, A. N., Pradhan, S. D., Pathak, G., Kulkarni, S. S., *Fuel* **79**, 821 (2000).
[21] Pan, Z. J., Yang, R. T., *J. Catal.* **130**, 161 (1991).
[22] Silva, I. F., Palma, C., Klimkiewicz, M., Eser, S., *Carbon* **36**, 861 (1998).
[23] Ahlström, A. F., Odenbrand, C. U. I., *Appl. Catal.* **60**, 143 (1990).
[24] Neeft, J. P. A., Makkee, M., Moulijn, J. A., *Chem. Eng. J.* **64**, 295 (1996).
[25] Neeft, J. P. A., Makkee, M., Moulijn, J. A., *Appl. Catal. B: Environ.* **8**, 57 (1996).

Chapter 5. Conclusions and Recommendations for Future Work

5.1 Conclusions

This thesis focused on materials development for emission control of diesel engines and H_2 provision for fuel cells. A new catalyst, 40 wt% CuO-Ag/CeO_2 was developed to completely oxidize carbon black by 400°C. It could be applied towards the effective combustion of soot particulates at diesel engine exhaust temperatures. The high dispersion of CuO and Ag on nanocrystalline CeO_2, and the synergism between these three components provided for superior catalyst reducibility at low temperatures. This led to a unique nanocomposite catalyst with outstanding performance in carbon black combustion.

Steam reforming of propane was investigated over nickel aluminate catalysts. The optimal Ni/Al molar ratio was found to be 1.10, based on propane conversion and H_2 yield. Upon reduction of the Ni-rich nickel aluminate, highly dispersed active Ni species were stably obtained for the catalytic steam reforming of propane. To further improve the catalytic activity and coke resistance of nickel aluminates, various additives were examined. Re was the most effective promoter for improving the low-temperature catalytic activity. Re-promoted nickel aluminate possessed a higher active surface area associated with improved reducibility, compared to the unmodified nickel aluminate. V was shown to inhibit coke formation dramatically by facilitating carbon gasification, without sacrificing the catalytic activity. The Re,V-promoted nickel aluminate catalyzed propane steam reforming effectively even under low H_2O/C ratios (e.g. 1). The promoters also helped to suppress sintering and grain growth of the active species during reaction, providing for excellent thermal and hydrothermal stability.

5.2 Recommendations for Future Work

This work demonstrated CuO-Ag/CeO_2 as an excellent catalyst for the combustion of carbon black. For the application of soot emission control, it is also important for the catalyst to possess poisoning resistance against sulfur dioxide. Alkali metals such as K and Cs have been shown to improve sulfur poisoning resistance [1, 2]. It would be of interest to introduce alkali metals to CuO-Ag/CeO_2, and examine the resulting catalyst for soot combustion under simulated diesel engine exhaust conditions.

For nickel-based catalysts to be applied industrially in steam reforming reactions, they have to possess excellent catalytic activity, and resistance against coking, sintering and sulfur poisoning [3]. In this thesis, Re,V-promoted nickel aluminate has demonstrated excellent activity, coke resistance and stability against sintering. Further study is needed to determine the sulfur resistance of this system. Sulfur is a common poison to nickel-based catalysts since the adsorbed sulfur can block the active nickel sites and decrease the catalytic activity. Thus, the sulfur adsorption capacity of Re,V-promoted nickel aluminate should be established. Where necessary, additives may be introduced to improve the sulfur resistance of the Re,V-promoted nickel aluminate system for industrial applications.

5.3 References

[1] Neri, G., Rizzo, G., Galvagno, S., Donato, A., Musolino, M. G., Pietropaolo, R., *Appl. Catal. B: Enviorn.* **42**, 381 (2003).

[2] Tikhomirov, K., Kröcher, O., Wokaun, A., *Catal. Lett.* **109**, 49 (2006).

[3] Sehested, J., *Catal. Today* **111**, 103 (2006).